"Modeling of Spatial and Temporal Dynamics in Biological Olfactory Systems"
Final Technical Report, ONR Grant N00014-01-1-0630

Dr. Jacek M. Zurada*, Dr. Andy G. Lozowski**, and Mykola Lysetskiy*

* University of Louisville
** Southern Illinois University at Edwardsville

Consultant: John S. Kauer, Tufts University

04/01/2001 - 12/31/2004

Report Date:

September 21, 2007

REPORT DOCUMENTATION PAGE

Form Approved
OMB No. 0704-0188

1. REPORT DATE *(DD-MM-YYYY)*	2. REPORT TYPE	3. DATES COVERED *(From - To)*
20-09-2007	Research	From 04-01-2001 To 12-31-2004

4. TITLE AND SUBTITLE
Modeling of Spatial and Temporal Dynamics in Biological Olfactory Systems

5a. CONTRACT NUMBER

5b. GRANT NUMBER
N00014-01-1-0630

5c. PROGRAM ELEMENT NUMBER

6. AUTHOR(S)
Dr. Jacek M. Zurada (PI), Dr. Andy G. Lozowski (Co-PI)

5d. PROJECT NUMBER

5e. TASK NUMBER

5f. WORK UNIT NUMBER

7. PERFORMING ORGANIZATION NAME(S) AND ADDRESS(ES)
University of Louisville Research Foundation

8. PERFORMING ORGANIZATION REPORT NUMBER
994 561

9. SPONSORING/MONITORING AGENCY NAME(S) AND ADDRESS(ES)
Office of Naval Research
Ballston Centre Tower One
800 N. Quincy Street
Arlington, VA 22217-5660
Div. of Cognitive and Neural Science/Technology/Neuromorphic Systems

10. SPONSOR/MONITOR'S ACRONYM(S)
ONR-DEPSCOR

11. SPONSOR/MONITOR'S REPORT NUMBER(S)

12. DISTRIBUTION/AVAILABILITY STATEMENT
For Public Release, Unlimited Distribution

13. SUPPLEMENTARY NOTES

14. ABSTRACT

The olfactory system is a very efficient biological setup capable of odor information processing with neural signals. The nature of neural signals restricts the information representation to multidimensional temporal sequences of spikes. The information is contained in the inter-spike intervals in each individual neural signal and in inter-spike intervals between multiple signals. A mechanism of interactions between random excitations evoked by odorants in the olfactory receptors of the epithelium and deterministic operation of the olfactory bulb is proposed and evaluated in this project. Inverse Frobenius-Perron models of the bulb's temporal sequences are fitted to the inter-spike distributions of temporally modulated receptor signals. Ultimately, such pattern matching results in an ability to recognize odors and offers a hypothetical model for signal processing occurring in the primary stage of the olfactory system.

15. SUBJECT TERMS
Olfactory system, temporal dynamics, inverse Frobenius-Perron model, interspike intervals

16. SECURITY CLASSIFICATION OF:			17. LIMITATION OF ABSTRACT	18. NUMBER OF PAGES	19a. NAME OF RESPONSIBLE PERSON
a. REPORT	b. ABSTRACT	c. THIS PAGE			Jacek M. Zurada
					19b. TELEPHONE NUMBER *(Include area code)* 502 852 5314

Contents

"Modeling of Spatial and Temporal Dynamics in Biological Olfactory Systems"
Final Technical Report, ONR Grant N00014-01-1-0630

Dr. Jacek M. Zurada*, Dr. Andy G. Lozowski**, and Mykola Lysetskiy*

* University of Louisville
** Southern Illinois University at Edwardsville

Consultant: John S. Kauer, Tufts University

04/01/2001 - 12/31/2004

Report Date:

September 21, 2007

List of Figures

List of Tables

"Modeling of Spatial and Temporal Dynamics in Biological Olfactory Systems"

December 2006

Summary

The olfactory system is a very efficient biological setup capable of odor information processing with neural signals. The nature of neural signals restricts the information representation to multidimensional temporal sequences of spikes. The information is contained in the inter-spike intervals in each individual neural signal and in inter-spike intervals between multiple signals. A mechanism of interactions between random excitations evoked by odorants in the olfactory receptors of the epithelium and deterministic operation of the olfactory bulb is evaluated in this project. Inverse Frobenius-Perron models of the bulb's temporal sequences are fitted to the interspike distributions of temporally modulated receptor signals. Ultimately, such pattern matching results in an ability to recognize odors, and it offers a hypothetical model for signal processing occurring in the primary stage of the olfactory system.

Chapter 1

Objectives

Understanding the computational principles of the biological neural circuits is a great scientific challenge of the current century. The olfactory neural circuits are relatively well accessible and studied, and are often believed to be the one that could provide great insights and even a significant breakthrough in our understanding of "How the brain works".

Not only a scientific curiosity drives the interest of studying the olfactory neural circuits, but also the potential benefits of discovering new neural computation principles. Indeed, computational abilities of the olfactory system are often superior to the ones offered by the engineering pattern recognition techniques. Thus, better understanding of the olfactory pattern processing could open new directions not only in neuroscience, but in computer science as well.

The aim of the research presented in this report is to study the principles of signal processing occurring in the olfactory bulb. A new concept of the olfactory neural encoding with the interspike interval (ISI) statistics has been suggested, and proposed to mimic the dynamics of the olfactory bulb. The idea is that the stored odor pattern (ISI distribution) corresponds to one of the eigenvectors of the transition matrix of associated Markov process.

A step towards implementation of this concept in a biologically realistic neural circuit, a circuit of integrate-and-fire neurons, has also been made. The basic principle used in the model is that the probabilities of occurrence of particular interspike intervals in the generated spike train are controlled by a pattern of applied input currents. This way the model maps input patterns to the ISI distributions. It is also suggested how such encoding with the ISI statistics could take place in biological olfactory systems.

The idea of controlling the dynamics and statistics of a neural dynamical system with an external input has been also studied in a theoretical model of a chaotic system, based on the macro-dynamics of the olfactory bulb (OB). The mechanism of the input-controlled bifurcation in a model of chaotic neuron has been proposed. This mechanism enables the neural system to map the input space to the different modes of its own dynamics.

The mapping of input patterns to the neural output dynamics has also been studied in the proposed model of the olfactory cortex dynamics, where the cortical pattern recognition has been investigated. In the developed model the temporal structure of the olfactory bulb input controls spatial dynamics of the cortical neural ensemble.

Chapter 2

Neural Encoding in the Olfactory Bulb

Biological olfactory system can be seen as an engineering device working as a pattern recognition machine with associative memory. It maps specific features of the odor molecules detected by the sensors of the receptor neurons in the olfactory epithelium to the inherent dynamics of the olfactory subsystem called olfactory bulb (OB) in mammals and antennal lobe (AL) in insects [1, 2, 3, 4, 5, 6, 7]. The spatio-temporal patterns of this dynamics are then processed and recognized by the olfactory cortex in mammals and mushroom body (MB) in insects [8, 9].

Variety of computational models and abstract concepts attempt to explain how olfactory system functions. A number of them study the global neural dynamics of the olfactory bulb, in particular, the possible role of chaos and bifurcations [10, 11, 12, 13] as well as statistics [14] in the the olfactory information processing. More biologically oriented models explore the dynamics of the olfactory bulb microcircuits focusing on the coupling of neural oscillators [15], emergence of synchronization [16, 17] and the mechanism of pattern formation [18, 19]. The recognition of these spatio-temporal patterns is then studied in the models of olfactory cortex [8, 9]. Still, more experimental and computational efforts are needed to clarify the basic information processing principles of the olfactory system.

2.1 Olfactory epithelium

The receptor neurons of olfactory epithelium in nasal cavity transform certain properties of the odor molecules to the spike trains which they send to olfactory bulb (Fig 2.1). The odorant receptors on the cilia of the sensory neurons react with the molecules having specific features. An individual sensory neuron posses one or a few kinds of this receptors, the total number of which is about 1000 [20, 21]. Thus each sensory neurons is sensitive to one or a few properties of the odor molecule, although, the origin of these molecules' properties crucial for odor identification is not clear [22]. The sensory neurons with identical receptors are spread uniformly in the epithelium in the 4 zones [20]. The larger the concentration of the odor presented in the nasal cavity, the more receptors are bound by the molecules, the larger the number of the sensory neurons are excited and the larger are the frequencies of their firing. This way epithelium seem to encode the concentration of the odor molecules with the number of activated sensory neurons

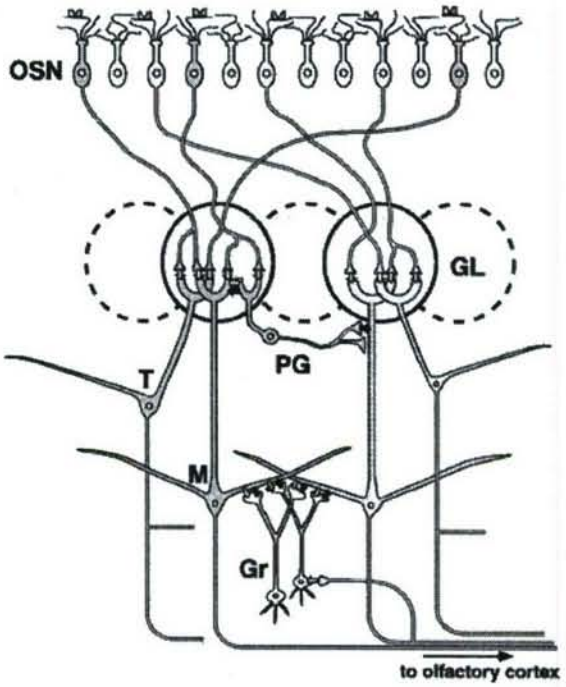

Figure 2.1: Olfactory bulb functional anatomy. Abbreviations: M - Mitral cells; T - tufted cells; Gr - Granulle cells; PG - Periglomerular cells; OSN - Olfactory sensory neurons;(From Mori K, Nagao H, and Yoshihara, Y, *Science*, 286(5540):711-715, 1999).

and the frequency of their firing [23, 21]. These spike trains from the input which olfactory bulb receives from the olfactory epithelium.

2.2 Functional anatomy of olfactory bulb

2.2.1 Glomeruli layer

The axons (output cables) of the sensory neurons with the same receptor type converge in the OB/AL to a tight axon bundle which is called glomerulus [20, 6, 21]. Although the glomeruli might receive some inputs from a different receptor types [20], it is generally assumed that each glomerulus corresponds to a specific odor feature [5]. This is the first and basic signal transformation in the olfactory bulb: Different odors form specific spatial patterns of the excited glomeruli, which are activated by the corresponding receptor neurons. Neighboring glomeruli are interconnected via periglomerular interneurons (Fig. 2.1). The glomeruli excite the adjacent periglomerular cells and get inhibitory feedback from them, which modulates the glomeruli activity. It is suggested that this modulation could be sharpening the spatial patterns, which might be realized via winner-take-all competition [21], as in the the visual system, although there are arguments against it [24].

2.2.2 Mitral cells layer

Each glomerulus sends signals to one or a few of the specific mitral cells (MC) in OB or to the projection neurons (PN) in AL. MC and PN are the principal (output) neurons of the OB/AL (Fig. 2.1). The dynamics of mitral cells gets modulated by the interneurons in the similar way as is the dynamics of glomeruli: Mitral cells excite the granule cells in return get inhibited by them [21].

Interactions in this excitatory-inhibitory circuit supposedly shape the odor-specific temporal patterns of the mitral cells/projection neurons [25, 26]. However, the exact mechanism of formation of the spatio-temporal patterns and their correlation with the input odor patterns is not clear [27].

2.3 Spatio-temporal dynamics

2.3.1 Spatial patterns

The only clearly known encoding principle in the olfactory bulb is that the odor invoked spatial activation patterns of the glomeruli and mitral cells of OB/AL are correlated with the odor components [2, 3, 4, 5, 6]. Invoked spatial patterns also proved to be unique for different odors and their concentrations [1, 7].

A number of experiments show that the neighboring glomeruli and corresponding mitral cells demonstrate similar tuning properties [4, 5]. This suggests that the OB/AL might work as an analog of a Kohonen map [28]. There is data that shows that the mapping of the olfactory bulb may be more complicated than that: Odor receptor map in the glomeruli array seems to have hierarchical and fractal-like structure [1]. It should be noted that the idea that spatial proximity of the glomeruli and mitral cells corresponds to the similarity of their tuning properties is not universally accepted [27], and it is also not clear how the tuning properties should be defined when a neuron participates in a spatio-temporal dynamics (described in the following sections). Overall, it is widely believed that spatial activity patterns of mitral cells and glomeruli are closely related to the odor encoding, but the exact structure of the odor-spatial pattern correspondence is unclear.

2.3.2 Spatio-temporal activity

Not only spatial, but also temporal patterns of activation proved to contribute to the odor encoding in the mammal olfactory bulb [29, 3, 7] and insect antennal lobe [30, 31, 26]. As was mentioned above, the neighboring glomeruli inhibit each other via periglomerular cells do the same with each other via granule interneurons [21]. These interactions are believed to be the the origin of the temporal dynamics in olfactory bulb. The initial odor-invoked spatial pattern of the mitral cells activity undergoes certain transformations as some of the mitral cells, active at first, become inhibited, while the others, silent/suppressed at the beginning of the odor onset, get excited later (Figs. 2.2 and 2.3).

Experimental data suggests two basic ideas about the nature of spatio-temporal dynamics. Some of the experiments report slow dynamics of the spatio-temporal patterns in a "diffusive" manner [29], where the initial spatial pattern does not change significantly: only fraction of the initially active regions stops firing, and some of the neighboring cells get recruited later

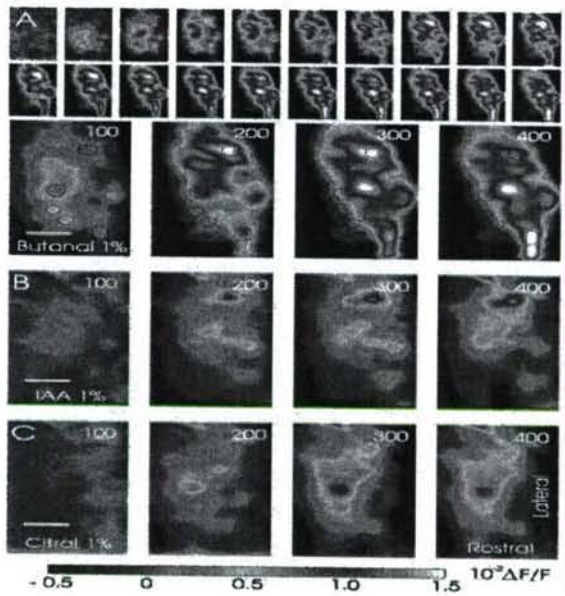

Figure 2.2: Activation patterns in the olfactory bulb (From Spors H, and Grinvald A, *Neuron*, 34(2):301-15, 2002.)

(Fig. 2.2). It was shown that such transformation optimizes the odor representation [29]. The similar odors which are close to each other in the odor space would also produce similar initial spatial representations in the mitral cells activity. During the transformation, the spatial activity patterns of the similar odors would become more and more distinct, which, supposedly, facilitates their recognition further in the olfactory cortex.

Another, more radical idea about the role of spatio-temporal sequences in the odor encoding is based on experimental data on the insect antennal lobe. In the locust AL, an initial spatial pattern of odor invoked activity undergoes dramatic, often cyclic changes [30, 26], in contrast to comparatively smaller changes in the olfactory bulb spatial dynamics described above. This data clearly shows that it is not just the initial spatial pattern, but it is the whole spatio-temporal dynamics that encodes the odors [24, 27] (See Fig 2.3).

So, in olfactory bulb and antennal lobe an odor invokes, at first, a spatial activation pattern of the principal (mitral or projection) neurons, which, then, transforms gradually, in a certain spatio-temporal sequence, which is shown to be odor specific. However, what exactly the sequence of spatial patterns and the latencies of their appearance encodes is yet to be clarified.

Some of the hypothesis suggest that the temporal structure of these sequences may be related to the concentration of the odors [32, 19]. Indeed, it was shown that the increasing odor concentrations reduce response latencies of the mitral cells in the odor specific sequences, and recruited new glomerular units [7].

These and other results suggest that both odor identity and its concentrations are encoded by both spatial and temporal structure of the activity of mitral cells. Interactions in the excitatory-inhibitory mitral-granule and glomeruli-periglomeruli circuit shape the odor-specific temporal patterns of the mitral cells [29, 7]. However, the exact mechanism of the spatio-temporal pattern formation and their correlation with the input odor patterns is still unclear [27].

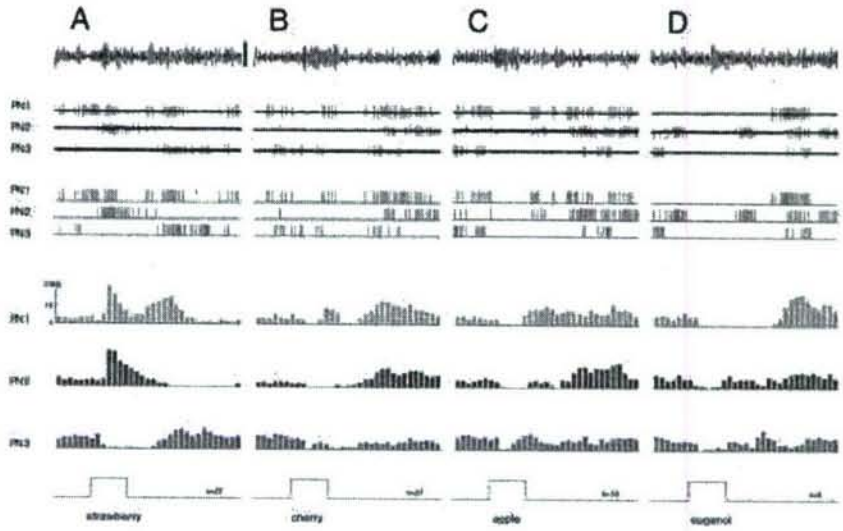

Figure 2.3: Odor-specific spatio-temporal dynamics of the principal neurons in the locust antennal lobe. Four columns (A-D)correspond to the application of four different odors. The upper rows show the spike train of the projection neurons (PN1, PN2 and PN3), and the lower rows demonstrate the histograms of the spike trains, repeatedly induced by the same odor (From Laurent G, Wehr M, and Davidowitz H, *Journal of Neuroscience*, 16(12):3837-47, 1996.)

2.4 Encoding with transient synchronization

In addition to spatio-temporal dynamics, another mechanism of encoding, synchronization, proved to work in olfactory system. There have been debates for a long time about the origin and functional significance of oscillatory activity and its synchronization in the brain in general and in the the olfactory system in particular [27]. One of the possible mechanisms of the emergence of synchronization is believed to be based on the interaction between excitatory and inhibitory circuits [21]. When excitatory neurons (mitral cells in OB and projection neurons in AL) get excited and start to fire (probably, incoherently at first), they activate common inhibitory cells (periglomerular and granule cells in OB and local interneurons in AL). Inhibitory cells, in their turn, send their feedback simultaneously to several excitatory neurons (mitral cells/projection neurons), and this common inhibition presumably synchronizes these microcircuits [33, 21].

Experimental data on the insect olfactory system provided neuroscience with one of the clearest demonstrations of the role of synchronization in neural encoding [31, 26]. It was shown that information is encoded not only by the activity of the individual neurons, but also by the fine structure and mutual correlations of neurons, in particular, by their synchronization. In the locust antennal lobe the sequences of the transient synchronizations of specific neural ensembles turned out to be responsible for the encoding and fine discrimination [30, 31, 26]. During the stimulus onset, specific groups of neurons synchronize their activity at specific cycles of their activation. The timing of this synchronization and the sequence of transient synchronization of different groups of neurons proved to be odor-specific and reproducible for a given odor for different trials [26].

Moreover, in the experiments with the honeybees [31] where synchronization was selectively blocked, but the patterns of individual neurons remained unchanged, the bees still could dis-

criminate between distinct odors, but were no longer able to distinguish similar ones. This experimental data suggests that the transient synchronization phenomenon in a sense, adds a new dimension to the input space. It amplifies the difference between similar odor patterns and optimizes the stimulus representation [27].

2.5 Modeling of the olfactory bulb dynamics

Two basic approaches could be distinguished in the olfactory bulb modeling. One of them deals with the macrodynamics of the whole olfactory bulb, assuming that it works as a dynamical system [10, 27, 13]. The microdynamics approach, instead, studies the dynamics of the local circuits and interactions between mitral cells, interneurons and others OB components [15, 18, 19, 34].

2.5.1 Macrodynamics

Historically, W.Freeman and co-workers [10] were the first to suggest that macrodynamics of the olfactory bulb could be seen in terms of chaotic dynamics. Their experiments with the olfactory bulb of a rabbit support the following concept: When there is no odor applied, the macro state of the olfactory bulb is wandering within a chaotic attractor and this may be seen as the process of the solution search. Applied input (odor) shifts the system to the one of its low-dimensional attractors ("wings") that represent the recognized odor [10]. This concept inspired a number of models of chaotic networks and chaotic neurons [15, 35, 11, 12]

Recently, the idea that one should analyze the olfactory circuit activity in terms of a dynamical systems was developed further. Based on the experimental data on the antennal lobe dynamics [30, 26], it was proposed that the sequences of the spatial activity patterns in the locust antennal lobe can be interpreted and modeled as the state of the system visiting low-dimensional attractors in the specific sequence and that its trajectory is what encodes information [27, 13]. This idea employs the concept of "winnerless competition"': the "winning" attractor of the network's dynamics is unstable, so the global state of the system does not get stuck there forever, but, after being in its vicinity for a while, moves on to another attractor [13]. Such dynamics has been also simulated in a biologically realistic neural circuit [36].

It should be emphasized that this kind of dynamics is completely different from the one of the Hopfield neural networks, where the state is just converging to the energy minimum from the given initial condition. One of the reasons behind it is that in the biological neural circuits input may not be presented by initial conditions as it is in ANN. The input can be assumed rather as a set of the bifurcation parameters that control the system's dynamics [15]. Another idea about global dynamics of the olfactory bulb was developed in [37]. The authors used the Hopfield neural network with non-symmetric weight matrix to reproduce the experimental spatio-temporal dynamics of the antennal lobe [26, 27].

It should be noted that despite the efforts in modeling and theory of the macrodynamics of the olfactory bulb, it is still to be shown that the principles of dynamical systems do indeed apply to the information processing in this system. More experimental data and biologically realistic models are needed to clarify the issue of the encoding with global dynamics in the olfactory bulb.

2.5.2 Dynamics of OB microcircuits

The mitral-granule cell microcircuit is believed to work as a nonlinear oscillator, which is assumed to be the origin of the OB and olfactory cortex oscillations [15, 21]. One of the first models which used coupled nonlinear oscillators to simulate olfactory bulb dynamics was proposed by Li and Hopfield [34]. Their model responded with specific oscillation modes to different odors in accordance to the Freeman experimental data and concepts [10].

The modes of dynamics of a mitral-granule pair of neurons in olfactory bulb was studied in [15]. It was shown that the synaptic strength of lateral (mitral-to-mitral) connection may serve as a bifurcation parameter for the mitral-granule cells oscillator. Different values of synaptic strength produced, via variety of bifurcations, a number of different dynamics: from fixed point and limit cycle to strange attractors and chaos.

Majority of the latest models of olfactory bulb focus on its potential role of segmentation of odor representation into simpler patterns [18, 19, 38]. This idea is based on the the concept of temporal binding and segmentation [39], which is presumably at work in the visual system. The idea is that different components of OB activity could be segregated in time and processed separately.

The modeling efforts have been put recently into studying the phenomenon of transient synchronization in the model of the locust antennal lobe [16]. It was shown that the mechanism behind this phenomenon could be based on the interactions between inhibitory local neurons and excitatory projection neurons, and the competition between inhibitory circuits. However, the mechanism of the transient synchrony and its role in the neural encoding is yet to be clarified.

2.6 Encoding with statistics of the olfactory bulb dynamics

The characteristic feature of the information processing in olfactory system is the transformation of the static odor signature (molecular structure) into the temporal sequence of neural activities [29, 3, 30, 31, 7, 26]. However, the principles of such transformation are unknown.

Most of the computational models reproducing temporal sequences of the olfactory bulb/antennal lobe rely on the different forms of neural competition. The main idea is that different neural ensembles win and loose the mutual competition at different times and, correspondingly, get activated and suppressed in a specific sequence [36, 18, 19, 34, 38].

However, there is an an alternative hypothesis, which links neural encoding with the statistical properties of the spike trains [40]. In this spirit, it was proposed that the odor features (molecules) could be encoded with the probability density function of the interspike intervals produced by the olfactory bulb dynamics [14]. This way the odors are stored as the invariant distribution of the probabilities of the interspike intervals, which corresponds to the one of the the eigenvectors of the transition matrix of associated Markov process. So, the odors are represented by a dynamical system which produces corresponding interspike interval distribution.

This concept may provide certain advantages. The encoding with the statistics of neural dynamics is invariant in time: the information can be read out from any long enough part of the spike train. It may be important, as the brains do not really "know" when exactly the message in the spike train starts and ends.

The idea of encoding with statistics [14] is also supported by the nature of the biological neuron. The neuron is a very unreliable mechanism: there is no strict correlation between

applied stimulus and produced spike train. Thus, neural encoding should be based, at least in part, on the probabilistic, rather than deterministic principles [40].

2.7 Discussion

There has been a significant progress in the studying of the olfactory system recently, but still, some major advances are needed in the experimental measurements and the theoretical approaches to better understand its functioning. Experimental data provides some insights about the role of spatio-temporal patterns of neural dynamics in the olfactory bulb [1, 2, 3, 4, 5, 6, 7], and suggests a role of the neural synchrony in the odor encoding [30, 27, 33, 31, 26].

The first models of the olfactory bulb focused on its global dynamics, applying principles of dynamical systems to the olfactory information processing [10]. These ideas have been developed further in modeling olfactory [27, 13], and other neural circuits [11, 12]. Later, a large body of computational work studied the formation of spatio-temporal patterns [36, 18, 19, 38] and different modes of synchrony [16, 34, 17] in olfactory bulb microcircuits. Principles of recognition of these patterns in the olfactory cortex were also explored [8, 9]. Recently, a new concept suggesting that the olfactory bulb dynamics encodes information by means of its statistics was developed [14].

The large number of theoretical approaches and computational models related to olfactory system points out that, probably, neither of them is capable to explain fully the olfactory system information processing. What restricts them from being conclusive is the general lack of our understanding of some basic principles of functioning of a single neuron, not to mention the large networks. It is not clear what exactly a single neurons does in the brain, and what governs its dynamics and plasticity. So, the future theoretical exploration of olfactory system is expected to evolve in two directions: developing biologically detailed models that reproduce experimentally measured dynamics, and the generation of new concepts about the principles of the global olfactory system dynamics. The cooperation of these approaches should produce a better understanding of the olfactory system dynamics.

Chapter 3

Signal Processing with Temporal Sequences in Olfactory Systems

Living organisms perceive odors as sensations caused by mixtures of odorant molecules. Such molecules excite the olfactory receptors to respond with increased activity which is then passed on to the olfactory bulb for detection. Various odorant molecules excite different groups of receptors. A superposition of these excitations constitute the odor as detected by the olfactory bulb [41]. The relative concentrations of individual components constitute the odor type, whereas the absolute concentrations determine the odor intensity. The olfactory bulb has the task of transforming the input obtained from the receptors into a set of signals to be interpreted by the brain.

The continuous quantities, such as molecule concentrations, cannot be directly represented by the signals produced by biological neurons. Neurons produce spikes and only indirectly their presence or absence, or time location may carry continuum of information. The nature of *neural signals* is assumed to have the following characteristics:

1. There is no significance of the shape of individual spikes. They simply mark instances of time when the neurons fire.

2. The signal is a time sequence of spikes. Spikes may occur more or less frequently which has an effect on the average value of the signal.

3. Spikes may occur in a certain temporal pattern. More precisely, the inter-spike intervals may follow a distinct and repetitive behavior. This allows for code division of information conveyed by a single signal.

4. Two or more signals may exhibit cross-correlation which typically results from synchronization between the signal sources. If the synchronized signals assume a certain spatial distribution, a set of such signals will manifest a spatio-temporal pattern.

The neural signals of the olfactory bulb representing the information about odors and intensities are further interpreted by the brain. The olfactory bulb functions as the first signal processing stage. In all non-biological designs the first stage is responsible for the sensitivity and noise performance of the entire detection system. The same should hold true in case of the olfactory bulb.

The goal of this project is to identify the simplest method of encoding odor information in temporal sequences. The input-output interactions between temporal sequences can lead to an odor detection and encoding mechanism in the olfactory bulb.

3.1 Temporal modulation

The very input of the olfactory system, the epithelium, produces an enormous number of signals. Receptors are hard-wired to detect specific odor components and are uniformly distributed in the epithelium. The odor information is therefore spatially distributed across the epithelium and is assumed to have no temporal dependency. Every odor and concentration can be represented by its "black-and-white photo" in which the gray-levels of pixels encode spiking activities of the receptors. In this paper, the odor information is assumed to be spatially distributed and static, although there is a strong evidence of various significant aspects of the inhale/exhale rhythm and the impulse response of the olfactory bulb [42].

No temporal coding of information is performed by the individual receptors. Simply, the more molecules are present at the docking sites of the receptors, the more frequent their spiking. Based on response measurements and fitting of concentration-response curves presented in [23] and [43], the spiking frequency f of the receptors has an asymptotic dependency on the odorant concentration c (molarity). When the odorant concentration is at the lowest detectable level $c = c_t$, the receptor fires at the very slow rate of spontaneous activity. When the concentration grows infinitely large, the frequency reaches saturation at the maximum firing rate of f_m. The curve $f(c)$ fits the following definition:

$$f = \frac{2}{\pi} f_m \arctan \beta(c - c_t) \tag{3.1}$$

The slope factor β is expressed in terms of the dynamic range Δc defined as the odor concentration at which the frequency reaches 80% maximum, $f(c_t + \Delta c) = 0.8 f_m$. Given the dynamic range, the slope factor can be determined as $\beta = \tan(0.8\pi/2)/\Delta c$.

Concentration c, used in [23] and [43], is a logarithmic quantity related to the odorant molarity $c = \log m$, with m in mol/l. The investigated odorants were anisole, camphor, isoamyle acetate, and limonene, denoted by ANI, CAM, ISO, and LIM, respectively. The curve fitting resulted in the following parameters for each odorant [23]:

	ANI	CAM	ISO	LIM
f_m	11 Hz	15 Hz	11 Hz	8 Hz
c_t	-6.7	-8.6	-7.0	-7.7
Δc	1.1	1.1	0.5	0.3

Remarkably linear curves are obtained if instead of spiking frequency f, the interspike intervals $\tau = 1/f$ are graphed versus the reciprocal of molarity, referred to as *sparsity* s. Since different odorants may have largely different molarity threshold levels $c_t = \log m_t$, the reciprocal of the incremental molarity $s = 1/(m - m_t)$ rather than the absolute value can be used in the joint graph for various odorants. The parametric representation of relationship (3.1) in the new coordinates (s, τ) for the introduced odorants is shown in Fig. 3.1. The horizontal and vertical axes are the incremental sparsity s and the interspike interval τ expressed in terms of molarity

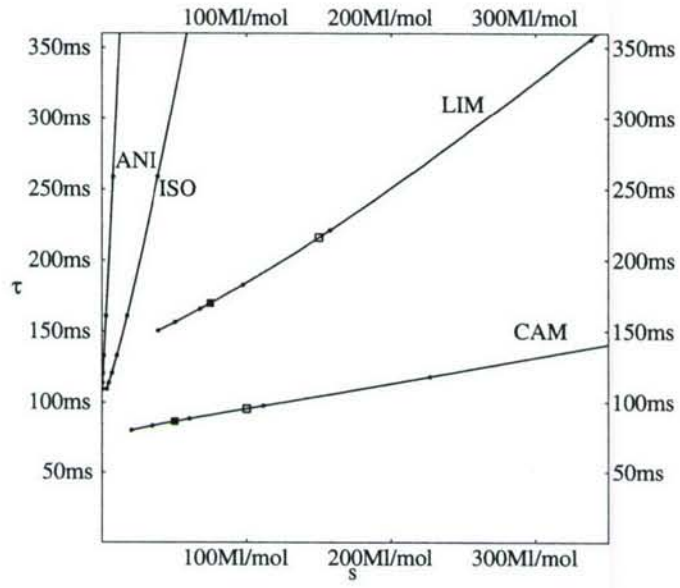

Figure 3.1: Interspike intervals τ of receptor firing versus incremental sparsity s of odorant. Six points on each curve correspond to the following logarithmic concentration levels (left-to-right): $1.2\Delta c$, Δc, $0.8\Delta c$, $0.6\Delta c$, $0.4\Delta c$, and $0.2\Delta c$ above c_t. The axes units are milliseconds (ms) and megaliters per moll (Ml/ mol).

m as follows:

$$s(m) = \frac{1}{m - m_t} \tag{3.2}$$

$$\tau(m) = \left(\frac{2}{\pi} f_m \arctan \beta \log \frac{m}{m_t}\right)^{-1} \tag{3.3}$$

As can be seen in the figure, diluting the odorant in the air increases the interspike intervals at an approximately constant rate. This may be regarded as temporal modulation[1] with the conversion gain $G = \mathrm{d}\tau/\mathrm{d}s$, which is the slope of the line. The left side of each curve corresponds to the receptor saturation region. By extrapolating the curves to the intersections with the vertical axis, a minimum interval τ_0 for each receptor type can be found of value roughly around 100 ms. This minimum interval may be regarded the refractory period of the receptor. With just two parameters τ_0 and G for each receptor type, the temporal modulation illustrated in Fig. 3.1 can be readily described using first-order approximation:

$$\tau = \tau_0 + Gs \tag{3.4}$$

The approximation can be validated only within the dynamic range of the receptor, that is outside the saturation $s > 1/(m_t 10^{\Delta c})$.

3.2 Odor characterization with interspike distributions

An odor is a superposition of a number of basic odorants. The concentration information is temporally modulated at the glomerular inputs of the olfactory bulb, therefore the perception of

[1]Term *temporal modulation* is adopted from [29]

odor intensity must be related to the interspike intervals. Increasing the odor intensity shortens the intervals at different rates for each basic odorant due to the differences in their conversion gains. This provides some explanation why responses of the mitral outputs can be different for the same odor at different intensities [44].

In the glomerular layer the enormous number of inputs converge into much less dimensional connections to the mitral cells. The glomeruli are also highly interconnected between each other via periglomerular interneurons [45]. Both inhibitory and excitatory connections are present within the glomeruli which indicates that a winner-take-all mechanism could be involved before the input to the mitral cells. The presence of such a mechanism would enable arranging of the input interspike intervals into distributions statistically representing the odor information.

Let R be the number of all types of receptors in the epithelium. This makes R also the number of distinct basic odorants, the basis for the odor space. Suppose the first four, out of all R odorants, are the ones shown in Fig. 3.1. An odor at a given intensity can be uniquely represented by a vector $\boldsymbol{s}$ of sparsities of the basic odorants. For instance, an odor created by mixing $0.5\,\mathrm{mol}$ of CAM and $0.75\,\mathrm{mol}$ of LIM with $100\,\mathrm{Ml}$ of air would be represented by vector $\boldsymbol{s} = (\infty, 50, \infty, 75, \infty, \ldots, \infty)\,\mathrm{Ml/\,mol}$. Vector $2\boldsymbol{s}$ would represent the same mixture diluted in twice the amount of air. In general, an odor, as seen by the epithelium, is $\boldsymbol{s} = (s_1, s_2, \ldots, s_R)$. Terms "vector" and "basis" are understood to be suitable ways to arrange numbers rather than the strictly defined terms used in linear spaces.

A much more compressed way to describe odors is through distributions of interspike interval probabilities. This formalism may also be more relevant to the signals presented to the mitral inputs. Let the interspike intervals be quantized into N ranges with cutoff $\tau_{\max}$. Interval $\tau_{\max}$ is considered to be a borderline between evoked and spontaneous activity of the receptors. A single neural signal can represent an odor with the interspike interval τ probability distribution $\boldsymbol{p} = (p_1, p_2, \ldots, p_N)$, which is formally a vector of probabilities:

$$p_n = \begin{cases} \Pr\left(\frac{n-1}{N}\tau_{\max} < \tau \leq \frac{n}{N}\tau_{\max}\right) & \text{if } n < N \\ \Pr\left(\tau_{\max} < \tau\right) & \text{if } n = N \end{cases} \tag{3.5}$$

The quantized representation of the interspike interval distribution is chosen because it is more suitable for numeric computations than the probability density function. A satisfactory approximation of continuum can be achieved provided that N is large enough.

Suppose the $0.5\,\mathrm{mol}$ of CAM and $0.75\,\mathrm{mol}$ of LIM mixture with $100\,\mathrm{Ml}$ of air, indicated by the filled squares in Fig. 3.1, is presented to the olfactory epithelium. Two kinds of receptors would be activated, each responding with spikes separated by roughly $90\,\mathrm{ms}$ intervals and $175\,\mathrm{ms}$ intervals, respectively, according to Fig. 3.1. Suppose also there is twice as many LIM receptors as those detecting CAM. In the winner-take-all competitions, the LIM receptors would have a better chance passing its signal compared to the CAM receptors. The described odor is represented by the filled bars of interspike interval probabilities in Fig. 3.2. The probability of the $175\,\mathrm{ms}$ LIM intervals is twice the probability of the $90\,\mathrm{ms}$ CAM intervals.

Suppose further that the same odor mixture is now diluted in twice the amount of air. This doubles the sparsity of the odor, hence increasing the interspike intervals of both odorants present in the mixture. The diluted odors are represented in Fig. 3.2 by the empty bars of probabilities. Now the LIM intervals are about $220\,\mathrm{ms}$ and the CAM intervals increased to about $100\,\mathrm{ms}$ without a change to the probability levels. Note that the two odorants have different conversion gains and modulate the temporal intervals at different rates. As the odor intensity changes, this

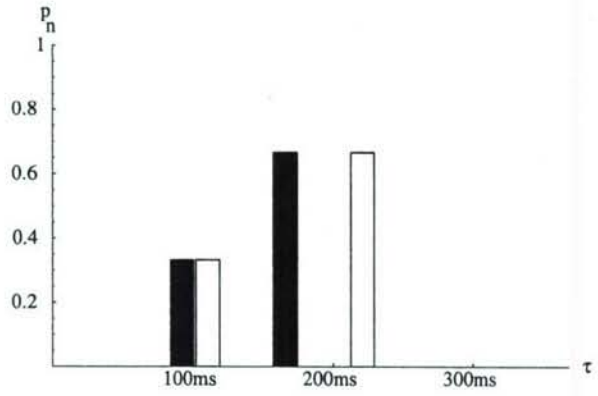

Figure 3.2: Odor composed of 0.5 mol of CAM odorant and 0.75 mol of LIM odorant mixed with 100 Ml of air (filled bars) and then diluted in additional 100 Ml of air (empty bars). The bars have width $\tau_{\max}/N$ and represent probabilities of respective time intervals as defined by (3.5). Example with $N = 20$ and $\tau_{\max} = 350$ ms shown.

changes the probability pattern. A different hypothesis of time advance modulation where the resulting pattern is invariant under the concentration level was introduced in [32] and leads to functional models [9]. However, the neurophysiological evidence suggests that the patterns of bulbar activity actually do change when varying the odor intensity [44].

The signal processing occurring between the mitral cells and glomerular layer is a dynamical process. The information is embedded in the time realizations of signals. It may be retrieved only through observation of these signals for a period of time. The probability distribution of the interspike intervals may be retrieved by statistically analyzing the neural signals. Likewise, a simple stochastic process can be modeled to have the statistical properties representing a given odor through the probability distribution.

Suppose, in steady-state after all the transient response has vanished the odor is represented by the probability distribution $\boldsymbol{p}^*$ defined according to (3.5). A Markov process [46] with the invariant distribution equal $\boldsymbol{p}^*$ could serve as a first order approximation of a dynamical system for that odor. Let $N \times N$ matrix P be the transition matrix of the Markov process

$$\boldsymbol{p}(k+1) = P\boldsymbol{p}(k) \tag{3.6}$$

Also, let the process converge to $\boldsymbol{p}^*$ in a sense that $\boldsymbol{p}^* = \lim_{k\to\infty} \boldsymbol{p}(k)$ for almost every initial distribution $\boldsymbol{p}(0)$. The invariant distribution is the eigenvector of transition matrix P associated with the unit eigenvalue: $\boldsymbol{p}^* = P\boldsymbol{p}^*$. In this respect, the Markov process is a dynamical system in probabilistic space $S = \{\boldsymbol{p} \in [0;1]^N \,|\, \sum_n p_n = 1\}$ with a stable fixed point $\boldsymbol{p}^*$. Further on, space S will be referred to as the odor space.

Consequently, an odor may be associated with an operator $P : S \to S$ in the odor space. The odor itself is the stable fixed point of the operator. There is a benefit of such a representation of odors. Operator P defines an odor indirectly through a definition of a dynamical system. It is easy and natural to generate realizations of neural signals using such operators, which is suitable in the modeling effort. There are many operators that have the same invariant distribution. Hence, the same odor information may be redundantly embedded in many different processes.

Formally, a realization of the introduced Markov process is a sequence of interspike intervals

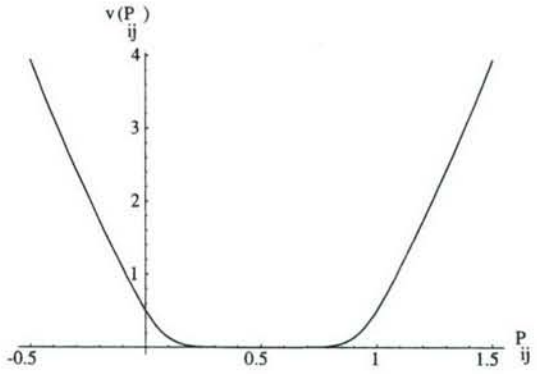

Figure 3.3: Unit segment potential function. In the total cost function, numbers $P_{ij} \in [0;1]$ contribute much less than numbers P_{ij} outside this range. Minimization of w will attract all P_{ij}'s toward the inside of the unit segment.

$\{\tau_k\}$. Define the interval range to be $T_n = [\frac{n-1}{N}\tau_{\max}; \tau_{\max})$ if $n < N$, and $T_N = [\tau_{\max}; \infty)$ otherwise, where the interval range index n is defined in the same manner as in (3.5). For the sake of modeling, through optimization, a particular operator P may be developed to have $\boldsymbol{p}^*$ as its invariant distribution of interspike intervals over time. Denote the elements of the operator by P_{ij}, so that $P = [P_{ij}]$, where i and j are the row and column indices. Number P_{ij} is the probability that in the Markov process (3.6) an interval from the range T_i will follow the interval from the range T_j:

$$P_{ij} = \frac{\Pr(\tau_{k+1} \in T_i \text{ and } \tau_k \in T_j)}{\Pr(\tau_k \in T_j)} \tag{3.7}$$

There is no closed-form formula for selecting P_{ij}'s for a given $\boldsymbol{p}^*$. However, starting with some random P_{ij}'s, an optimization algorithm can be used to find the P_{ij}'s as the minimum of a suitable cost function. Since all P_{ij}'s are probabilities, they must be numbers in the unit segment from 0 to 1. This fact allows for constructing one of the components to be included in the cost function, namely the unit segment potential. For each number P_{ij}, a potential function $v(P_{ij})$, shown in Fig. 3.3 describes how distant P_{ij} is from the unit segment:

$$v(P_{ij}) = \frac{(2P_{ij} - 1)^2}{1 + (2P_{ij} - 1)^{-6}} \tag{3.8}$$

Function v attains the minimum in the middle of the unit segment and is maximally flat within the segment. The maximally flat approximation [47] with a rational function is chosen to facilitate the optimization process. The partial costs $v(P_{ij})$ sum up to the cost function component $E_v(P)$ responsible for keeping all the entries of P within the unit segment:

$$E_v(P) = \sum_{i=1}^{N}\sum_{j=1}^{N} v(P_{ij}) \tag{3.9}$$

Operator P is a probabilistic matrix in a sense that all its column vectors are normalized probability distributions. Therefore, the column sums of P must sum up to 1. Another cost function component $E_c(P)$ measures the deviation from this requirement:

$$E_c(P) = \sum_{j=1}^{N}\left(1 - \sum_{i=1}^{N} P_{ij}\right)^2 \tag{3.10}$$

Operator P is a well defined transition matrix of Markov process (3.6) if $E_v(P) + E_c(P) = 0$. The goal of the optimization procedure is to develop operator P with the constraint that $\boldsymbol{p}^*$ is it's principal eigenvector associated with eigenvalue 1. To simplify the operator synthesis, matrix P will be assumed to be diagonalizable: $P = B\Lambda B^{-1}$. The diagonal matrix $\Lambda = \text{diag}(\boldsymbol{\lambda})$ is composed of N eigenvalues $\boldsymbol{\lambda} = (\lambda_1, \lambda_2, \ldots, \lambda_N)$ of P. Let $\lambda_1 = 1$. The convergence rate of the dynamical system (3.6) heavily depends on the radius of the remaining λ_i's for $i > 1$. Operator P is synthesized with random λ_i's, for $i > 1$, with the assumption that $|\lambda_i| < r < 1$ and the radius r is kept low to improve the convergence rate. In the numerical experiment r was selected to be equal to 0.2. Operator P is diagonal in the basis constructed with the column vectors of B. Since $\lambda_1 = 1$, the first column vector of B is $\boldsymbol{p}^*$. More precisely, $B_{ij} = p_i^*$ for $j = 1$. All other entries B_{ij}, for $j > 1$, are variables in the optimization process. Their initial values are selected randomly from the uniform distribution in the range $(-1; 1)$. Final matrix B is found using an optimization algorithm to minimize the cost function as in the following expression:

$$\min_{B_{ij}|_{j>1}} \left[E_v(P) + E_c(P)\right] \tag{3.11}$$

The minimized solution oftentimes needs a final touch to make sure that P has no negative entries, no entries greater than one and that column sums of P are indeed 1. This can be done by zeroing of negative values and normalization of columns. The principal eigenvector of P is not very sensitive to such trimming of P. Software package MATRIX has been developed (See Section 5.1) in order to generate a probabilistic matrix according to the principles described in this section.

3.3 Embedding distributions in temporal sequences

As illustrated in the example shown in Fig. 3.2, the probabilistic representation of odors and intensities fits well the random nature of excitations received from the olfactory epithelium. The Markov model is also a natural candidate for a simple approximation of the dynamics behind spike interactions driven by the receptors. The olfactory bulb, however, should be considered a deterministic system which has no random variables other than the input received from the epithelium. Moreover, the olfactory bulb is capable of self-excitatory activity in response to the input. This may be the factor contributing to both high sensitivity and high selectivity of the sense of smell [48]. From this perspective, it seems reasonable to regard the olfactory bulb as an active medium rather than a passive relay of receptor signals. The olfactory bulb actively produces firing activity in response to the receptor signals [49].

A sequence of interspike intervals complying with a given interval distribution can be generated in a deterministic dynamical system. The simplest such system is a one-dimensional map constructed by solving the inverse Frobenius-Perron problem [50]. The overall goal of the search for a sequence generator is to be able to represent the odor information by a distribution of interspike intervals. A simple shift-map can be constructed directly from the probabilistic operator used in approximation (3.6), as described in detail in [51].

First, a piece-wise linear map $f : [0; N] \to [0; N]$, $[0; N] \subset R$ is derived from probabilities included in the operator P:

$$f(x) = \frac{1}{P_{ij}} \left(x - j + \sum_{m=1}^{i} P_{mj} \right) + N - i, \quad \text{if} \quad j - \sum_{m=1}^{i} P_{mj} \leq x < j + P_{ij} - \sum_{m=1}^{i} P_{mj} \tag{3.12}$$

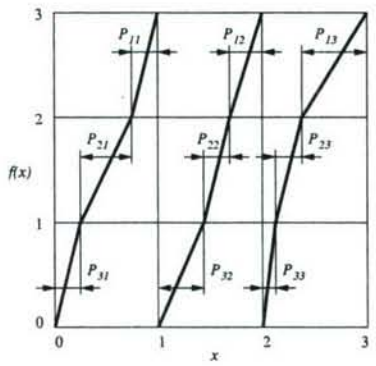

Figure 3.4: Example of a piece-wise linear shift map $f(x)$. Function f is composed of N continuous branches $f_j : [j-1; j) \to [0; N]$. If x is chosen randomly from the uniform distribution over the range $(0; N)$, the conditional probability P_{ij} that $f(x) \in (i-1; i)$ given the fact $x \in (j-1; j)$ can be evaluated by $P_{ij} = ||f_j^{-1}([i-1; i])||$. Example with $N = 3$ shown.

As shown in Fig. 3.4, map f is composed of N^2 linear segments corresponding to N^2 numbers P_{ij}. The slopes of the segments are simply $1/P_{ij}$. To evaluate $f(x)$, the pair of indices i and j appropriate for a given x needs to be identified using the condition provided by (3.12).

By scaling the domain and range of map f, the dynamical system generating temporal sequence $\{\tau_k\}$ can be defined with the help of shift map h:

$$h(\tau) = \frac{\tau_{\max}}{N-1} f\left(\frac{N-1}{\tau_{\max}}\tau\right) \tag{3.13}$$

Regardless of the initial condition chosen, subsequent mappings with h will determine sequence $\{\tau_k\}$ whose distribution of values converges to the invariant distribution of process (3.6). A deterministic dynamical system

$$\tau_{k+1} = h(\tau_k) \tag{3.14}$$

may be regarded as a generator of realizations of neural signals for a given distribution of interspike intervals.

A numeric example of shift-map synthesis is shown in Fig. 3.5. Three interspike interval distributions $\boldsymbol{p}_A^*$, $\boldsymbol{p}_B^*$, and $\boldsymbol{p}_C^*$ are selected randomly to characterize three hypothetical odors A, B, and C. The bars represent probabilities p_n of respective time intervals as defined by (3.5). The horizontal axis is normalized such that interval $N\tau_{\max}/(N-1)$ corresponds to 1. Shift-maps h_A, h_B, and h_C are evaluated for the example odors and shown in the middle row of figures also in time-normalized coordinates. The maps have N disconnected branches, however, vertical lines connecting the branches are added to enhance the graphs. Starting with a random initial interval, each map iterated 3000 times according to (3.14) produced a temporal sequence. The sequences are shown in the bottom row of figures. Each interval in a sequence is indicated as a point whose vertical coordinate is the normalized time. This way the density of points reflects the original distribution plots if rotated clockwise by 90°.

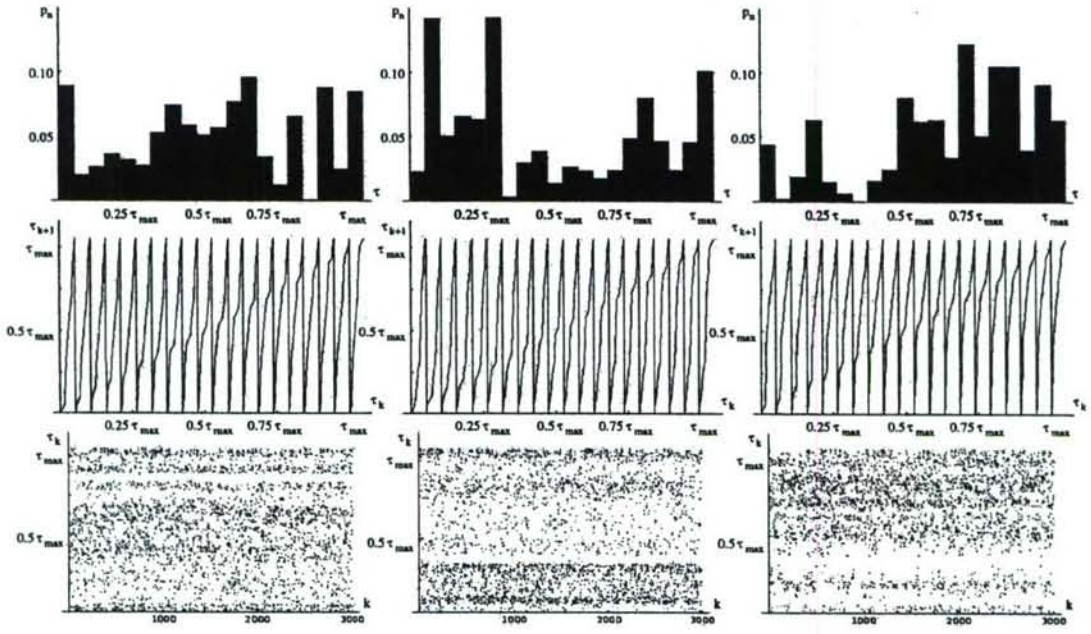

Figure 3.5: Synthesis of temporal sequence generators. Three example interspike interval distributions with $N = 20$ representing three different odors are shown in the top row. The corresponding shift-maps and distributions of values of generated temporal sequences are shown underneath. The time interval axes are normalized to the range of $(0; 1)$. Each graph in the bottom row contains 3000 points representing interspike intervals placed vertically according to the length of the interval.

3.4 Frobenius filter for temporal sequences

It is broadly accepted that the olfactory bulb provides support for a pattern recognition mechanism for odor detection and classification. Not all of the recognition is taking place there, but definitely the process is initiated in the olfactory bulb. Assuming that the temporal sequences of interspike intervals are carriers for the odor information, an implementation of signal processing system (3.14) can be proposed. Ultimately, the goal is to demonstrate usefulness of the proposed mechanism in odor recognition.

The proposed signal processing scheme is shown in Fig. 3.6 and will be referred to as the Frobenius filter. The input to the filter is a temporal sequence whose interspike intervals are determined by the random variable τ_{in} with values governed by the probability distribution $\boldsymbol{p}_{\text{in}}$ defined as in (3.5). Distribution $\boldsymbol{p}_{\text{in}}$ characterizes an odor.

The Frobenius filter is simply a shift-map with the feedback loop controlled by a random switch. The switch operation is described by a two-valued stochastic process $\xi : \{0,1\} \times N \to R$. The filter is producing time intervals based on the switch position. At every interval k, the switch position depends on the value of ξ_k governed by probabilities:

$$\Pr(\xi_k = 1) = c \tag{3.15}$$

$$\Pr(\xi_k = 0) = 1 - c \tag{3.16}$$

where $c \in [0;1]$ is a constant parameter. When this is the case, the filter is receiving the input τ_{in}. The opposite position of the switch lets the shift-map determine the output time interval based on the previous interval as in (3.14). The overall filter equation reads:

$$\tau_{k+1} = h\big[\xi_k \tau_{\text{in}} + (1 - \xi_k)\tau_k\big] \tag{3.17}$$

The notion of the switch is an attempt to model a competition between the input and the feedback. Its random operation is inherited from the random nature of the input temporal sequence.

The three shift-maps h_A, h_B, and h_C, introduced in Fig. 3.5, are used to illustrate the function of the Frobenius filter. Each of the shift-maps was stimulated at the input by values generated by probability distributions $\boldsymbol{p}_A^*$, $\boldsymbol{p}_B^*$, and $\boldsymbol{p}_C^*$ representing three different odors. Figure 3.7 shows all possible input-filter combinations arranged in the following nine pairs:

$$\begin{array}{lll} (\boldsymbol{p}_A^*, h_A) & (\boldsymbol{p}_B^*, h_A) & (\boldsymbol{p}_C^*, h_A) \\ (\boldsymbol{p}_A^*, h_B) & (\boldsymbol{p}_B^*, h_B) & (\boldsymbol{p}_C^*, h_B) \\ (\boldsymbol{p}_A^*, h_C) & (\boldsymbol{p}_B^*, h_C) & (\boldsymbol{p}_C^*, h_C) \end{array} \tag{3.18}$$

In each instance, $K = 20000$ values random values τ_{in} were drawn from the input distribution and applied with probability $c = 0.5$ to the filter. The values drawn were also sorted in the ascending

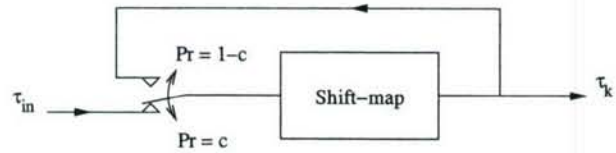

Figure 3.6: Frobenius filter is a shift-map with input. Either the input interval τ_{in} or the present output interval τ_k is transformed into the next output interval τ_{k+1}.

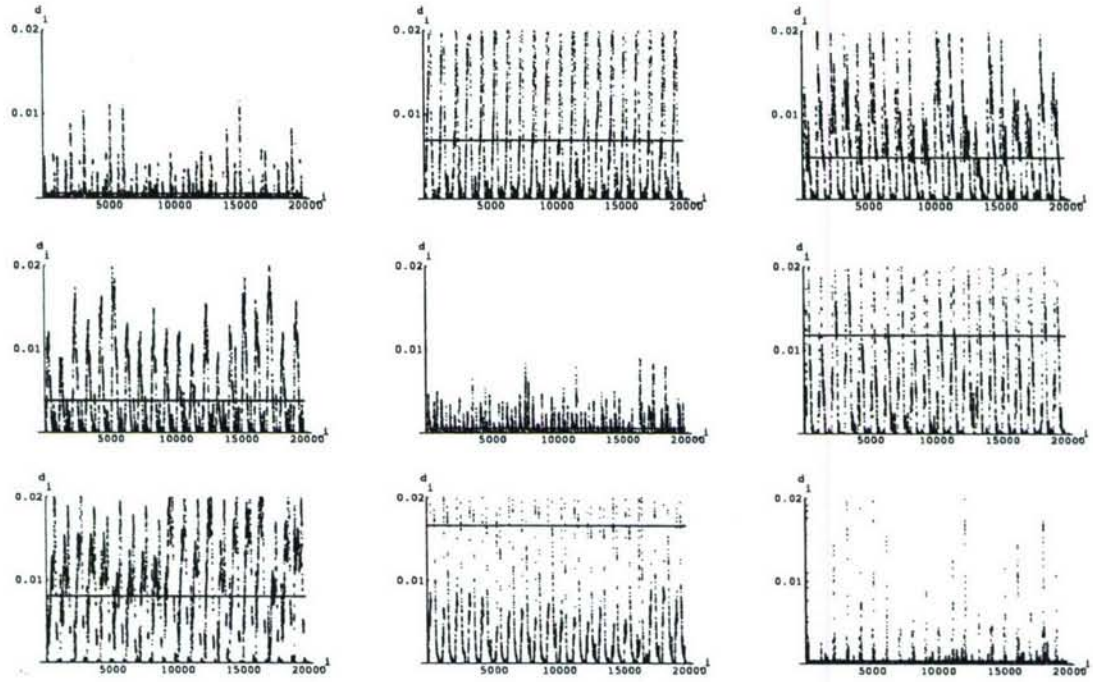

Figure 3.7: Nine instances of a Frobenius filter stimulated by an input distribution for 20000 iterations. Quadratic distance $d_i = (u_i - t_i)^2$ between cumulative distributions of interspike intervals at the input u_i and output t_i of the filter shown. The graphs are arranged according to (3.18).

order and stored. In the sorted input sequence $\{u_i\}$ the following property holds: $i < j \Rightarrow u_i \leq u_j$. When plotted, the graph of the sorted sequence would resemble the shape of the cumulative distribution function of the random variable τ_{in}.

The realization of the sequence $\{\tau_k\}$ generated by the Frobenius filter for K iterations were also sorted in the same manner. The sorted output sequence $\{t_i\}$ was then compared to the sorted input sequence in Fig. 3.7. More precisely, the graphs in the figure are the sequences of quadratic distances $\{(u_i - t_i)^2\}$ in each of the nine instances. The horizontal line is the mean square value of the distance $\overline{(u_i - t_i)^2}$. As seen in the figure, the input-output sequences generated in pairs $(\boldsymbol{p}_A^*, h_A)$, $(\boldsymbol{p}_B^*, h_B)$, and $(\boldsymbol{p}_C^*, h_C)$ are synchronized in a sense that the quadratic distance between input and output interval distributions is small. The distances in all the other pairs are significantly larger. By detecting low distance between the input and the output of the filter, an odor recognition mechanism can be devised.

Two examples of realizations of the input and output temporal sequences are shown in Fig. 3.8 and Fig. 3.9. The proposed mechanism uses a pattern matching phenomenon which signals successful detection as a decreased distance between parameters of the input and the output neural signals. The pattern matching is not based on coherence of the two signals. As shown in the figures, no similarity in realizations of the input and the output can be observed in either the matched or unmatched odor-filter pairs. In case of the matched pair, the similarity is in the statistical properties of the input and the output signals.

Figure 3.8: Realizations of the input (top) and output (bottom) temporal sequences for a matched pair $(\boldsymbol{p}_A^*, h_A)$. A fragment containing 100 spikes shown.

Figure 3.9: Realizations of the input (top) and output (bottom) temporal sequences for unmatched matched pair $(\boldsymbol{p}_B^*, h_A)$. A fragment containing 100 spikes shown.

3.5 Discussion

The details of how the cells of the olfactory bulb could encode the information in the way described in this project are not discussed here. The goal set for this work was to describe the simplest method of encoding information in temporal sequences and show the input-output interactions which can lead to an odor detection and encoding mechanism. All the computations are very simple. No memory is necessary, only the last time interval is locally kept in the evaluation of the next time interval in the output sequence. Actual neurons are capable of performing such a storage with their inherent leaky integration.

The shapes of the shift-maps shown in Fig. 3.5 are not crucial for in the operation of the Frobenius filters. The proposed shapes are just samples of infinite possibilities chosen for mathematical simplicity. In fact, any mapping that is mixing and expanding [52] can be used in the Frobenius filter. Such mappings develop continuous invariant distributions and guarantee ergodicity of the temporal sequence in a sense that the invariant distribution is reachable from any initial condition. Temporal sequences at the output of the filter have a very strong ability of encoding information in the time scale. It is sufficient to isolate just a few consecutive spikes to be able to identify the shift-map which generated the spikes and effectively identify the encoded odor.

How exactly the proposed encoding concept may be implemented in a biological neural circuit is not directly addressed here. However, it would be an intriguing subject for a possible future research. A circuit of integrate-and-fire neurons can be designed to produce spike trains with controlled interspike interval statistics. The software GENERATOR developed for these simulations is presented later in Section 5.2.

4. References

[1] R. W. Friedrich and S. I. Korsching, "Combinatorial and chemotopic odorant coding in the zebrafish olfactory bulb visualized by optical imaging," *Neuron*, vol. 18, pp. 737–752, 1997.

[2] J. Joerges, A. Kuttner, C. G. Galizia, and R. Menzel, "Representations of odour mixtures visualized in the honeybee brain," *Nature*, vol. 387, no. 6630, pp. 285–288, 1997.

[3] J. S. Kauer, "On the scent of smell in the salamander," *Nature*, vol. 417, pp. 336–342, 2002.

[4] M. Meister and T. Bonhoeffer, "Tuning and topography in an odor map in the olfactory bulb," *The Journal of Neuroscience*, vol. 21, no. 4, pp. 1351–1360, 2001.

[5] K. Mori and G. M. Shepherd, "Emerging principles of molecular signal processing by mitral/tufted cells in the olfactory bulb," *Semin. Cell Biol.*, vol. 5, no. 1, pp. 65–74, 1994.

[6] K. Ressler, S. Sullivan, and L. Buck, "Information coding in the olfactory system: Evidence for a stereotyped and highly organized epitope map in the olfactory bulb," *Cell*, vol. 79, pp. 1245–1255, 1994.

[7] H. Spors and A. Grinvald, "Spatio-temporal dynamics of odor representations in the mammalian olfactory bulb," *Neuron*, vol. 34, no. 2, pp. 301–315, 2002.

[8] M. Lysetskiy, A. Lozowski, and J. M. Zurada, "Temporal-to-spatial dynamic mapping, flexible recognition, and temporal correlations in olfactory cortex model," *Biological Cybernetics*, vol. 87, no. 1, pp. 58–67, 2002.

[9] M. Lysetskiy, A. Lozowski, and J. M. Zurada, "Invariant recognition of spatio-temporal patterns in the olfactory system model," *Neural Processing Letters*, vol. 15, pp. 225–234, June 2002.

[10] W. Freeman, "Strange attractors that govern mammalian brain dynamics shown by trajectories of electroencephalographic (EEG) potential," *IEEE Transactions on Circuits and Systems*, no. 35, pp. 781–783, 1988.

[11] M. Lysetskiy, J. M. Zurada, and A. G. Lozowski, "Bifurcation-based neural computation," in *Proc. of the International Joint Conference on Neural Networks*, vol. 3, (Honolulu, HI), pp. 2716–2720, May 12–17, 2002.

[12] M. Lysetskiy and J. M. Zurada, "Bifurcating neuron: Computation and learning." *Neural Networks*, 17(2): 225-232, 2004.

[13] M. Rabinovich, A. Volkovskii, P. Lecanda, R. Huerta, H. Abarbanel, and G. Laurent, "Dynamical encoding by network of competing neuron groups: Winnerless competition," *Physical Review Letters*, vol. 87, 2001.

[14] A. G. Lozowski, M. Lysetskiy, and J. M. Zurada, "Signal processing with temporal sequences in olfactory systems." *IEEE Transactions on Neural Networks*, vol. 15, no. 5, pp. 1268–1275, 2004.

[15] P. Erdi, T. Grobler, G. Barna, and K. Kaski, "Dynamics of the olfactory bulb: bifurcations, learning, and memory," *Biological Cybernetics*, vol. 69, no. 1, pp. 57–66, 1993.

[16] M. Bazhenov, M. Stopfer, M. Rabinovich, R. Huerta, H. Abarbanel, T. Sejnowski, and G. Laurent, "Model of transient oscillatory synchronization in the locust antennal lobe," *Neuron*, vol. 30, pp. 553–567, 2001.

[17] M. Lysetskiy, A. G. Lozowski, and J. M. Zurada, "Neural encoding with transient synchronization in olfactory system," in *Computational Neuroscience Meeting*, (Chicago, Illinois), Jul. 21–25, 2002.

[18] O. Hendin, D. Horn, and J. Hopfield, "Decomposition of a mixture of signals in a model of the olfactory bulb," *Proceedings of the National Academy of Sciences*, vol. 91, no. 13, pp. 5942–5946, 1994.

[19] O. Hoshino, Y. Kashimori, and T. Kambara, "An olfactory recognition model based on spatiotemporal encoding of odor quality in the olfactory bulb," *Biological Cybernetics*, vol. 79, no. 2, pp. 109–120, 1998.

[20] K. Mori, H. Nagao, and Y. Yoshihara, "The olfactory bulb: Coding and processing of odor molecule information," *Science*, vol. 286, no. 5540, pp. 711–715, 1999.

[21] G. M. Shepherd and C. A. Greer, "Olfactory bulb," in *The synaptic organization of the brain* (G. M. Shepherd, ed.), pp. 159–204, New York: Oxford University Press, 1998.

[22] P. Wise, J. Mats, and S. William, "Quantification of odor quality," *Chemical Senses*, vol. 25, pp. 429–443, 2000.

[23] J. P. Rospars, P. Lansky, P. Duchamp-Viret, and A. Duchamp, "Spiking frequency versus odorant concentration in olfactory receptor neurons," *BioSystems*, vol. 58, pp. 133–141, 2000.

[24] G. Laurent, "A systems perspective on early olfactory coding," *Science*, vol. 286, no. 5440, pp. 723–728, 1999.

[25] G. Laurent, M. Wehr, and H. Davidowitz, "Temporal representations of odors in an olfactory network," *Journal of Neuroscience*, vol. 16, no. 12, pp. 3837–3847, 1996.

[26] M. Wehr and G. Laurent, "Odour encoding by temporal sequences of firing in oscillating assemblies," *Nature*, vol. 384, no. 6630, pp. 162–166, 1996.

[27] G. Laurent, M. Stopfer, R. Friedrich, M. I. Rabinovich, A. Volkovskii, and H. Abarbanel, "Odor encoding as an active, dynamical process: Experiments, computation and theory," *Annual Review in Neuroscience*, vol. 24, pp. 263–297, 2001.

[28] T. Kohonen, "The self-organizing map," *Neurocomputing*, vol. 21, pp. 1–6, 1998.

[29] R. W. Friedrich and G. Laurent, "Dynamic optimization of odor representations by slow temporal patterning of mitral cell activity," *Science*, vol. 291, pp. 889–894, Feb. 2001.

[30] G. Laurent, "Dynamical representation of odors by oscillating and evolving neural assemblies," *Trends in Neuroscience*, vol. 19, pp. 489–496, 1996.

[31] M. Stopfer, S. Bhagavan, B. Smith, and G. Laurent, "Impaired odor discrimination on desynchronization of odor-encoding neural assemblies," *Nature*, vol. 390, pp. 70–74, 1997.

[32] J. Hopfield, "Pattern recognition computation using action potential timing stimulus representation," *Nature*, vol. 376, pp. 33–36, 1995.

[33] K. MacLeod and G. Laurent, "Distinct mechanisms for synchronization and temporal patterning of odor-encoding neural assemblies," *Science*, vol. 274, no. 5289, pp. 976–979, 1996.

[34] A. Li and J. J. Hopfield, "Modeling the olfactory bulb and its neural oscillatory processing," *Biological Cybernetics*, vol. 61, no. 5, pp. 379–392, 1989.

[35] W. Freeman, R. Kozma, and P. Werbos, "Biocomplexity: adaptive behavior in complex stochastic dynamical systems," *Biosystems*, vol. 59, pp. 109–123, 2001.

[36] M. Bazhenov, M. Stopfer, M. Rabinovich, H. Abarbanel, T. Sejnowski, and G. Laurent, "Model of cellular and network mechanisms for odor-evoked temporal patterning in the locust antennal lobe," *Neuron*, 2001.

[37] B. Quenet, D. Horn, G. Dreyfus, and R. Dubois, "Temporal coding in an olfactory oscillatory model," *Neurocomputing*, vol. 38–40, pp. 831–836, 2001.

[38] Z. Li and J. Hertz, "Odour recognition and segmentation by coupled olfactory bulb and cortical networks," *Neurocomputing*, vol. 26–27, pp. 789–794, 1999.

[39] C. Marlsburg, "The what and why of binding: The modeler's perspective," *Neuron*, vol. 24, pp. 95–104, 1992.

[40] F. Rieke, D. Warland, R. R. Steveninck, and W. Bialek, *Spikes*. Cambridge, Massachusetts: MIT Press, 1997.

[41] T. A. Dickinson, J. White, J. S. Kauer, and D. R. Walt, "Current trends in 'artificial-nose' technology," *Trends in Biotechnology*, vol. 16, pp. 250–258, Jun 1998.

[42] J. S. Kauer, "Real-time imaging of evoked activity in local circuits of the salamander olfactory bulb," *Nature*, vol. 331, pp. 166–168, Jul 1988.

[43] J. P. Rospars, P. Lansky, P. Duchamp-Viret, and A. Duchamp, "Characterizing and modeling concentration-response curves of olfactory receptor cells," *Neurocomputing*, vol. 38–40, pp. 319–325, 2001.

[44] J. White, K. A. Hamilton, S. R. Neff, and J. S. Kauer, "Emergent properties of odor information coding in a representational model of the salamander olfactory bulb," *Journal of Neuroscience*, vol. 12, pp. 1772–1780, May 1992.

[45] J. S. Kauer, "Contributions of topography and parallel processing to odor coding in the vertebrate olfactory pathway," *Trends in Neurosciences*, vol. 14, pp. 79–85, Feb 1991.

[46] A. G. Lozowski and B. L. Noble, "Processing temporal sequences," in *Proc. of the 45th Midwest Symposium on Circuits and Systems (MSCAS'02)*, vol. 1, (Tulsa, Oklahoma), pp. 180–183, Aug. 4–7, 2002.

[47] A. Budak, *Passive and active network analysis and synthesis*. Waveland Press, 1991.

[48] T. A. Dickinson, J. White, J. S. Kauer, and D. R. Walt, "A chemical-detecting system based on a cross-reactive optical sensor array," *Nature*, vol. 382, pp. 697–700, 22 Aug 1996.

[49] J. White, T. A. Dickinson, D. R. Walt, and J. S. Kauer, "An olfactory neuronal network for vapor recognition in an artificial nose," *Biological Cybernetics*, vol. 78, pp. 245–251, Apr 1998.

[50] E. M. Bollt, "Controlling chaos and the inverse frobenius-perron problem: Global stabilization of arbitrary invariant measures," *Int. Journal of Bifurcation and Chaos*, vol. 10, no. 5, pp. 1033–1050, 2000.

[51] D. Pingel, P. Schmelcher, and F. K. Diakonos, "Theory and examples of the inverse Frobenius-Perron problem for complete chaotic maps," *Chaos*, vol. 9, no. 2, pp. 357–366, 2000.

[52] G. Mazzini, R. Rovatti, and G. Setti, "Chaos-based DS-CDMA:Introduction. Some tools for studying chaos with densities." Winter School in Chaotic Communications, University of California in San Diego, Jan. 23–26, 2000.

Chapter 5

Appendix

5.1 MATRIX User Manual

This software generates a transition matrix of Markov process. The optimization technique produces a corresponding operator **A** with a target principal eigenvector **v** associated with eigenvalue 1.

MATRIX Installation

1. Copy all files into an arbitrarily selected directory e.g. `C:/MATLAB/MATRIX`.
2. Launch MATLAB.

File list:

```
colwise.m
cost.m
DiagonalMatrix.m
eigv.m
formA.m
penalty.m
vector.m
Umin.m
```

MATRIX Tutorial

Task:
Use the MATRIX algorithm to generate matrix **A** with a target principal eigenvector **v** associated with eigenvalue 1.

Solution:

Step 1. Choose the matrix size N:

```
>> N=20;
```

Step 2. Define global variables:

```
>> global v e
```

Step 3. Store the target eigenvector **v** and the array of target eigenvalues **e**:

```
>> v=vector(N)
>> e=eigv(N)
```

Step 4. Define initial matrix **U**:

```
>> U=rand(N,N-1)
```

Step 5. Optimize initial matrix **U**:

```
>> Uopt=Umin(U)
```

Step 6. Generate target matrix **A**:

```
>> A=formA(v,e,Uopt)
```

Step 7. Save matrix **A** to the file "matrixA".

```
>> save matrixA A -ASCII
```

MATRIX Function Reference

The following function prototypes are provided for the advanced user. These prototypes are useful to the programmer if additional features are to be added to the software.

`colwise.m`
USAGE: `colwise(m)`
Evaluates the quadratic distance between 1 and the column sum, for each of the columns **m** of the matrix **A**.

`cost.m`
USAGE: `cost(U)`
Matrix cost function, which defines the optimization process of the matrix **A**.

`DiagonalMatrix.m`
USAGE: `DiagonalMatrix(e)`
Creates a diagonal matrix with specified column of eigenvalues **e** on its diagonal.

`eigv.m`
USAGE: `eigv(N)`
Creates a column of eigenvalues **e** of dimension N, where the first one is equal to 1 and the rest are equal to 0.2.

`formA.m`
USAGE: `formA(v,e,U)`
Creates matrix **A** with specified eigenvectors **v** and corresponding eigenvalues **e**.

`penalty.m`
USAGE: `penalty(x)`
Penalty function imposing constraints on the matrix **A**.

`vector.m`
USAGE: `vector(N)`
Creates a random normalized vector of dimension N

`Umin.m`
USAGE: `Umin(U)`
Optimizes the initial matrix **U** in order to create matrix **A** with minimal cost function.

The code of the corresponding files can be downloaded from:
http://ci.uofl.edu/currentwork/lozowski/depscor01/report.final/MATRIX/

5.2 GENERATOR User Manual

GENERATOR Tutorial

This software generates a transition matrix of Markov process. The optimization technique produces a corresponding operator **A** with a target principal eigenvector **v** associated with eigenvalue 1.

GENERATOR Installation

1. Copy all files into an arbitrarily selected directory e.g. `C:/MATLAB/GENERATOR`.
2. Launch MATLAB.

File list:

```
diagr.m
filter1.m
isi.m
prob.m
```

GENERATOR Tutorial

Task:
Use the GENERATOR algorithm to produce a spike train with the input-controlled interspike interval distribution.

Solution:

Step 1. Set an example input pattern: **Input5**=[0.41, 0.28, 0.41, 0.31, 0.34]:

```
>> Input5=[0.41; 0.28; 0.41; 0.31; 0.34];
```

Step 2. Evaluate and plot the normalized input pattern **Input5norm**:

```
>>Input5norm = Input5/sum(Input5)
ans =
    0.2343
    0.1600
    0.2343
    0.1771
    0.1943

>> bar(Input5norm)
```

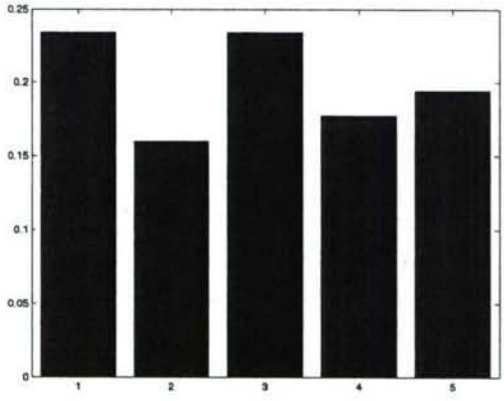

Step 3. Generate the corresponding spike train **train** of the length **T** seconds

```
>> T=10;
>> train=prob(T,Input5);
```

Step 4. Plot the diagram of the interspike interval distribution of the generated spike train:

```
>> bar(diagr(train,Input5))
```

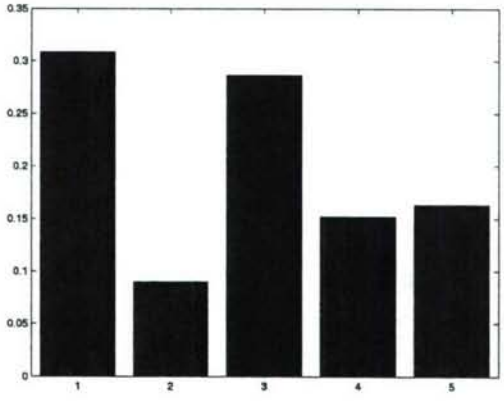

GENERATOR Function Reference

The following function prototypes are provided for the advanced user. These prototypes are useful to the programmer if additional features are to be added to the software.

`prob.m`
USAGE: `prob(T,Input5)`
Creates a spike train of length T, controlled by the input vector **Input5**. In the output array the "1" and "0" represent, respectively, the presence or absence of a spike in a 1ms interval.

`isi.m`
USAGE: `isi(train)`
Produces an array of the interspike intervals of the spike train **train** created by the *prob.m* function.

`diagr.m`
USAGE: `diagr(train,Input)`
Creates the diagram of the probabilities of occurrence of the the corresponding interspike intervals in the generated spike train **train** controlled by the input pattern **Input**.

`filter1.m`
USAGE: `filter1(u)`
Realizes the winner-take-all competition: limits the number of firing neurons in the neuron array **u** during one cycle to one.

The code of the corresponding files can be downloaded from:
http://ci.uofl.edu/currentwork/lozowski/depscor01/report.final/GENERATOR/

5.3 List of Published Papers

Journal Papers

Lysetskiy M, Lozowski A, and Zurada JM, "Temporal-to-spatial dynamic mapping, flexible recognition and temporal correlations in olfactory cortex", Biological Cybernetics, 87(1):58-67, 2002.

Lysetskiy M, Lozowski A, Zurada, JM, "Invariant Recognition of Spatio-temporal Patterns in the Olfactory System Model", Neural Processing Letters, 15(3):225-234, 2002.

Lozowski A.G., Lysetskiy M., and Zurada J.M., "Signal Processing with Temporal Sequences in Olfactory System", IEEE Transactions on Neural Networks, vol.15, No.5, September 2004, pp.1268-1275

Lysetskiy M and Zurada JM, "Bifurcating neuron: Computation and Learning", Neural Networks, 17(2): 225-232, 2004.

Conference Papers Published in Proceedings

Lysetskiy M, Zurada, J.M., Temporal Binding, Segmentation and Attention Focusing in the Olfactory Model, Proc. International Joint Conference on Neural Networks, pp.1095-1100, Washington, D.C., July 16-19, 2001.

Lozowski A.G. and Noble B.L., Processing temporal sequences, Proc. of the 45th Midwest Symposium on Circuits and Systems, vol. 1, (Tulsa, Oklahoma), pp. 180-183, Aug. 4-7, 2002.

Lysetskiy M, Zurada, JM., Lozowski, A., Bifurcation-based Neural Computation, Proc. of the International Joint Conference on Neural Networks, pp. 2716-2720, Honolulu, Hawaii, May 12-17, 2002

Hemachand Narem, Zurada, JM., Lozowski, A., Simulation of Pulse Distibution Observed in Olfactory Bulb, Proc. of the Artificial Neural Networks in Engineering (ANNIE 2004) Conference, St. Louis, Missouri, November 7-10, 2004, pp.791-799

Progress Report

Zurada JM, Lozowski AG, Modeling of Spatial and Temporal Dynamics in Biological Olfactory Systems, Presentation at ONR, April 8, 2004, 20pp (in landscape format)

Other Conference Presentations

Lysetskiy M, Lozowski A, Zurada, JM., "Invariant Recognition of Spatio-temporal Patterns in the Olfactory System Model", Fifth International Conference on Cognitive and Neural Systems, Boston, Mass., 2001

Lysetskiy M, Zurada, JM, Synaptic balancing guided by spike-timing-dependent plasticity in olfactory cortex model, Neural Information and Coding Workshop (NICW), Snowbird, Utah, 2003

Lysetskiy M., Lozowski A.G., and Zurada J.M., "Neural Dynamics: Encoding with Chaos and Statistics", Ninth Annual Kentucky EPSCoR Conference, Lexington, Kentucky, Abstract no. 54, May 12, 2003

Lysetskiy M., Zurada, J.M., "Possibility of synaptic balancing and spike-timing-dependent synap-

tic plasticity in the olfactory cortex", Seventh International Conference on Cognitive and Neural Systems, Abstract no. 13, p. 95, Boston, Mass., May 29-31, 2003

Chapter 6

Papers

Biol. Cybern. 87, 58–67 (2002)
DOI 10.1007/s00422-002-0319-0

Biological Cybernetics

Temporal-to-spatial dynamic mapping, flexible recognition, and temporal correlations in an olfactory cortex model

Mykola Lysetskiy[1], Andrzej Lozowski[2], Jacek M. Zurada[1]

[1] Department of Electrical and Computer Engineering, University of Louisville, Louisville, KY 40292, USA
[2] Department of Electrical and Computer Engineering, Southern Illinois University at Edwardsville, Edwardsville, IL, USA

Received: 16 October 2001 / Accepted in revised form: 7 February 2002

Abstract. This paper proposes temporal-to-spatial dynamic mapping inspired by neural dynamics of the olfactory cortex. In our model the temporal structure of olfactory-bulb patterns is mapped to the spatial dynamics of the ensemble of cortical neurons. This mapping is based on the following biological mechanism: while anterior part of piriform cortex can be excited by the afferent input alone, the posterior areas require both afferent and association signals, which are temporally correlated in a specific way. One of the functional types of the neurons in our model corresponds to the cortical spatial dynamics and encodes odor components, and another represents temporal activity of association-fiber signals, which, we suggest, may be relevant to the encoding of odor concentrations. The temporal-to-spatial mapping and distributed representation of the model enable simultaneous rough cluster classification and fine recognition of patterns within a cluster as parts of the same dynamic process. The model is able to extract and segment the components of complex odor patterns which are spatiotemporal sequences of neural activity.

1 Introduction

Flexible object recognition, feature binding and segmentation, attention focusing, and other pattern processing tasks are hardly handled by computational techniques based on stationary principles. On the other hand, they are successfully resolved by biological neural systems, where not only spatial, but also different kinds of temporal dynamics and correlation are believed to be the underlying principles of the brain's abilities (Fujii et al. 1996; Malsburg 1992).

Olfaction is an example of such a system in which spatiotemporal dynamics has been the subject of both numerous experimental studies (Duchamp-Viret et al. 1996; Joerges et al. 1997; Ressler et al. 1994; Scarda and Freeman 1987; Wehr and Laurent 1996) and theoretical modeling (Haberly and Bower 1989; Hendin et al. 1998; Hoshino et al. 1998; Wilson and Bower 1992). However, most odor recognition techniques do not make use of temporal encoding and processing. In static systems patterns are recognized by the stationary pattern recognition methods, which do not appear to be linked to biological temporal dynamics. The lack of such dynamics and dynamic processing principles in pattern recognition systems is one of the reasons for their poor computational abilities in comparison to biological neural circuits.

On the other hand, there are a number of olfactory cortex models which are based strictly on the system's neurobiological description and produce spatiotemporal dynamics similar to the experimental data (Ballain et al. 1998; Wilson and Bower 1992). Although such models do not clarify the functional significance of this dynamics, they provide insights about its possible role in cortical information processing.

Indeed, biological data demonstrate that pyramidal cells are principal neurons of olfactory cortex that receive and integrate four major types of input signals: from the olfactory bulb (OB) through afferent fibers, and also from three functional cortical areas via association fibers. These four signals are delayed differently by different branches of fibers, and arrive to the area of convergence at different times. Moreover, their signals need different times to propagate through the dendrites and reach the cell body. Temporal correlation of incoming afferent and associative signals proved to be crucial for the signal integration by a pyramidal cell (see Sect. 6.1 for details) (Haberly 1998). We explore this type of temporal correlation in our model and suggest that it could give some cues to understand how a recognition of multicomponent odors and their mixtures is realized in the olfactory cortex.

In the ensemble of spiking neurons described in Sect. 3, the neurons at different layers have different functional properties. The dynamics of the neurons

Correspondence to: J. M. Zurada (e-mail: j.zurada@ieee.org, Tel.: +1-502-8526314; Fax: +1-502-8523940)

which are sensitive to the odor components represents the activity of the neural pool corresponding to the spatial pattern of activity induced by this component (Haberly 1998). Although another type of neuron, sensitive to the concentrations of the odor components, also proved to have its biological analog in the frog olfactory cortex (Duchamp-Viret et al. 1996), its function can be interpreted more generally. The activity of this neuron delivers OB signals to the cortical neurons with different delays, so it may correspond to the dynamics of association fibers.

This ensemble's architecture, due to its distributed and dynamical representation of memory, provides the basis for solution of the coarseness-sensitivity flexibility problem. A coarse-enough system cannot distinguish fine variations of the patterns within a cluster. On the other hand, a sensitive-enough system is not able to detect what cluster these slightly different patterns belong to. The temporal-to-spatial mapping and distributed representation of the model enable simultaneous rough cluster classification and fine recognition of patterns within a cluster as parts of the same dynamic process.

Another group of tasks handled by biological systems includes feature binding, segmentation, attention focusing, and other multipattern recognition problems. There are experimental data that suggest that in the brain these tasks are solved with temporal processing (Fujii et al. 1996; Jinks and Laing 1999), and there are models that propose possible mechanisms (Ambros-Ingerson et al. 1990; Campbell and Wang 1998; Grossberg 1999; Hendin et al. 1998; Lysetskiy et al. 2001; Malsburg 1992). In Sect. 4 we show that the temporal structure of our model allows us to realize this multipattern processing.

In Sect. 2 we introduce the biological olfactory system and its functional properties, Sect. 3 describes the basic block layout of the model and its spatiotemporal dynamics which ensures the recognition flexibility. An example of temporal segmentation of odor patterns in a mixture is presented in Sect. 4. Methods and parameters of the simulation are shown in Sect. 5, which is followed by discussion and conclusions in Sect. 6.

2 Olfactory system

2.1 Olfactory bulb

An odor identity is defined by a group of physical and chemical parameters of the odor's constituent molecules and their relative concentrations. However, these parameters are not clearly determined, nor is the correlation between their candidates and the odor properties (Wise et al. 2000). For the sake of simplicity we assume that one constituent molecule possesses one of these crucial parameters and corresponds to one of the odor components. The odors can therefore be presented by the concentration vector $\boldsymbol{C} = \{c_1, c_2, \ldots, c_n\}$, where c_j is the concentration of jth molecule.

In the olfactory system, odors are first perceived in the olfactory epithelium by different types of receptor neurons. These neurons are sensitive to different kinds of molecules and respond selectively to their presence with oscillatory firing. An odor is further encoded into a quasiperiodic temporal sequence of spatial patterns of synchronized oscillatory neural activity of the olfactory bulb or antennal lobe (Hoshino et al. 1998; Laurent 1996; Scarda and Freeman 1987; Wehr and Laurent 1996).

The spatial patterns of the olfactory bulb/antennal lobe have been proved to be correlated with the odor components (Joerges et al. 1997; Laurent 1996; Ressler et al. 1994), but the functional significance of their temporal structure is unclear. There are two major hypotheses of its possible role. Experiments such as these of Laurent et al. (1996) and Wehr and Laurent (1996) show that the temporal structure of firing of different ensembles contributes to encoding of odor identity in a certain combinatorial way. Another idea is that temporal dynamics of the olfactory bulb encodes the concentrations of the odor components. According to the concept that the odor components are encoded as dynamic attractors of neural activity (Scarda and Freeman 1987), the order in which the state of the system visits these attractors and the time the state spends wandering around them could be correlated with the concentrations of the odor components (Hoshino et al. 1998). There is also experimental and theoretical support for the idea that a component's concentrations can be encoded by precise timing of a spike, a burst, or the phase of the periodic firing of corresponding neuron or ensemble (Duchamp-Viret et al. 1996; Hopfield 1995). These hypothesis do not necessarily contradict each other; they could coexist and complement one another or be the parts of a more complicated neural coding scheme.

Our model realizes a mapping of the temporal relations of input patterns into spatiotemporal dynamics of the output activity. We follow the idea proposed by Hopfield (1995) and assume that the precise time advance of a pattern's firing encodes the concentration of an odor, though it is a simplification of the real olfactory code that is yet to be discovered. However, the idea of the temporal-to-spatial mapping could still be applicable if the temporal structure carried some other functional significance.

We assume that spatiotemporal patterns in the olfactory bulb are formed in the following way: the greater the concentration of the odor component applied, the earlier the correspondent neural ensemble synchronizes its activity and fires (Hoshino et al. 1998), and the greater is the time φ_j that the jth ensemble fires in advance of the moment of the maximum of its subthreshold activation, which serves as a reference time (Hopfield 1995).

According to the Hopfield's (1995) hypothesis, the corresponding concentrations c_j of n constituent molecules are encoded as time advances $\varphi_1, \varphi_2, \ldots, \varphi_n$ of the ensemble's firing:

$$\varphi_j = t_j - t^{(r)} \tag{1}$$

where t_j is the time of the ensemble's spike and $t^{(r)}$ is the reference time mentioned above. The functional relation

between stimulus intensity and time advance of the spikes has been proposed by Hopfield:

$$\varphi_j = \alpha \ln(c_j/\delta) \quad (2)$$

where each time advance is assumed to be proportional to the logarithm of the corresponding concentration, α is a coefficient, and δ is a scale factor (Hopfield 1995).

Such logarithmic scaling makes the relative time advances of spatial patterns invariant to different concentrations of the same odor. The changing of the concentration of a multicomponent odor results in a time advance of the whole pattern, while the relative time advances remain constant.

2.2 Olfactory cortex

2.2.1 Synaptic organization. The piriform cortex (PC), the part of the olfactory cortex we focus on, is divided in three functional areas: ventral and dorsal parts of the anterior PC (APCv and APCd), and the posterior PC (PPC).

The input (spatial activation patterns) from the OB is delivered directly to the APCv by the lateral olfactory tract (LOT), and via LOT collaterals further to the PPC. The conduction velocities along the LOT (7.0 m/s) are greater than along its collaterals (1.6 m/s) (Wilson and Bower 1992). Thus, there is a time delay of about 5–7 ms between the arrivals of the OB signal to anterior and posterior parts of the PC, as measured by Ketchum and Haberly (1993a,b).

In addition to afferent input from the OB, pyramidal cells also receive association projections from each other, which are distinguished by the area they come from: APCv, APCd, and PPC. The striking feature of the PC is the spatiotemporal organization of its afferent and association connections: four major fiber systems, afferent input from OB, and association projections from APCv, APCd, and PPC make synapses in distinct sublayers of the PC.

The closer the source of the signal is to the LOT, the further from the cell body corresponding fibers synapse and the greater is the time of the signal's propagation along the dendritic tree to the cell body. Afferent axons synapse on the dendrites of pyramidal cells in layer Ia (the closest one to the cortical surface). Association axons from the APCv and the APCd synapse, respectively, in superficial (sup Ib) and deep (deep Ib) parts of layer Ib. Association axons from the PPC excite the same dendrites deeper in layer deep Ib and in layer III.

2.2.2 Spatiotemporal dynamics. The temporal dynamics of the dendritic trees in response to LOT activation is also strictly structured. It includes four peaks of inward currents: excitatory postsynaptic current (EPSC) in layer Ia (caused by the signals of afferent fibers), disynaptic EPSC in layer sup Ib (mediated by association fibers from the APCv), small EPSC in deep Ib (which is due, in part, to the APCd's signals), and inhibitory PSC in layer II.

The structure of this temporal sequence of the dendritic inward currents proved to be crucial for their integration at the cell body. In order to produce maximum activity, the cell body needs not only for both afferent and association signals to be applied, but also for them to be temporally correlated in a specific way (Ketchum and Haberly 1993a,c). This idea is also supported by the results of Wilson et al. (1992) (see Sect. 6.1). We explore this integration mechanism in our model and suggest that it could be employed by the olfactory cortex for the recognition of complex odors.

Another question we focus on in this paper is: how is the concentration of odor components encoded in the cortex? The experimental data of Duchamp-Viret et al. (1996) show that in a frog olfactory cortex there is a special class of neurons which do not discriminate well between different odors, but instead seem to encode odor concentration. The latency of their bursting was found to be correlated to the odor concentration: the greater the concentration, the smaller is the latency. This data is in accordance with the idea of Hopfield (1995), and suggests that odor components and odor concentrations may be encoded by different populations of neurons.

However, such "concentration neurons" were not found in other olfactory systems, where intensity encoding may be different. In various olfactory systems odor concentrations influence the temporal structure of OB activity patterns. When they are injected to the PC, the resulting temporal patterns of incoming signals to different PC regions invoke corresponding sequences of inward dendritic currents at the dendritic trees. As well as the integration of EPSCs in the cell body depending crucially on this pattern of inward currents (Haberly 1998; Ketchum and Haberly 1993b,c), we conclude that the dynamics of association-fiber signals could be correlated with the concentrations of odor components. We explore these ideas in our model, where there is a special type of neurons sensitive to different concentrations.

3 The model

Let an odor be a mixture of two components A and B. For recognition of this mixture as a whole, some kind of AND logic gate ODOR = A AND B has to be realized at some level of a recognition system: in our model this AND function is performed by integration of afferent and association signals by an integrate- and-fire neuron, which fires if these signals arrive within a close-enough time window.

We define an odor as a cluster of odor patterns that have identical components with different relative concentrations. An odor recognition system has to be rough enough to be able to recognize that different patterns may belong to the same cluster. On the other hand, it has to be sensitive enough to distinguish slightly different odors within a cluster.

In our model the recognition of an odor is represented by the firing of the neurons of a specific ensemble in a specific sequence. Cluster recognition and fine

recognition are represented by activation of different neural subensembles.

Our network consists of a layer of leaky integrate-and-fire neurons u_j, interconnected via arrays of intermediate-delay neurons d_k^{ji} (Fig. 1). The neurons u_j are also connected with the layer of temporal inputs $s_j(t)$. These inputs simulate activity of the OB and the neural layer functionally corresponds to the olfactory cortex that receives and processes those patterns.

The periodic inputs $s_j(t)$, $j = 1, \ldots, n$, represent n spatial patterns which correspond to n components of odor concentration vector $C = \{c_1, c_2, \ldots, c_n\}$. The inputs are presented as follows:

$$s_j(t) = s \sum_{k=1}^{\infty} \delta(t + \varphi_j - kT) \tag{3}$$

where $\delta(t)$ is Dirac delta function, T is the signal's oscillation period, s is a spike's amplitude, and the time advances φ_j encode concentrations of constituent molecules according to (2). An example of input pattern is shown in Fig. 1.

There are three types of neurons in the layer. Each neuron is characterized by its state, that is the neuron's membrane potential: $u_j(t)$ for the principal neurons, $d_k^{ji}(t)$ for the delay neurons, and $x_k^{ji}(t)$ for the selective neurons. The neurons and inputs are connected with weights $w^{(\text{neur})}$, $w^{(\text{del})}$, and $w^{(\text{sup})}$ (Fig. 1).

As described below in (4), a neuron u_j receives corresponding input signal $s_j(t)$ from the jth input and lateral signals $l_k^{ji}(t) = L[d_k^{ji}(t)]$ (operator L is defined below) from the activated neuron u_i, which are propagated and delayed by the delay neurons d_k^{ji}.

The operator L used above maps the functions of a neuron membrane potential to the function of the spikes $l(t)$ which this neuron produces. So, for example, $L[u_j(t)] = l_j(t)$ where $l_j(t)$ is equal to $\sum_k s\delta(t - t_{\text{thresh}}^k)$, and where t_{thresh}^k are the times when the value of membrane potential u_j reaches its threshold.

If a neuron receives a spike at time t_s, its potential $u_j(t)$ is increased by the weighted value

$$w^{(\text{neur})} \int s_j(t)\mathrm{d}t = w^{(\text{neur})} s \ ,$$

if it is a spike from the input level, or

$$w^{(\text{neur})} \int l_k^{ji}(t)\mathrm{d}t = w^{(\text{neur})} \int L[d_k^{ji}(t)]\mathrm{d}t = w^{(\text{neur})} S \ ,$$

if it is a spike propagated though a delayneuron d_k^{ji}. If the potential of a neuron reaches its threshold value u_{thresh}, the neuron fires. Its output signal $l_j(t) = L[u_j(t)]$ produces a spike which is propagated to the array of delayneurons that transfer the spike to all other neurons in the layer. At the same time its potential u_j is instantly reset to 0, as shown in (5). Additionally, the potential u_j is constantly decreasing with decay coefficient k. These mechanisms are employed by all the neurons in the model:

$$\frac{\mathrm{d}u_j(t)}{\mathrm{d}t} = -ku_j(t) + w^{(\text{neur})} s_j(t) + \sum_{i:i\neq j}^{n} \sum_{k=1}^{m} w^{(\text{neur})} L[d_k^{ji}(t)] \tag{4}$$

$$u_i(t^-) = u_{\text{thresh}} \Rightarrow u_i(t^+) = 0 \tag{5}$$

The parameters of the equation are set in such a way that in order for a neuron u_j to fire it needs to receive two spikes in the narrow time window $\Delta t^{(u)}$: one spike, $s_j(t)$, from the corresponding input; and another, $l(t) = L[d_k^{ji}(t)]$, from one of the delay neurons (see details in Sect. 5). An exception is made for the very first input spike in the first cycle, which alone is able to activate the corresponding neuron. This adds to the model the functional property of the networks like the so-called LEGION, where the global inhibition of the neurons depends on the number of the activated neurons (Campbell and Wang 1998). Such inhibition

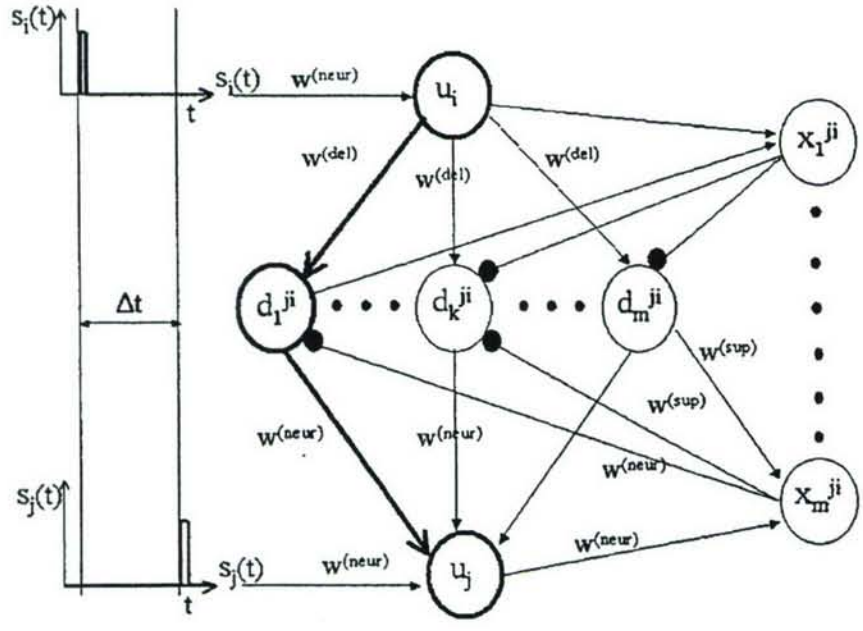

Fig. 1. Network architecture. The neurons of activated sub-ensemble $\{u_i, d_1^{ji}, u_j\}$ are shown in *bold*. *Arrows* and *black circles* represent excitatory and inhibitory connections, respectively

ensures that when fewer neurons are activated, the greater is the probability for a neuron to fire. In our model the neurons are made more sensitive to the very first input spike, because there is no activation yet in the neuron layer. The biological correspondence of this assumption is discussed in Sect. 6.1.

Delay neurons in the arrays are integrate-and-fire neurons with added inherent propagation delays D_k, $k = 1, \ldots, m$, defined as

$$\frac{\mathrm{d}d_k^{ji}(t)}{\mathrm{d}t} = -kd_k^{ji}(t) + w^{(\mathrm{del})}L[u_i(t - D_k)] + \sum_{q:q\neq k}^{m} w^{(\mathrm{sup})}L[x_k^{ji}(t)] \quad (6)$$

The parameters of the equation make the delay neuron work as a delay operator (details in Sect. 5). When d_k^{ji} receives a spike at time t it fires at $t + D_k$. Functionally, d_k^{ji} are equivalent to the ordinary integrate-and-fire neurons as in (4), connected to the principal neuron u_i via corresponding delay D_k. The values of delays D_k change gradually across the array as follows:

$$D_k = \frac{T(k - 1/2)}{m}, \quad k = 1, \ldots, m \quad (7)$$

where T is the oscillation period (3), and m is the number of the delay neurons in the array. This specific delay distribution ensures recognition properties of the system which are discussed below.

As a pattern processing example we consider a simple case where an odor with two components $\{0, \ldots, c_I, c_J, \ldots, 0\}$ is applied with $c_I > c_J$. For convenience we will be presenting this as $\{c_I, c_J\}$. When this odor is applied, the neuron u_I receives the input spike $s_I(t)$ first, at the moment t_1, and then u_J receives $s_J(t)$ at t_2.

The single spike s_I is enough for u_I to fire because of the exception mentioned above. The neuron u_I fires at the moment t_1 and sends spikes $L[u_I(t)]$ to all other neurons u_j, $j = 1, \ldots, n$, $j \neq I$ via delay arrays d_k^{ji}. The neurons u_j receive the delayed signals from d_k^{ji} at times $t + D_k$, $k = 1, \ldots, m$. However, this is not enough for them to fire because a spike from the input level is also needed. Although all of them show subthreshold activation, only the neuron u_J which will receive the input spike s_J will actually reach the threshold and fire. Finally, the neurons that fire are u_I, u_J, and all intermediate neurons d_k^{JI} in the array which connects them.

The values of D_k set by (7) ensure that one and only one of the delay neurons fires and sends a spike to the neuron u_J within the time window $\Delta t^{(x)}$. Thus, although all of the delay neurons in the array fired, only one of them actually contributes to the firing of the neuron u_J. To distinguish this contributing delay neuron from others, an additional layer of selective neurons x_k^{ji} is added (Fig. 1).

Selective neurons x_k^{ji} are functionally equivalent to the principal neurons u_j. They work as coincident time detectors and fire if spikes from neurons u_j and d_k^{ji} arrive at x_k^{ji} within time window Δt:

$$\frac{\mathrm{d}x_k^{ji}(t)}{\mathrm{d}t} = -kx_i(t) + w^{(\mathrm{neur})}L[d_k^{(Ji)}] + w^{(\mathrm{neur})}L[u_j(t)] \quad (8)$$

Selective neurons provide negative feedback $\sum_{q:q\neq k}^{m} w^{(\mathrm{sup})}L[x_k^{ji}(t)]$ to the delay neurons $d_k^{(JI)}$ that did not contribute to the firing of u_J (6). Because of this selective feedback, neurons d_k^{JI} which contributed to the firing of u_J stay unchanged, while the rest of the delay neurons are suppressed and will not be sensitive to the spikes from u_i during suppression time T_S, defined as follows:

$$T_S = \frac{1}{k}\ln\left(\frac{w^{(\mathrm{sup})}s}{d_{\mathrm{thresh}}/s - w^{(\mathrm{del})}}\right) \quad (9)$$

At the output level there is now a sequence of firing of neurons u_I, d_K^{JI}, and u_I one after another. Firing of the neurons u_I and u_J indicates that an odor of the cluster $\{c_I, c_J\}$ is recognized. The firing of the specific delay neuron d_K^{JI} defines the relative concentration of two components, the logarithm of which lays in the vicinity of the delay D_K of the corresponding delay neuron:

$$D_K - \frac{T}{2m} < \alpha\ln\left[\frac{c_I}{c_J}\right] < D_K + \frac{T}{2m} \quad (10)$$

An example of the system's dynamics is shown in Figs. 2 and 3. During the first cycle ($0 < t < T$), neurons d_k^{JI} are activated by u_I and fire consequently in the order of their inherent delays D_K, starting from the one with the smallest D_K, until d_3^{JI} gets activated, which fires within time window Δt with u_J. The correlated firing of u_J and d_3^{JI} makes x_3^{JI} fire. Selective neuron x_3^{JI} suppresses the remaining delay neurons for the suppression time T_S, which is equal to the oscillation period $T = 20$. After time T, selective neuron x_3^{JI} will suppress them again. So, the only delay neuron that will fire during the second and following cycles is d_3^{JI}. The parameters used in the simulation are described in Sect. 5.

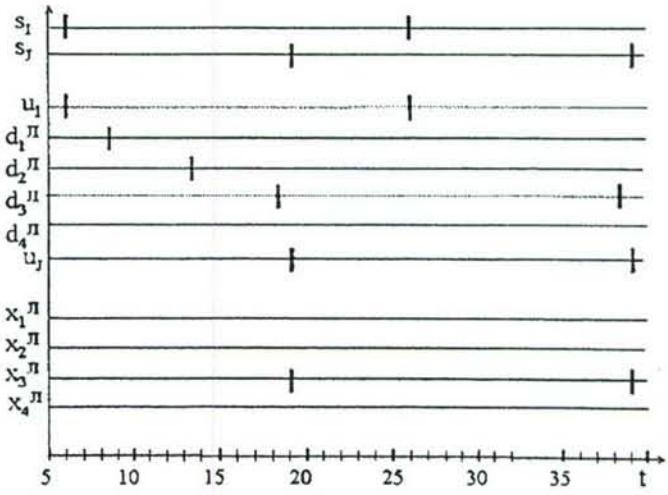

Fig. 2. Dynamics of the neural ensemble during the recognition process. The *bars* represent the spikes of the corresponding neurons

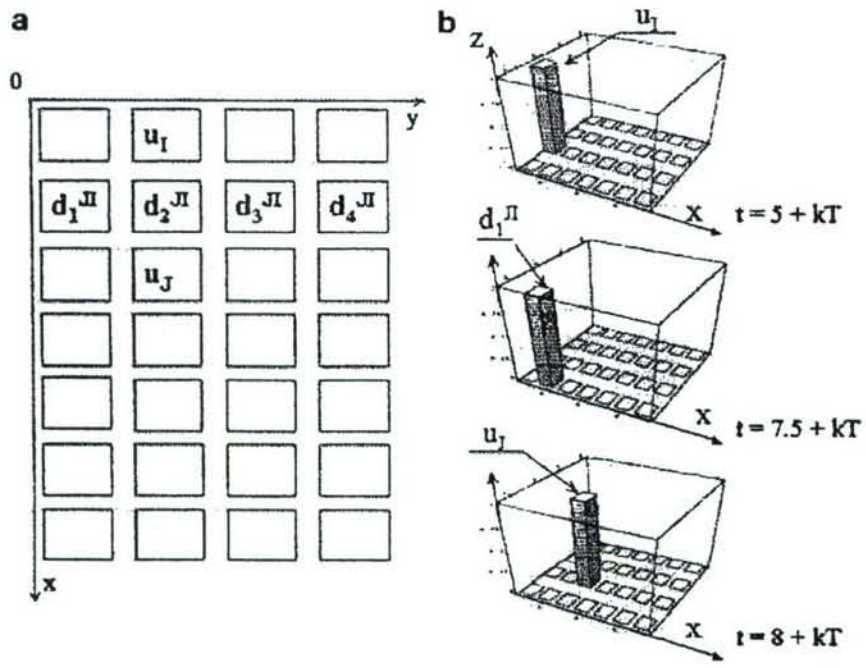

Fig. 3a,b. Simulation of spatiotemporal dynamics of the ensemble: a distribution of the neurons in the layer; b spatiotemporal neural dynamics. Axis z corresponds to the membrane potentials $u(t)$ or $d(t)$: $k = 1, 2, \ldots, N$; and T is the period of the oscillations

4 Temporal segmentation

According to Hopfield's (1985) mechanism of formation of the input temporal sequence, if a mixture of several odors is applied, the corresponding spatiotemporal sequences are superimposed and the resulting input sequence contains patterns of all components of each odor. The stronger the component, the earlier its pattern fires, no matter which odor the component belongs to.

In order to segregate the odor patterns in time, one of the ensembles should win and hence suppress the others for a period of several cycles. After that, due to the neural fatigue, the winning ensemble stops firing and the second-strongest ensemble wins and fires during the next several cycles (Campbell and Wang 1998; Hoshino et al. 1998; Malsburg 1992). To realize such pattern segmentation, the modified network from Sect. 2 with additional neural interaction and neural fatigue function $F(p)$ is used:

$$\frac{\mathrm{d}u_j(t)}{\mathrm{d}t} = -ku_j(t) + \{w^{(\mathrm{neur})}s_j(t) + \sum_{i:i\neq j}^{n}\sum_{k=1}^{m} w^{(\mathrm{neur})}L[d_k^{ji}(t)] + \sum_{i:\forall z,u_i\cup u_j\notin E_z}^{n} w_{ji}^{(\mathrm{inter})}L[u_i(t)]\}F(p) \tag{11}$$

where $F(p)$ is defined as a step function, with $F(p) = 1$ if $2kp_f < p < (2k+1)p_f$, and $F(p) = 0$ if $(2k+1)p_f < p < (2k+2)p_f$; $\forall k : k = 1, 2, \ldots, K$. The variable p is the number of times the potential of neuron u_j reached its threshold, and p_f is the number of firings after which the neuron becomes insensitive to the inputs and stays silent for another p_f cycles.

Neural ensemble E_z, $z = 1, \ldots, Z$, is a group of neurons that correspond to the components of the same odor. All neurons which are not members of the same ensemble are interconnected with negative weights $w_{ji}^{(\mathrm{inter})}$. When a neuron u_i fires, it sends inhibitory signals $w_{ji}^{(\mathrm{inter})}L[u_i(t)]$ to the neurons that do not belong to any of the ensembles E_z in which the neuron u_i participates. The membrane potentials of those neurons are decreased by $w_{ji}^{(\mathrm{inter})}L[u_i(t)]$. They stay suppressed for the refractory period T_R during which they cannot fire regardless of the input signals received. T_R is determined as follows:

$$T_R = \frac{1}{k}\ln\left(\frac{w^{(\mathrm{inter})}s}{u_{\mathrm{thresh}} - 2w^{(\mathrm{neur})}s}\right) \tag{12}$$

The dynamics of the competition between ensembles is quite a complicated process (Campbell and Wang 1998; Hoshino et al. 1998), because for a neuron in the ensemble, its probability of being suppressed depends on the statistical value of the difference of received inhibitory and excitatory spikes.

In our model, according to (11) and the exception for the first spike in the input sequence (Sect. 3), the first activated neuron suppresses the others which are not in its ensemble, and does not allow them to fire with 100% probability. So, the ensemble which contains the winning neuron, or, in other words, the odor with the strongest component, always wins the competition first.

As an example we consider the case where two odors $\{c_I, c_J\}$ and $\{c_P, c_Q\}$ are applied to the network with the following order of the concentrations of their components: $c_I > c_P > c_J > c_Q$. The temporal sequence of input spikes is the same, $\{s_I(t), s_P(t), s_J(t), s_Q(t)\}$, as shown in Fig. 4. The first of them, $s_I(t)$, activates neuron u_I, which sends inhibitory signals to u_P and u_Q, and excitatory signal

to u_J via an array of the delay neurons. When input spike $s_P(t)$ appears, the corresponding output neuron u_P is suppressed and will not respond to the impulse. Then input s_J activates neuron u_J, which already received an excitatory signal from u_I: After that $s_Q(t)$ fails to activate neuron u_Q. Finally the neurons u_I and u_J fire, while u_P and u_Q remain silent. In this way the odor $\{u_I, u_J\}$ is segmented from the background and attention is focused on it for the period of $p_f = 2$ cycles (Fig. 3). Then, due to the neural fatigue $F[p]$, the neurons u_I and u_J stop firing and u_P and u_Q become activated, so the attention is now refocused on this odor. So, the odor patterns are temporally segregated and processed one at a time, as is shown in Figs. 4 and 5. The parameters used in the simulation are specified in Sect. 5.

5 Simulation

The neurons described by (4) and (8) work as coincident time detectors. They fire if two spikes arrive at a neuron within time window Δt, the size of which is defined by the parameters of the integrate-and-fire neurons as follows:

$$\Delta t^{(u)} = -\frac{1}{k}\ln\left(\frac{u_{\text{thresh}}}{w^{(\text{neur})}s} - 1\right)$$
$$\Delta t^{(x)} = -\frac{1}{k}\ln\left(\frac{x_{\text{thresh}}}{w^{(\text{neur})}s} - 1\right) \tag{13}$$

where $\Delta t^{(u)}$ and $\Delta t^{(x)}$ are the time windows of neurons u_j and x_k^{ji}, respectively. In our simulation $u_{\text{thresh}} = x_{\text{thresh}}$, so $\Delta t^{(u)} = \Delta t^{(x)}$, and we will represent them both as Δt.

Since this is essentially the property of the neurons used in the model, there was no need to implement them by the actual integrate-and-fire neurons. The neurons u_j were replaced by logic units u_j^*, characterized by its state $u_j^*(t)$ that has the following properties. Without inputs, $u^*(t)$ is equal to 0. If u_j^* receives two spikes with weights $w^{(\text{neur})}$ at the moments t_1 and t_2 with $t_2 > t_1$, then

$$\text{if } |t^2 - t^1| < \Delta t$$
$$\text{then } u^*(t_2^+) = u_{\text{thresh}}$$
$$\text{else } u^*(t) = 0 \tag{14}$$

If the state $u_j^*(t)$ of logic unit u_j^* reaches its threshhold value u_{thresh}^* at time t_{thresh}, it behaves in the same way as neurons u_j do. The value of $u_j^*(t)$ is reset to 0 and the output function of the unit, $L[u_j^*(t)]$, is equal to $\Delta(t - t_{\text{thresh}})$. The rules for units x_k^{*ji} are analogous to the rules of u_j^*. The state of d_k^{*ji} is defined as $d_k^{*ji}(t) = d_k^{ji}(t) = L[u_i(t)]$.

The focus of the model is the computational abilities of spatiotemporal integration and temporal dynamics discussed in Sect. 3. For this reason, temporal parameters have been assigned biologically realistic values, such as the period of oscillations, $T = 20$ ms, which corresponds to 50-Hz oscillations observed in the olfactory cortex. This also makes the values of time delays D_K, defined by (7), comparable with the delays of 5–7 ms, related to different association fibers (see Sect. 6.1 for details).

The values of the following parameters were chosen arbitrarily: $T = T_R = T_S = 20$, $\Delta t = 5$, $\alpha = 4$, $\delta = 1$, $s = 1$, $u_{\text{thresh}} = x_{\text{thresh}} = d_{\text{thresh}} = 1$, $p_f = 2$, $n = 4$, and $m = 4$.

The weights $w^{(\text{del})} = 1.1$ were assigned their values in order to make a single weighted spike $sw^{(\text{del})}$ be enough to fire a delay neuron. The values of weights $w^{(\text{neur})} = 0.75$ were defined so as to ensure that not one, but two weighted spikes $sw^{(\text{neur})}$ (and in a small-enough time window) are needed to activate a principal neuron. The parameters $w^{(\text{sup})} = -8.0963$, $w^{(\text{int})} = -39.91$, and $k = 0.2197$ were defined by (9), (12), and (13), respectively.

The dynamics of an example simulation is shown in Fig. 5, where the mixture of odors $\{u_I, u_J\} = \{100, 50\}$

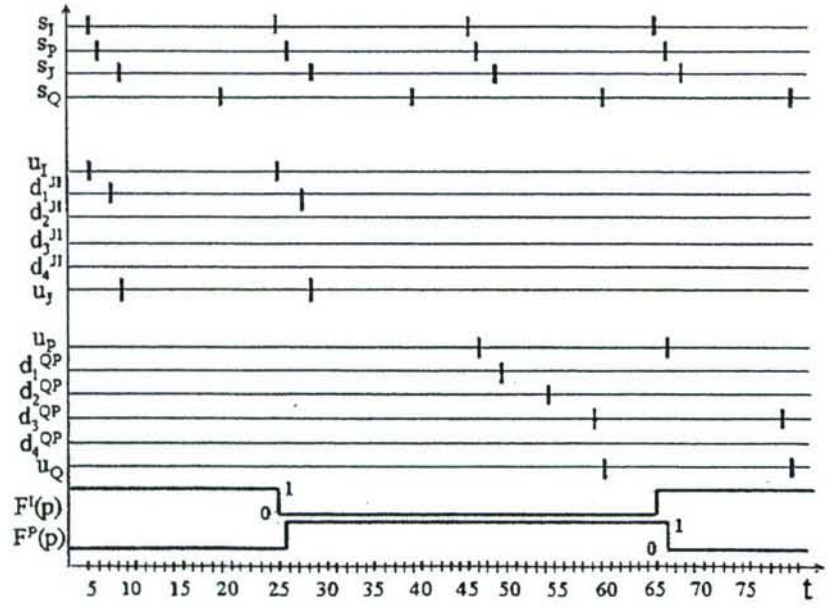

Fig. 4. Dynamics of two neural ensembles during processes of temporal binding, segmentation, and attention

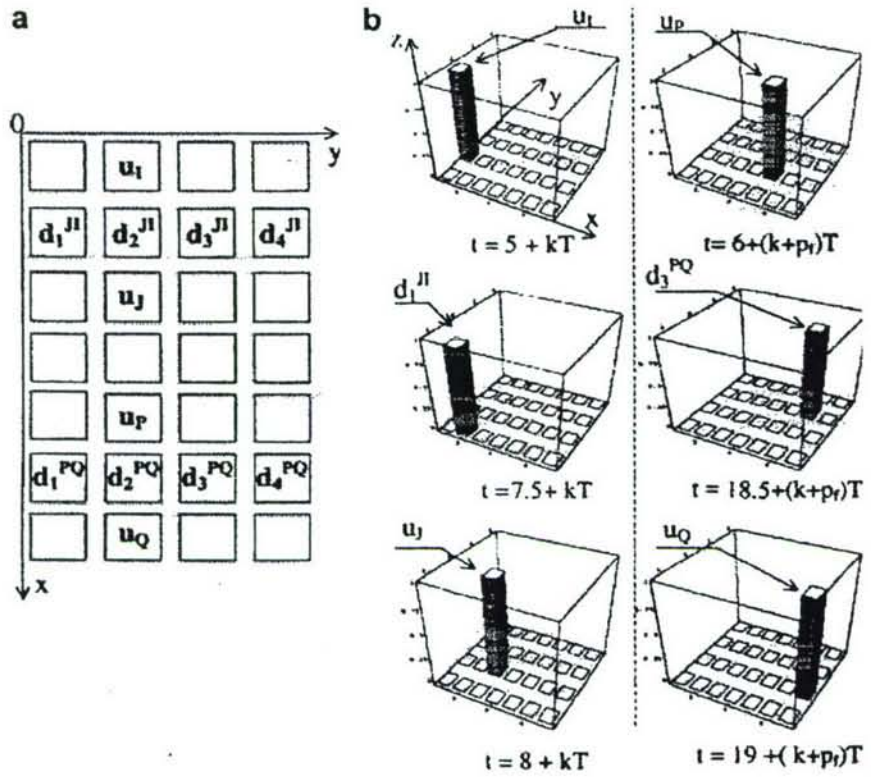

Fig. 5a,b. Simulation of the neural dynamics of pattern segmentation and attention focusing: **a** distribution of the neurons in the layer; **b** spatiotemporal neural dynamics during the first p_f (*left column*) and second p_f (*right column*) cycles. Axis z corresponds to the membrane potentials $u(t)$ or $d(t)$: $k = 1, \ldots, p_f$; and T is the period of the oscillation

and $\{u_P, u_Q\} = \{80, 3\}$ is applied. During the first three cycles the neurons of the first odor fire in the following sequence: u_I, d_1^{JI}, and u_J (Fig. 5b, left column). This indicates that the odor $\{u_I, u_J\}$ is recognized with the relative concentrations of its components defined by (9) as $0 < \ln[\frac{c_I}{c_J}] < 1.25$. After three cycles $\{u_P, d_3^{JI}, u_Q\}$ becomes activated and suppresses in its turn the first ensemble (Fig. 5b, right column). So, the ratio of the concentrations of the components of this odor is $2.5 < \ln[\frac{c_P}{c_Q}] < 3.75$.

6 Discussion

6.1 Biological correspondence

We argue that the dynamics of our model reflects certain aspects of olfactory cortex activity related to information processing. The key principles of mixture recognition in our system are that a single input spike from the OB is enough to activate a certain neuron (e.g., u_i, in the model) while the others (e.g., u_j) need signals both from the OB and from another principal neuron, propagated by the delay neurons.

Experimental results (Wilson and Bower 1992) indeed suggest that while anterior areas of the cortex may be activated by afferent input only, the posterior parts require both afferent and association signals. This mechanism rises from the properties of the relative density of association and afferent terminals, defined by the association-to-afferent dominance ratio (AADR). The AADR increases along the distance from the LOT: in the APCv (the closest area to the LOT), afferent fibers prevail over the association ones, and the opposite is true for the PPC (Haberly 1998). The results of Wilson and Bower (1992) show that when the afferent activity is not strong enough, it can only activate the APC, where the AADR is low. Activation of the posterior cortex (with a high AADR) results mostly from delayed arrival of association-fiber activity. These results suggest that the areas with medium AADRs, such as the APCd, may need equally both afferent and association inputs to be activated.

In Sect. 2.2.2 we described the spatiotemporal sequence of the dendritic currents, produced by afferent and association signals. Its correspondence with the dynamics of our model is the following: neuron u_j receives the spikes $s_j(t)$ from the OB, and $L[d_k^{ji}]$ from the principal neurons, differently delayed by delay neurons (or association fibers, as in the real PC), as shown in Fig. 2. Each of the incoming signals increases the state of the neuron (i.e., produces a peak of inward current). u_j is activated only if afferent input $s_j(t)$, and one of the association inputs $L[d_k^{ji}]$, arrive in a small-enough time window (in terms of the PC, the induced EPSCs are close enough in time).

This mechanism is supported by experimental results described in Ketchum and Haberly (1993b,c) and Haberly (1998), which show that the optimal temporal correlation of inward currents is the one which ensures their roughly synchronous arrival at the cell body. In these experiments, when three EPSCs were presented in their natural sequence (with interpeak latencies of several milliseconds), the induced potential at the cell body was 50% greater than the one caused by the same EPSCs applied simultaneously.

Moreover, the delays produced by propagation along the dendritic tree could synchronize the incoming signals, as did delay neurons in our model. Indeed, different fibers synapse at distinct distances from the cell body, and thus require different times for a postsynaptic spike to propagate to it via the dendritic tree. The latency between peak depolarization in afferent input in layer Ia and the peak depolarization of the cell body is approximately 6 ms (Haberly 1998).

The repetitive temporal dynamics in our model is also related to the one of the real PC, where the temporal sequence of dendritic postsynaptic currents evolves in each cycle of 50-Hz cortical oscillations. Odor components are also segregated temporally, with each of them processed during different oscillation cycles. Thus, the temporal sequence of EPSCs, whatever functional role it plays, participates repetitively in the processing of each odor component.

Selective suppression of the delay neurons in our model, which corresponds to the suppression of association-fiber signals, also has its prototype in the PC. As shown in Ketchum and Haberly (1993a), when two successive shocks are applied to the LOT, the first one induces the full sequence of the peaks of inward currents, but the second one produces only an isolated monosynaptic EPSC coming from the APCv. The association-fiber signals are blocked by inhibitory postsynaptic currents evoked by the first shock. However, there is not enough biological evidence yet to specify functional significance of this suppression and compare it to the one of our model, where all delay neurons are active at the first cycle and get selectively suppressed at the second one (Fig. 2).

In our model, activity of a delay neuron represents corresponding concentration of the odor component. Such behavior, although detected in the frog olfactory cortex (Duchamp-Viret et al. 1996), was not observed in other olfactory systems. We argue that the dynamics of delay neuron in our model can be seen as differently delayed activity of association fibers coming from different cortical areas: APCv, APCd, and PPC. They also are of the same range: the time of signal propagation along the cortex – from anterior to posterior parts – is 5–7 ms.

6.2 Olfactory system models

The general idea behind most of the odor recognition models is that an odor pattern is temporally segregated in the patterns of its components, which are processed in the order of their significance or intensity (the strongest one is processed first). However, it is not absolutely clear which parts of the olfactory system are involved in this process, and to what degree.

In the model of Ambros-Ingerson et al. (1990), temporal segmentation of the bulbar activation patterns is realized by the selective inhibitory cortical feedback. During each cycle, OB activity is projected to the cortex where the pattern of its strongest component suppress the other ones (the winner-takes-all mechanism) and activates inhibitory feedback to the bulb. This feedback suppresses the part of the bulbar activity which corresponds to this strongest component. During the following cycles, the normalized remainder of the input is presented to the cortex and the same process occurs repetitively. During different cycles, input is classified as a part of a cluster of the corresponding hierarchical level. Processing during the first cycle corresponds to the first level clusters (rough recognition), subcluster recognition is realized at the second cycle, and so on.

Input segmentation in this model is due to the corticobulbar interaction. However, it may be also realized in the OB without corticobulbar interplay. In the model of Hoshino et al. (1998) the winner-takes-all competition occurs in the OB itself. The winning pattern suppresses the others, stays active during several cycles, and then stops firing due to the neural fatigue. The second-strongest pattern then wins, and the process repeats. Chaotic dynamics, which is believed to be crucial for bulbar information processing, is also taken into account in this system.

The models discussed above deal with odors which have distinct components. If, instead, complex odors with the same components but in different concentrations are ideally mixed, the information about them is lost, and their separation is impossible. An odor mixture {4A, 7B} may be composed of an infinite number of odor combinations, such as {2A, B} + {2A, 6B} or {A, 3B} + {3A, 4B}. However, the problem becomes solvable if temporal fluctuations of the odors are independent. This is the case when, for example, the sources of odors are spatially distinct and there is enough turbulence in the airflow. This idea was explored in the models of Hendin et al. (1994, 1998), where temporal segmentations of the bulbar activity is based on the temporal fluctuations of input odors.

In our model we focus on the recognition of the odor mixtures which are already segmented into spatiotemporal patterns of OB activity, after the temporal fluctuations of odors, if any, were employed by the OB. We propose a new possible functional role of temporal correlation of association-fiber signals, activity of which is influenced by the temporal structure of the OB signals, which, in turn, is assumed to be correlated with the odor concentrations.

The advantage of the distributed representation of our model is its flexible recognition ability. Speaking of the olfactory system, where the number of odors and their mixtures the brain can possibly perceive is enormous, one of the computational problems is how to preserve the hierarchy and similarity in the representation of odor memory. In our system the neural ensemble which corresponds to the odor of coffee would be a part of a bigger ensemble that represents more complicated odors of a coffee house. The dynamics of the smaller ensemble also would be part of the bigger ensemble's dynamics. On the other hand, two similar odors (odors with some common components) would activate two similar neural ensembles with close spatial dynamics. This would happen because common components and their relative concentrations would

activate the same spatial dynamics of the same ensemble. The neural processing of spatiotemporal patterns is one of the key principles for the brain's fast flexible pattern recognition that is still beyond the reach of modern computational techniques. In this paper we present an attempt to understand the principles of how the brain could use its spatiotemporal dynamics for recognition tasks.

Acknowledgment. This work was sponsored in part by the Department of the Navy, Office of Naval Research, Grant N000 14-01-1-0630. The content of this information does not necessarily reflect the position of the U.S. government.

References

Ambros-Ingerson J, Granger R, Lynch G (1990) Simulation of paleocortex performs hierarchical clustering. Science 247: 1344–1348

Ballain T, Litaudon P, Martiel JL, Cattarelli M (1998) Role of the net architecture in piriform cortex activity analysis by a mathematical model. Biol Cybern 79: 323–336

Campbell S, Wang D (1998) Synchrony and desynchrony in integrate-and-fire oscillators. In: Proceedings of the IEEE International Joint Conference on Neural Networks, Anchorage, Alaska, 4–9 May 2: 1498–1503

Duchamp-Viret P, Palouzier-Paulignan B, Duchamp A (1996) Odor coding properties of frog olfactory cortical neurons. Neuroscience 74: 885–895

Fujii H, Ito H, Aihara K, Ichinose N, Tsukada M (1996) Dynamical cell assembly hypothesis – the theoretical possibility of spatiotemporal coding in the cortex. Neural Netw 9: 1303–1350

Grossberg S (1999) How does the cerebral cortex work? Learning, attention and grouping by the laminar circuits of visual cortex. Spat Vis 12: 163–186

Haberly L (1998) Olfactory cortex. In: Shepherd G (ed) The synaptic organization of the brain. Oxford University Press, New York, pp 377–416

Haberly L, Bower J (1989) Olfactory cortex: model circuit for study of associative memory? Trends Neurosci 12: 258–264

Hendin O, Horn D, Hopfield J (1994) Decomposition of a mixture of signals in a model of the olfactory bulb. Proc Abtl Acad Sci USA 91: 5942–5946

Hendin O, Horn D, Tsodyks M (1998) Associative memory and segmentation in an oscillatory neural model of the olfactory bulb. J Comput Neurosci 5: 157–169

Hopfield JJ (1995) Pattern recognition computation using action potential timing stimulus representation. Nature 376: 33–36

Hoshino O, Kashimori Y, Kambara T (1998) An olfactory recognition model based on spatio-temporal encoding of odor quality in the olfactory bulb. Biol Cybern 79: 109–120

Jinks A, Laing D (1999) Temporal processing reveals a mechanism for limiting the capacity of humans to analyze odor mixtures. Cogn Brain Res 8: 311–325

Joerges J, Kuttner A, Galizia CG, Menzel R (1997) Representations of odour mixtures visualized in the honeybee brain. Nature 387: 285–288

Ketchum KL, Haberly LB (1993a) Synaptic events that generate fast oscillations in piriform cortex. J Neurosci 13: 3980–3985

Ketchum KL, Haberly LB (1993b) Membrane currents evoked by afferent fiber simulation in rat piriform cortex. I. Current source-density analysis. J Neurophysiol 69: 248–260

Ketchum KL, Haberly LB (1993c) Membrane currents evoked by afferent fiber simulation in rat piriform cortex. II. Analysis with a system model. J Neurophysiol 69: 261–281

Laurent G (1996) Dynamical representation of odors by oscillating and evolving neural assemblies. Trends Neurosci 19: 489–496

Lysetskiy M, Zurada JM (2001) Temporal binding, segmentation and attention focusing in the olfactory model. In: Proceedings of International Joint Conference on Neural Networks, Washington, D.C., 15–19 July, 2: 1095–1100

Malsburg C (1992) The what and why of binding: the modeler's perspective. Neuron 24: 95–104

Ressler K, Sullivan S, Buck L (1994) Information coding in the olfactory system: evidence for a stereotyped and highly organized epitope map in the olfactory bulb. Cell 79: 1245–1255

Scarda C, Freeman W (1987) How brains make chaos in order to make sense of the world. Behav Brain Sci 10: 161–195

Wehr M, Laurent G (1996) Odour encoding by temporal sequences of firing in oscillating assemblies. Nature 384: 162–166

Wilson M, Bower J (1992) Cortical oscillations and temporal interactions in a computer simulation of piriform cortex. J Neurophysiol 67: 981–995

Wise P, Mats J, William S (2000) Quantification of odor quality. Chem Senses 25: 429–443

Neural Processing Letters **15**: 225–234, 2002.

Invariant Recognition of Spatio-Temporal Patterns in The Olfactory System Model

MYKOLA LYSETSKIY,[1] ANDRZEJ LOZOWSKI[2] and JACEK M. ZURADA[1]
[1]*Department of Electrical and Computer Engineering, University of Louisville, KY.*
e-mail: m0lyse01@ubongo.spd.louisville.edu
[2]*Department of Electrical and Computer Engineering, Southern Illinois University at Edwardsville, IL*

Abstract. This paper presents a model of a network of integrate-and-fire neurons with time delay weights, capable of invariant spatio-temporal pattern recognition. Spatio-temporal patterns are formed by spikes according to the encoding principle that the phase shifts of the spikes encode the input stimulus intensity which corresponds to the concentration of constituent molecules of an odor. We applied the Hopfield's phase shift encoding principle at the output level for spatio-temporal pattern recognition: Firing of an output neuron indicates that corresponding odor is recognized and phase shift of its firing encodes the concentration of the recognized odor. The temporal structure of the model provides the base for the modeling of higher level tasks, where temporal correlation is involved, such as feature binding and segmentation, object recognition, etc.

Key words. integrate-and-fire neurons, olfactory cortex, phase shift encoding, spatio-temporal pattern recognition

1. Introduction

1.1. OLFACTION

In the olfactory bulb odor stimulus information is encoded into a periodic spatio-temporal pattern of oscillatory neural activity (Hoshino et al., 1998 Skarda and Freeman, 1987; Laurent and Davidowitz, 1994; Laurent, 1996). Specific spatial patterns of synchronized firing are correlated to a certain constituent molecules of the applied odor. Relative time advances of the appearances of these spatial patterns are correlated with the concentrations of the molecules. This spatio-temporal correlation enables odor recognition and concentration estimation in the olfactory cortex (Hopfield, 1995; Hoshino et al., 1998). The olfactory epithelium of a nasal cavity contains hundreds (say n) of receptors sensitive to various types of molecules (Ressler, 1994). Thus, epithelium perceives odors, basically, as the mixtures of their components (different molecules). It is convenient for the odors to be represented by the concentration vector $C = \{c_1, c_2, \ldots, c_n\}$, where c_j is the corresponding concentration of the jth odor component.

During sniffing constituent molecules of an odor cause receptor neurons (that are equally distributed in the olfactory epithelium) to fire, producing spikes (Duchamp-

Viret et al., 1998; Ressler, 1994). A firing pattern in the receptor field is then mapped to the olfactory bulb. Axons from the same receptors of olfactory epithelium go to the corresponding ensembles of the neurons in the olfactory bulb (Ressler, 1994). So, each ensemble of neurons in the olfactory bulb represents a corresponding constituent molecule of the odor. Once they receive impulses from the receptor level, the neurons in the ensembles synchronize their activity. They fire synchronously within each ensemble, and with the time shifts between different ensembles (Hoshino et al., 1998; Laurant and Davidowitz, 1994). As a result, the odors at the bulbar level are presented by the sequence of firing of different neural ensembles, where the specific neural ensembles represent the odor constituent molecules and the time shifts of the firing of these ensembles represent the concentrations of the constituent molecules (Hoshino et al., 1998; Duchamp-Viret et al., 1996).

The larger is the concentration c_j of a constituent molecule, the earlier the corresponding ensemble gets excited and synchronized (Campbell andWang, 1998) and the greater is the time φ_j the jth ensemble fires in advance of the moment of the maximum of its subthreshold activation, which serves as a reference time (Hopfield, 1995). So, the corresponding concentrations c_j of n constituent molecules can be encoded as time advances $\varphi_1, \varphi_2, \ldots, \varphi_n$ of ensemble's firing presented as:

$$\varphi_j = t_j - t^{(r)} \tag{1}$$

where t_j is the time of the ensemble's spike and $t^{(r)}$ is the reference time mentioned above. The relationship (2) between input concentrations c_j and corresponding time advances φ_j has been proposed in the Hopfield's model (Hopfield, 1995), where each time advance is proportional to the logarithm of the corresponding concentration, α is a coefficient and δ is a scale factor.

$$\varphi_j = \alpha \ln(c_j/\delta) \tag{2}$$

The logarithmic scaling makes the relative phase pattern invariant to the different concentrations of the same odor. In this case, not the relative, but the entire pattern is shifted when the odor concentration is changed.

1.2. OLFACTORY PATTERN RECOGNITION MODELING

In most of the functional olfactory models reported in the literature the authors focus on the spatio-temporal pattern formation at the olfactory bulb level. The basic principles of pattern formation presented above are more or less understood and they are supported by the biological experiments (Duchamp-Viret et al., 1998; Hoshino et al., 1998; Laurent and Davidowitz, 1994; Laurent, 1996). However, the mechanism by which these spatio-temporal patterns (Figure 1(a)) are recognized and then processed at the next, olfactory cortex level, remains, basically, unknown.

One of the plausible biological mechanisms of spatio-temporal pattern recognition is a system with an appropriate set of delays stored in synaptic memory followed by coincidence time detectors that receive these appropriately delayed (and now synchronized) signals. Recognition of a stored odor can be indicated by firing of the

corresponding coincidence time detector neuron (Hopfield, 1995; Natschlager and Ruf, 1998; White et al., 1998). The question that arises is how the concentration of the recognized multi-component odor is represented at the olfactory cortex?

Experimental evidence indicates that time shift encoding of stimulus intensity occurs not only at the bulb level, but at olfactory cortex level as well (Duchamp-Viret et al., 1996, 1998). This supports the idea that time shift encoding is also used at the 'output level' of the olfactory system, i.e. at the olfactory cortex. It also indicates that the mechanism of this encoding could be similar to the one at the olfactory bulb.

However, most of the olfactory pattern recognition models do not make use of temporal encoding and temporal processing. In such models the patterns to be recognized are ordinary time independent vectors that represent certain odor qualities. Those vectors are then recognized by one of the classical pattern recognition techniques, which do not have much in common with biological temporal processing.

Temporal encoding and temporal processing have only recently been included in the olfactory pattern recognition modeling. Significant progress in this direction has been made by White et al. (1998). In their model vapor identity is encoded by the spatial code across output units, and vapor intensity is represented by response latency. The system is not only biologically relevant (at some extent), but also proved to be more effective than classical neural networks models. Its percentage of correctly identified test patterns was higher than the one of the feed-forward neural network with hidden layer (82% and 71% correspondingly) (White et al., 1998).

However, the model of White et al. is not complete. Odor intensities are encoded just qualitatively: shorter response latency signifies greater concentration (and vice versa), but no precise functional correspondence exists between response latency and odor concentration. Moreover, the model as it is shown in (White et al., 1998) works only in the very narrow range of relative concentrations. Our proposed model implements precise functional encoding of the pattern intensity, that is odor concentration, with the phase shifts of the output neuron firing. The odor recognition remains invariant within broad range of concentrations due to the Hopfield's logarithmic intensity encoding.

2. Model

Our network consists of one layer of m leaky integrate-and-fire neurons fully connected with n temporal inputs. These inputs simulate spatio-temporal patterns formed in the olfactory bulb (Figure 1(a)), and the neural layer (Figure 1(b)) corresponds to the olfactory cortex that receives and recognizes those patterns. The periodic inputs $s_j(t)$ for $j = 1, \ldots, n$ are expressed by Dirac delta function:

$$s_j = \beta \sum_{k=1}^{\infty} \delta(t + \varphi_j - kT) \tag{3}$$

where T is the period of the signal's oscillation. The time advance φ_j of a periodical input spike can be expressed in terms of its phase advance ϕ_j related to the reference

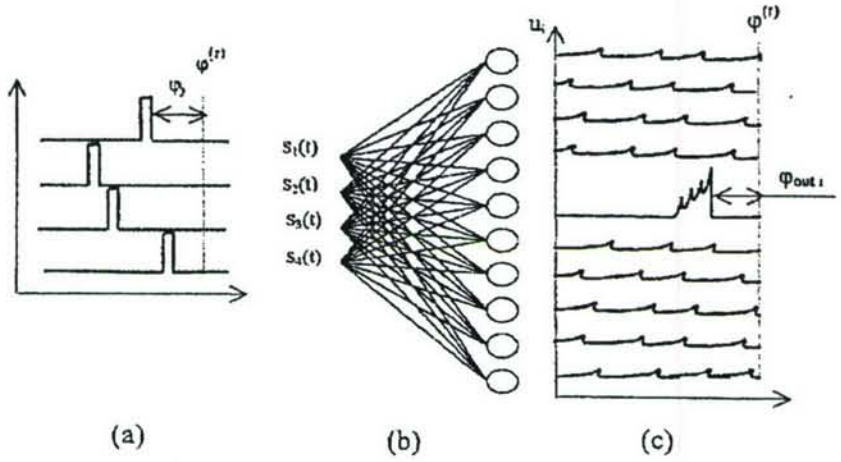

Figure 1. Pattern formation and encoding in the olfactory system model: (a) synthetic input pattern where $s_j(t)$ are the input signals, φ_j – phase shift of the input signals, $\varphi^{(r)}$ – reference phase as in Equation (1); (b) network of integrate and fire neurons; (c) output pattern: u_i – membrane potential of the output neurons.

phase $\phi^{(r)}$ (which corresponds to the zero time advance) as: $\varphi_j = \phi_j/\omega$, where $w = 2\pi/T$. In order to distinguish periodical time advances of the input spikes from the constant time delays stored in the network, further in the paper we will call the time advances φ_j as the phase shifts φ_j, related to the reference phase $\varphi^{(r)}$. Thus, the phase shifts φ_j of the signal's spikes encode concentrations of the n corresponding constituent molecules (2). An example of input pattern is shown at Figure 1(a).

During each cycle the spikes arrive to the neural layer with the delays equal to their phase shifts φ_j. Then the spikes acquire additional time delays d_{ij} stored in the synaptic connections. So, the total time delays of the signals that arrive to ith neuron are equal to $\varphi_j + d_{ij}$.

Each neuron in the layer (Figure 1(b)) is characterized by its state–membrane potential u_i, $(i = 1, \ldots, m)$. Every time a neuron receives a spike, its potential u_i is increased by the weighted value of that input spike: $w_{ij}s_j(t - d_{ij})$. At the same time the potential u_i is constantly decreasing with decay coefficient k as follows:

$$\frac{du_i(t)}{dt} = -ku_i(t) + \sum_{j=1}^{n} w_{ij}s_j(t - d_{ij}) \tag{4}$$

When the potential of a neuron reaches its threshold value u_{thresh}, neuron fires (Figure 1(c)), and its potential u_i is instantly reset to 0 as shown below.

$$u_i(t^-) = u_{\text{thresh}} \Rightarrow u_i(t^+) = 0 \tag{5}$$

The coefficient β in (3), that is equal to u_{thresh}/n, scales the value of input spikes. So, only all spikes added together are able to increase the value of potential to u_{thresh}. As well as the membrane potential u_i is constantly decreasing (4), the spikes that arrive with big time intervals one after another fail to significantly increase the potential's

value. They have to arrive within a narrow time interval (almost simultaneously) to the neuron in order to increase its value to u_{thresh}. Odor patterns are stored in the network memory by the delays d_{ij} between inputs and the neurons. The delays are set in such a way to make each of n spikes arrive simultaneously to the neuron if the applied pattern is equal to the pattern stored:

$$d_{ij} = \varphi_{st\,j}^{(i)} - \min_j\{\varphi_{st\,j}^{(i)}\} \tag{6}$$

where $\varphi_{st}^{(i)}$ is a phase vector of ith stored pattern.

When a stored odor pattern is applied, the total input $\sum_{j=1}^{n} w_{ij}s_j(t - d_{ij})$ to the neuron i has to be equal to or more than u_{thresh} in order to increase the membrane potential u_i by this value and make it fire (Figure 1c). So the weights have to be determined as follows:

$$w_{ij} \geqslant \frac{u_{\text{thresh}}}{\sum_{j=1}^{n} s_j(t - d_{ij})} \tag{7}$$

The neuron fires simultaneously with the last arriving spike, so the phase shift of the output spike is equal to the minimal input phase shift (or phase shift of the weakest component), as shown in Figure 2.

If the pattern applied is not close enough to any of stored odor patterns (of any concentration) spikes arriving with significant time intervals will not make output neuron fire because of its exponential decay. Output potentials in Figure 1(c) show a superthreshold firing of neuron #5 with the phase shift $\varphi_{\text{out}\,i}$ and subthreshold activity of all other neurons. This indicates that odor #5 with some concentration is recognized.

Due to logarithmic scaling in Equation (2) the global phase of the entire pattern is shifted when the odor concentration is changed, while the relative phase shifts remain

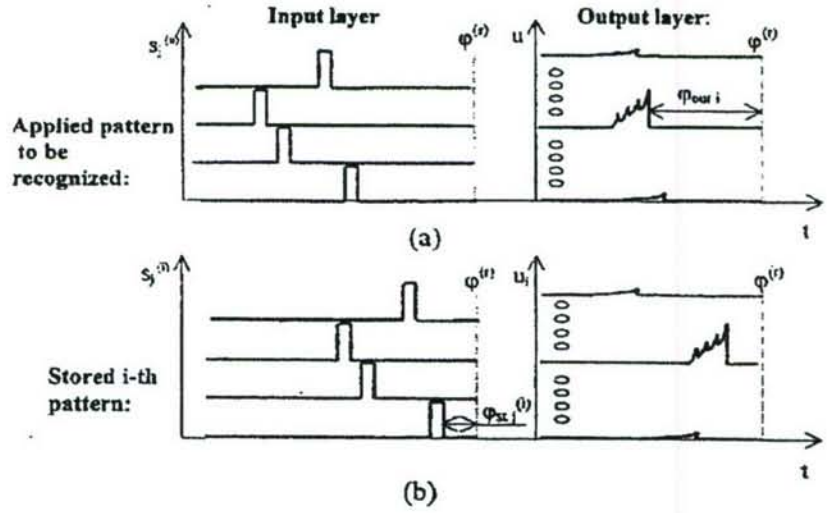

Figure 2. Recognition of the patterns of the same odor with different concentrations.

the same. This makes pattern recognition of the model invariant to the different concentrations of the same odor. Figure 2 shows an example of two patterns of the same odor with different concentrations. Phase shift of the entire pattern (a) is greater than of the pattern (b), though the pattern itself is the same. Thus, the output spike phase shift at (a) is greater than at (b). So, the odor concentration of the pattern (a) is greater.

Concentration of entire odor $c_{\text{out}\,i}$ is defined as relative concentration of odor applied to the corresponding odor stored. This concentration is decoded from the output spike phase shift $\varphi_{\text{out}\,i}$ and the minimum phase shift of the corresponding stored pattern $\min_j\{\varphi_{st\,j}^{(i)}\}$ (Figure 2) by the inverse function of Hopfield's encoding.

$$c_{\text{out}\,i} = \delta \exp[(\varphi_{\text{out}\,i} - \min_j\{\varphi_{st\,j}^{(i)}\})/\alpha] \tag{8}$$

3. Simulation Results

In our computational simulation the stimuli are 4-dimensional ($n = 4$) concentration vectors C (as defined above). Four input neurons produce the spatio-temporal patterns that correspond to the applied stimuli. 10 output neurons ($m = 10$) correspond to 10 stored odors. The concentration of their components varied from 1 (threshold concentration) to 10. Concentration of the components of the odors tested varied from 1 to 70.

Two basic parameters were to be optimized during the simulation: exponential decay coefficient k (4) and corresponding weights w_{ij} (7). The system is quite sensitive to both of them. With w_{ij} determined by Equation (7) with the equality sign, or with decay coefficient $k \gg 1$, the system can recognize undistorted stored patterns only. When weights increase or k decreases the network becomes more flexible (the receptive regions of the neurons get larger). However, the greater the receptive region, the worse the system accuracy is. So, certain compromise had to be found. For our system the highest success rate of recognition (shown in Table I) was achieved with $k = 6.3$, and $w_{ij} = 1.32$, $\forall i, j$. Period T and threshold u_{thresh} were arbitrary selected as follows: $T = 50$, $u_{\text{thresh}} = 1$. The coefficients α and δ define the scale of the transformation (2). They were chosen as: $\alpha = 10$, $\delta = 1$, that makes the maximum phase difference of the spikes (that is $T = 50$) correspond to the relative concentration of the odor components equal to 150.

Example of a simulated input pattern is shown at Figure 3(a). This signal is a repeating sequence of four spikes corresponding to applied odor {63, 96, 48, 10}

Table I. Characteristics of the model performance

Patterns applied	5000
Odors recognized	10.3%
Successful recognition	81%
Incorrect recognition	19%

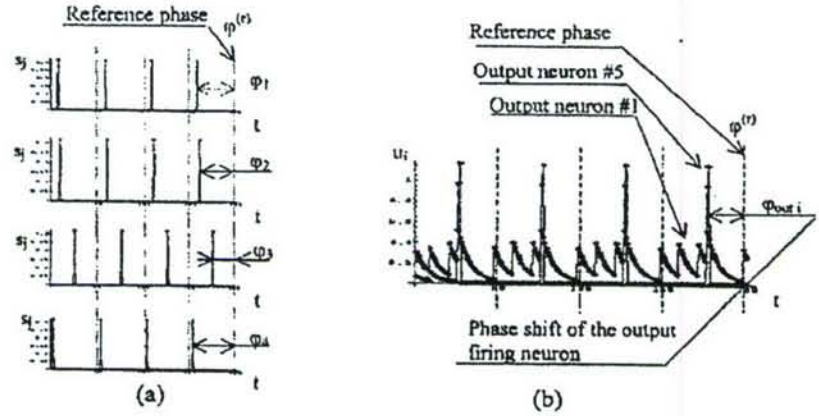

Figure 3. Simulated input and output patterns: (a) input pattern of an example odor (63, 96, 48, 10); (b) Output patterns of the 1st, and 5th neurons (both are shown on the same picture). There is a superthreshold firing of the neuron #5, and substhreshold activity of neuron #1. Odor #5 is recognized.

which was chosen for illustration purpose. Figure 3(a) shows the activity patterns of two neurons. Only neuron #5 reaches the threshold and fires. This indicates successful recognition of odor #5. Neuron #1 does not reach the firing level, so the odor #1 is not recognized.

In our experiment 5000 randomly generated test odors have been presented to the system. A total of 89.7% of them caused the output neurons to produce the subthreshold activity only (odors were not recognized). A total of 10.3% of the test-stimuli provoked superthreshold firing of output neurons (odors were recognized). A total of 81.0% of them were recognized correctly (both odor and concentration), with allowed concentration error equal to 20%.

For the sake of testing the proposed model, each applied odor is projected onto the distance–concentration coordinate system. The purpose of the test is to determine if our model correctly classifies an input odor as resembling one of the stored odors, or leaves the input odor unclassified if it does not resemble any of them. The resemblance is expressed using a metric introduced in the Appendix. The stored odors have a certain distribution in the concentration space. The distance D between the arbitrary input odor and its closest neighbor amongst the stored odors allows for testing our model.

The inputs that caused an output to fire are indicated as points in Figure 4(a). Majority of these points are gathered in the region of small D with various concentrations. This indicates that the odors which caused an output to fire were indeed close to one of the stored odor patterns. The concentration level of the input odor does not affect the models ability to classify the input as one of the known odor patterns.

On the other hand, all other input odors which did not cause an output to fire are shown as points in Figure 4(b). These points tend to have large values of distance function D. Any input odor that is too far from all of the stored patterns fails to

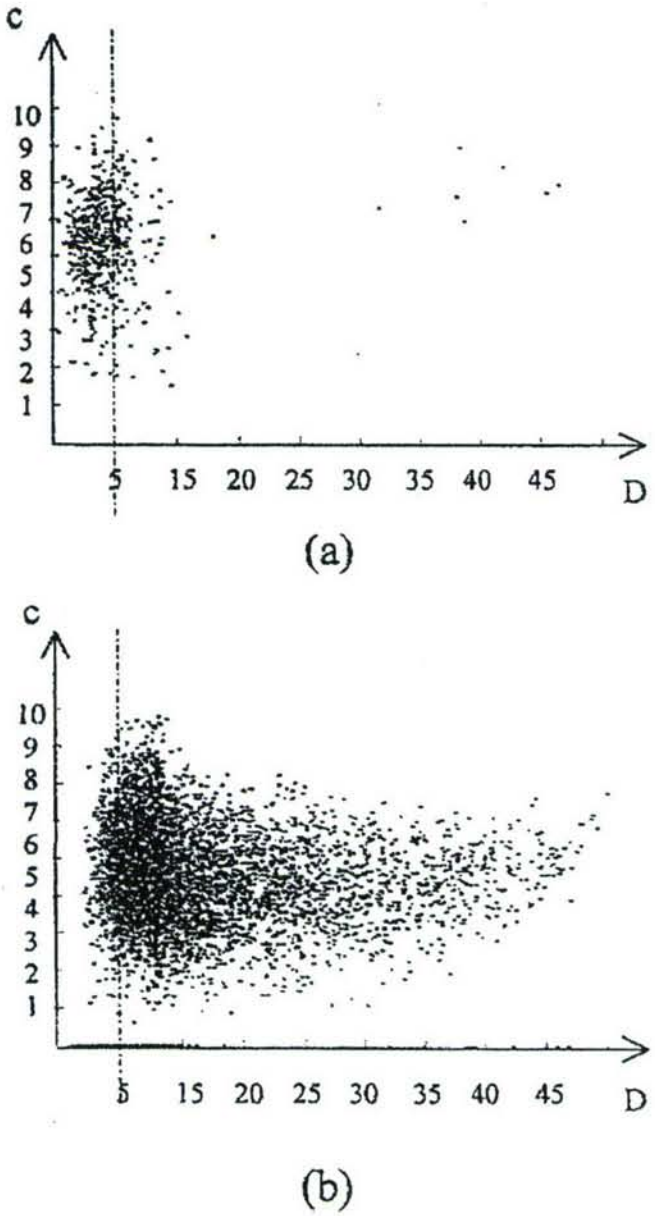

Figure 4. Distribution of the simulation results. (a) Patterns correctly recognized. (b) Patterns that are not recognized.

activate the model outputs. Even strongly concentrated odors stay unclassified if they lack resemblance to one of the stored patterns.

In order to compare Figure 4(a) and (b) a vertical division line is drawn. The line separates the classified points from the unclassified ones in terms of the distance

value D. Points to the left from the line manifest a resemblance to one of the stored pattern odors and hence activate the output of the model. Most of the points stay on the right side of the division line, as no stored pattern claims such resemblance. Remarkably, the division line is vertical, which means that Hopfield's principle works well separating the odor 'flavors' from their concentrations.

4. Discussion and Conclusion

Recognition of a single pattern is only one of the first stages of sensory information processing. The higher-level problems of multi-pattern processing, such as object recognition in real world, feature binding and segmentation, object-background separation, attention focusing, etc. are much more difficult to model and they are far from being handled by modern computational methods. However, all these tasks are efficiently performed by cortical neural networks of animals and humans, where different temporal correlation types are believed to be the underlying principle of these abilities (Campbell and Wang, 1998; Malsburg and Buhmann, 1992; Malsburg and Schneider, 1986).

Temporal correlation plays an essential role in olfactory systems as well. Experimental results prove that several odors in a mixture are separated temporally from each other at some of the higher levels (Jinks and Laing, 1999). One of the possible ways to do such a temporal segregation is using temporal correlation and competition of output neurons (or neural ensembles) and inhibitory top-down feedback to input level in order to temporally segregate recognition of different odors, suppress noise or irrelevant inputs and focus attention on the necessary odor (Campbell and Wang, 1998; Malsburg and Buhmann, 1992; Malsburg and Schneider, 1986). Phase encoding, that is a specific example of temporal correlation is the basic principle of our model and we believe it provides the base for the solution of the higher level processing tasks presented above.

Appendix

This section introduces the transformation of odor vectors to the distance-concentration space. Each component c_j of applied odor vector, C, is logarithmically transformed as in (2) to the corresponding components φ_j of phase vector φ. In the same way m stored vectors $c_{st}^{(i)}$, $i = 1, \ldots, m$ are transformed to m vectors $\varphi_{st}^{(i)}$, where $\varphi_{st}^{(i)} = \{\varphi_{stj}^{(i)}, j = 1, \ldots, n\}$.

Vectors $\varphi_{st}^{(i)}$ and φ are normalized in the phase space in the following way:

$$\varphi_{st}^{(i)*} = \{\varphi_{stj}^{(i)} - \min_j\{\varphi_{stj}^{(i)}\}, j = 1, \ldots, n\} \tag{9}$$

$$\varphi^* = \{\varphi_j - \min_j\{\varphi_j\}, j = 1, \ldots, n\} \tag{10}$$

Each applied and then normalized phase vector $\varphi^* = \{\varphi_j, j = 1, \ldots, n\}$. is characterized by its distance D to the closest of the $\varphi_{st}^{(i)*}$. This distance D is defined as:

$$D = \min_i \{\|\varphi^* - \varphi_{st}^{(i)*}\|\} \tag{11}$$

Thus D defines distance in the phase space from the vector applied to the closest of the stored vectors.

Acknowledgements

This work was sponsored in part by the Department of the Navy, Office of Naval Research, Grant N000 14-01-1-0630. The content of this information does not necessarily reflect the position of the government.

References

Campbell, S. and Wang, D.: Synchrony and desynchrony in integrate-and-fire oscillators. *Proceedings of the IEEE International Joint Conference on Neural Networks*, Anchorage, Alaska, **2** (1998), 1498–1503.

Duchamp-Viret, P. and Palouzier-Paulignan, B. and Duchamp A.: Sensory information processing in the frog olfactory pathways. Experimental basis for modeling studies. *Biosystems*, **48** (1998), 37–45.

Duchamp-Viret, P. and Palouzier-Paulignan, B. and Duchamp A.: Odor coding properties of frog olfactory cortical neurons. *Neuroscience*, **74** (1996), 885–895.

Hopfield J.: Pattern recognition computation using action potential timing stimulus representation. *Nature*, **376** (1995), 33–36.

Hoshino, O. and Kashimori, Y. and Kambara, T.: An olfactory recognition model based on spatio-temporal encoding of odor quality in the olfactory bulb. *Biological Cybernetics*, **79** (1998), 109–120.

Jinks, A. and Laing, D.: Temporal processing reveals a mechanism for limiting the capacity of humans to analyze odor mixtures. *Cognitive Brain Research*, **8** (1999), 311–325.

Laurent, G. and Davidowitz, H.: Encoding of olfactory information with oscillating neural assemblies. *Science*, **265** (1994), 1872–1875.

Laurent G.: Dynamical representation of odors by oscillating and evolving neural assemblies. *Trends in Neuroscience*, **19** (1996), 489–496.

Malsburg, C. von der, Buhmann, J.: Sensory segmentation with coupled neural oscillators. *Biological Cybernetics*, **67** (1992), 233–242.

Malsburg, C. von der, Schneider W.: A neural cocktail-party processor. *Biological Cybernetics*, **54** (1986), 29–40.

Natschlager, T. and Ruf, R.: Spatial and temporal pattern analysis via spiking neurons. *Network*, **9**(3) (1998), 319–332.

Ressler, K. and Sullivan, S. and Buck, L.: Information coding in the olfactory system: evidence for a stereotyped and highly organized epitope map in the olfactory bulb. *Cell*, **79** (1994), 1245–1255.

Skarda, C. and Freeman, W.: How brains make chaos in order to make sense of the world. *Behavioral and Brain Sciences*, **10** (1987), 161–195.

White, J. and Dickinson, T. and Walt, D. and Kauer, J.: An olfactory neuronal network for vapor recognition in an artificial nose. *Biological Cybernetics*, **78** (1998), 245–251.

Signal Processing With Temporal Sequences in Olfactory Systems

Andrzej G. Lozowski, *Member, IEEE*, Mykola Lysetskiy, *Student Member, IEEE*, and Jacek M. Zurada, *Fellow, IEEE*

***Abstract*—The olfactory system is a very efficient biological setup capable of odor information processing with neural signals. The nature of neural signals restricts the information representation to multidimensional temporal sequences of spikes. The information is contained in the interspike intervals within each individual neural signal and interspike intervals between multiple signals. A mechanism of interactions between random excitations evoked by odorants in the olfactory receptors of the epithelium and deterministic operation of the olfactory bulb is proposed in this paper. Inverse Frobenius–Perron models of the bulb's temporal sequences are fitted to the interspike distributions of temporally modulated receptor signals. Ultimately, such pattern matching results in ability to recognize odors and offer a hypothetic model for signal processing occurring in the primary stage of the olfactory system.**

***Index Terms*—Frobenius filter, interspike intervals, inverse Frobenius problem, Markov process, odorant concentration, olfactory bulb, shift map, temporal sequence.**

I. Introduction

LIVING organisms perceive odors as sensations caused by mixtures of odorant molecules. Such molecules excite the olfactory receptors to respond with increased activity which is then passed on to the olfactory bulb for detection. Various odorant molecules excite different groups of receptors. A superposition of these excitations constitute the odor as detected by the olfactory bulb [1]. The relative concentrations of individual components constitute the odor type, whereas the absolute concentrations determine the odor intensity. The olfactory bulb has the task of transforming the input obtained from the receptors into a set of signals to be interpreted by the brain. The capacity of a simple discriminator to distinguish the target from background odorants has been statistically analyzed in [2].

The continuous quantities, such as molecule concentrations, cannot be directly represented by the signals produced by biological neurons. Neurons produce spikes and only indirectly their presence or absence, or time location may carry continuum of information. The nature of *neural signals* is assumed to have the following characteristics.

1) There is no significance of the shape of individual spikes. They simply mark instances of time when the neurons fire.
2) The signal is a time sequence of spikes. Spikes may occur more or less frequently which has an effect on the average value of the signal.
3) Spikes may occur in a certain temporal pattern. More precisely, the inter-spike intervals may follow a distinct and repetitive behavior. This allows for code division of information conveyed by a single signal.
4) Two or more signals may exhibit cross correlation which typically results from synchronization between the signal sources. If the synchronized signals assume a certain spatial distribution, a set of such signals will manifest a spatio-temporal pattern.

The neural signals of the olfactory bulb representing the information about odors and intensities are further interpreted by the brain. The olfactory bulb functions as the first signal processing stage. In all nonbiological designs the first stage is responsible for the sensitivity and noise performance of the entire detection system. The same should hold true in case of the olfactory bulb. A very detailed investigation of neuronal noise and spike propagation can be found in [3].

The goal of this article is to identify the simplest method of encoding odor information in temporal sequences. The input–output interactions between temporal sequences can lead to an odor detection and encoding mechanism in the olfactory bulb.

II. Temporal Modulation [1]

The very input of the olfactory system, the epithelium, produces an enormous number of signals. Receptors are hard-wired to detect specific odor components and are uniformly distributed in the epithelium. The odor information is therefore, spatially distributed across the epithelium and is assumed to have no temporal dependency. Every odor and concentration can be represented by its "black and white photo" in which the gray levels of pixels encode spiking activities of the receptors. In this paper, the odor information is assumed to be spatially distributed and static, although there is a strong evidence of various significant aspects of the inhale–exhale rhythm and the impulse response of the olfactory bulb [5].

No temporal coding of information is performed by the individual receptors. Simply, the more molecules are present at the docking sites of the receptors, the more frequent their spiking. Based on response measurements and fitting of concentration-response curves presented in [6] and [7], the spiking frequency f of the receptors has an asymptotic dependency on the odorant concentration c (molarity). When the odorant concentration is

[1]Term temporal modulation is adopted from [4].

Manuscript received June 20, 2003; revised January 8, 2004. This work was supported by the U.S. Department of Navy Office of Naval Research under Grant N00014-01-1-0630.

A. G. Lozowski is with the Department of Electrical and Computer Engineering, Southern Illinois University, Edwardsville, IL 62026 USA.

M. Lysetskiy and J. M. Zurada are with the Department of Electrical and Computer Engineering, University of Louisville, Louisville, KY 40208 USA.

Digital Object Identifier 10.1109/TNN.2004.832730

at the lowest detectable level $c = c_t$, the receptor fires at the very slow rate of spontaneous activity. When the concentration grows infinitely large, the frequency reaches saturation at the maximum firing rate of f_m. The curve $f(c)$ fits the following definition:

$$f = \frac{2}{\pi} f_m \arctan \beta(c - c_t). \tag{1}$$

The slope factor β is expressed in terms of the dynamic range Δc defined as the odor concentration at which the frequency reaches 80% maximum, $f(c_t + \Delta c) = 0.8 f_m$. Given the dynamic range, the slope factor can be determined as $\beta = \tan(0.8\pi/2)/\Delta c$.

Concentration c, used in [6] and [7], is a logarithmic quantity related to the odorant molarity $c = \log m$, with m in mol/l. The investigated odorants were anisole (ANI), camphor (CAM), isoamyle acetate (ISO), and limonene (LIM). The curve fitting resulted in the following parameters for each odorant [6]:

	ANI	CAM	ISO	LIM
f_m	11 Hz	15 Hz	11 Hz	8 Hz
c_t	−6.7	−8.6	−7.0	−7.7
Δ_c	1.1	1.1	0.5	0.3.

Remarkably, linear curves are obtained if instead of spiking frequency f, the interspike intervals $\tau = 1/f$ are graphed versus the reciprocal of molarity, referred to as *sparsity* s. Since different odorants may have largely different molarity threshold levels $c_t = \log m_t$, the reciprocal of the incremental molarity $s = 1/(m - m_t)$ rather than the absolute value can be used in the joint graph for various odorants. The parametric representation of relationship (1) in the new coordinates (s, τ) for the introduced odorants is shown in Fig. 1. The horizontal and vertical axes are the incremental sparsity s and the interspike interval τ expressed in terms of molarity m as follows:

$$s(m) = \frac{1}{m - m_t} \tag{2}$$

$$\tau(m) = \left(\frac{2}{\pi} f_m \arctan \beta \log \frac{m}{m_t} \right)^{-1}. \tag{3}$$

As can be seen in the figure, diluting the odorant in the air increases the interspike intervals at an approximately constant rate. This may be regarded as temporal modulation with the conversion gain $G = d\tau/ds$, which is the slope of the line. The left side of each curve corresponds to the receptor saturation region. By extrapolating the curves to the intersections with the vertical axis, a minimum interval τ_0 for each receptor type can be found of value roughly around 100 ms. This minimum interval may be regarded the refractory period of the receptor. With just two parameters τ_0 and G for each receptor type, the temporal modulation illustrated in Fig. 1 can be readily described using first-order approximation:

$$\tau = \tau_0 + Gs. \tag{4}$$

The approximation can be validated only within the dynamic range of the receptor, that is, outside the saturation $s > 1/(m_t 10^{\Delta c})$.

III. Odor Characterization With Interspike Distributions

An odor is a superposition of a number of basic odorants. The concentration information is temporally modulated at the glomerular inputs of the olfactory bulb, therefore, the perception of odor intensity must be related to the interspike intervals. Increasing the odor intensity shortens the intervals at different rates for each basic odorant due to the differences in their conversion gains. This provides some explanation why responses of the mitral outputs can be different for the same odor at different intensities [8].

In the glomerular layer the enormous number of inputs converge into much less dimensional connections to the mitral cells. The glomeruli are also highly interconnected between each other via periglomerular interneurons [9]. Both inhibitory and excitatory connections are present within the glomeruli which indicates that a winner-take-all mechanism could be involved before the input to the mitral cells. The presence of such a mechanism would enable arranging of the input interspike intervals into distributions statistically representing the odor information.

Let R be the number of all types of receptors in the epithelium. This makes R also the number of distinct basic odorants, the basis for the odor space. Suppose the first four, out of all R odorants, are the ones shown in Fig. 1. An odor at a given intensity can be uniquely represented by a vector $\boldsymbol{s}$ of sparsities of the basic odorants. For instance, an odor created by mixing 0.5 mol of CAM and 0.75 mol of LIM with 100 Ml of air would be represented by vector $\boldsymbol{s} = (\infty, 50, \infty, 75, \infty, \ldots, \infty)$ Ml/mol. Vector $2\boldsymbol{s}$ would represent the same mixture diluted in twice the amount of air. In general, an odor, as seen by the epithelium, is $\boldsymbol{s} = (s_1, s_2, \ldots, s_R)$. Terms "vector" and "basis" are understood to be suitable ways to arrange numbers rather than the strictly defined terms used in linear spaces.

A much more compressed way to describe odors is through distributions of interspike interval probabilities. This formalism may also be more relevant to the signals presented to the mitral inputs. Let the interspike intervals be quantized into N ranges with cutoff $\tau_{\max}$. Interval $\tau_{\max}$ is considered to be a borderline between evoked and spontaneous activity of the receptors. A single neural signal can represent an odor with the interspike interval τ probability distribution $\boldsymbol{p} = (p_1, p_2, \ldots, p_N)$, which is formally a vector of probabilities

$$p_n = \begin{cases} \Pr\left(\frac{n-1}{N}\tau_{\max} < \tau \le \frac{n}{N}\tau_{\max}\right), & \text{if } n < N \\ \Pr(\tau_{\max} < \tau), & \text{if } n = N. \end{cases} \tag{5}$$

The quantized representation of the interspike interval distribution is chosen because it is more suitable for numeric computations than the probability density function. A satisfactory approximation of continuum can be achieved provided that N is large enough.

Suppose the 0.5 mol of CAM and 0.75 mol of LIM mixture with 100 Ml of air, indicated by the filled squares in Fig. 1, is presented to the olfactory epithelium. Two kinds of receptors would be activated, each responding with spikes separated by

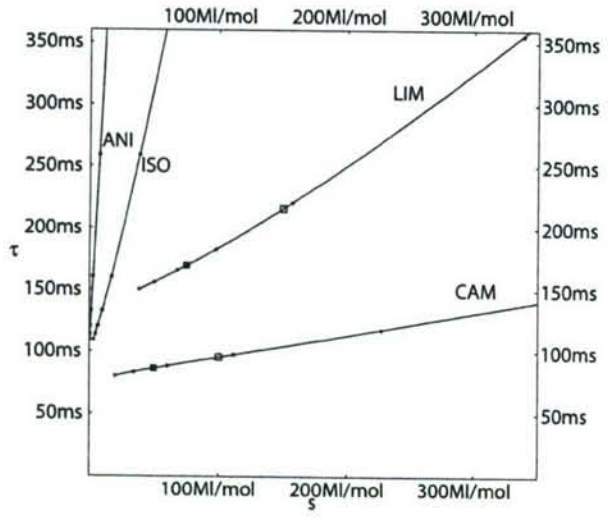

Fig. 1. Interspike intervals τ of receptor firing versus incremental sparsity s of odorant. Six points on each curve correspond to the following logarithmic concentration levels (left-to-right): $1.2\Delta c$, Δc, $0.8\Delta c$, $0.6\Delta c$, $0.4\Delta c$, and $0.2\Delta c$ above c_t. The axes units are ms and Ml/mol.

roughly 90-ms intervals and 175-ms intervals, respectively, according to Fig. 1. Suppose also that there is twice as many LIM receptors as those detecting CAM. In the winner-take-all competitions, the LIM receptors would have a better chance passing its signal compared to the CAM receptors. The described odor is represented by the filled bars of interspike interval probabilities in Fig. 2. The probability of the 175 ms LIM intervals is twice the probability of the 90 ms CAM intervals.

Suppose further that the same odor mixture is now diluted in twice the amount of air. This doubles the sparsity of the odor, hence, increasing the interspike intervals of both odorants present in the mixture. The diluted odors are represented in Fig. 2 by the empty bars of probabilities. Now the LIM intervals are about 220 ms and the CAM intervals increased to about 100 ms without a change to the probability levels. Note that the two odorants have different conversion gains and modulate the temporal intervals at different rates. As the odor intensity changes, this changes the probability pattern. A different hypothesis of time advance modulation where the resulting pattern is invariant under the concentration level was introduced in [10] and leads to functional models [11]. However, the neurophysiological evidence suggests that the patterns of bulbar activity actually do change when varying the odor intensity [8].

The signal processing occurring between the mitral cells and glomerular layer is a dynamical process. The information is embedded in the time realizations of signals. It may be retrieved only through observation of these signals for a period of time. The probability distribution of the interspike intervals may be retrieved by statistically analyzing the neural signals. Likewise, a simple stochastic process can be modeled to have the statistical properties representing a given odor through the probability distribution.

Suppose, in steady–state after all the transient response has vanished the odor is represented by the probability distribution $\boldsymbol{p}^*$ defined according to (5). A Markov process [12] with the

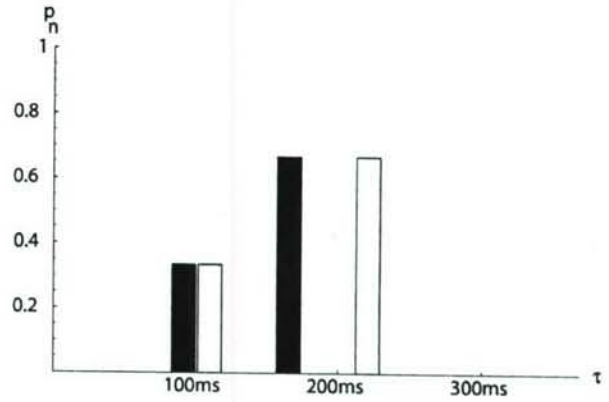

Fig. 2. Odor composed of 0.5 mol of CAM odorant and 0.75 mol of LIM odorant mixed with 100 Ml of air (filled bars) and then diluted in additional 100 Ml of air (empty bars). The bars have width $\tau_{\max}/N$ and represent probabilities of respective time intervals as defined by (5). Example with $N = 20$ and $\tau_{\max} = 350$ ms shown.

invariant distribution equal $\boldsymbol{p}^*$ could serve as a first-order approximation of a dynamical system for that odor. Let $N \times N$ matrix P be the transition matrix of the Markov process

$$\boldsymbol{p}(k+1) = P\boldsymbol{p}(k). \tag{6}$$

Also, let the process converge to $\boldsymbol{p}^*$ in a sense that $\boldsymbol{p}^* = \lim_{k\to\infty} \boldsymbol{p}(k)$ for almost every initial distribution $\boldsymbol{p}(0)$. The invariant distribution is the eigenvector of transition matrix P associated with the unit eigenvalue: $\boldsymbol{p}^* = P\boldsymbol{p}^*$. In this respect, the Markov process is a dynamical system in probabilistic space $S = \{\boldsymbol{p} \in [0;1]^N \big| \sum_n p_n = 1\}$ with a stable fixed point $\boldsymbol{p}^*$. Further on, space S will be referred to as the odor space.

Consequently, an odor may be associated with an operator $P : S \to S$ in the odor space. The odor itself is the stable fixed point of the operator. There is a benefit of such a representation of odors. Operator P defines an odor indirectly through a definition of a dynamical system. It is easy and natural to generate realizations of neural signals using such operators, which is suitable in the modeling effort. There are many operators that have the same invariant distribution. Hence, the same odor information may be redundantly embedded in many different processes. Another approach to representing odors with Markov processes is presented in [13].

Formally, a realization of the introduced Markov process is a sequence of interspike intervals $\{\tau_k\}$. Define the interval range to be $T_n = [(n-1/N)\tau_{\max}; \tau_{\max})$ if $n < N$, and $T_N = [\tau_{\max}; \infty)$ otherwise, where the interval range index n is defined in the same manner as in (5). For the sake of modeling through, optimization, a particular operator P may be developed to have $\boldsymbol{p}^*$ as its invariant distribution of interspike intervals over time. Denote the elements of the operator by P_{ij}, so that $P = [P_{ij}]$, where i and j are the row and column indexes. Number P_{ij} is the probability that in the Markov process (6) an interval from the range T_i will follow the interval from the range T_j:

$$P_{ij} = \frac{\Pr(\tau_{k+1} \in T_i \text{ and } \tau_k \in T_j)}{\Pr(\tau_k \in T_j)}. \tag{7}$$

There is no closed-form formula for selecting P_{ij}s for a given $\boldsymbol{p}^*$. However, starting with some random P_{ij}s, an optimization algorithm can be used to find the P_{ij}s as the minimum of a suitable cost function. Since all P_{ij}s are probabilities, they must be numbers in the unit segment from 0 to 1. This fact allows for constructing one of the components to be included in the cost function, namely, the unit segment potential. For each number P_{ij}, a potential function $v(P_{ij})$, shown in Fig. 3, describes how distant P_{ij} is from the unit segment

$$v(P_{ij}) = \frac{(2P_{ij}-1)^2}{1+(2P_{ij}-1)^{-6}}. \tag{8}$$

Function v attains the minimum in the middle of the unit segment and is maximally flat within the segment. The maximally flat approximation [14] with a rational function is chosen to facilitate the optimization process. The partial costs $v(P_{ij})$ sum up to the cost function component $E_v(P)$ responsible for keeping all the entries of P within the unit segment

$$E_v(P) = \sum_{i=1}^{N}\sum_{j=1}^{N} v(P_{ij}). \tag{9}$$

Operator P is a probabilistic matrix in a sense that all its column vectors are normalized probability distributions. Therefore, the column sums of P must sum up to 1. Another cost function component $E_c(P)$ measures the deviation from this requirement

$$E_c(P) = \sum_{j=1}^{N}\left(1-\sum_{i=1}^{N} P_{ij}\right)^2. \tag{10}$$

If operator P is a well defined transition matrix of Markov process (6), then the cost sum $E_v(P)+E_c(P)$ is low and close to its minimum attainable value. The goal of the cost minimization procedure is to develop operator P with the constraint that $\boldsymbol{p}^*$ is it's principal eigenvector associated with eigenvalue 1. To simplify the operator synthesis, matrix P will be assumed to be diagonalizable: $P = B\Lambda B^{-1}$. The diagonal matrix $\Lambda = \mathrm{diag}(\boldsymbol{\lambda})$ is composed of N eigenvalues $\boldsymbol{\lambda} = (\lambda_1, \lambda_2, \ldots, \lambda_N)$ of P. Let $\lambda_1 = 1$. The convergence rate of the dynamical system (6) heavily depends on the radius of the remaining λ_is for $i > 1$. Operator P is synthesized with random λ_is, for $i > 1$, with the assumption that $|\lambda_i| < r < 1$ and the radius r is kept low to improve the convergence rate. In the numerical experiment r was selected to be equal to 0.2. Operator P is diagonal in the basis constructed with the column vectors of B. Since $\lambda_1 = 1$, the first column vector of B is $\boldsymbol{p}^*$. More precisely, $B_{ij} = p_i^*$ for $j = 1$. All other entries B_{ij}, for $j > 1$, are variables in the optimization process. Their initial values are selected randomly from the uniform distribution in the range $(-1;1)$. Final matrix B is found using an optimization algorithm to minimize the cost function as in the following expression:

$$\min_{B_{ij}|_{j>1}} \left[E_v(P) + E_c(P)\right]. \tag{11}$$

The minimized solution oftentimes needs a final touch to make sure that P has no negative entries, no entries greater than one and that column sums of P are indeed 1. This can be done by zeroing of negative values and normalization of columns. The principal eigenvector of P is not very sensitive to such trimming of P.

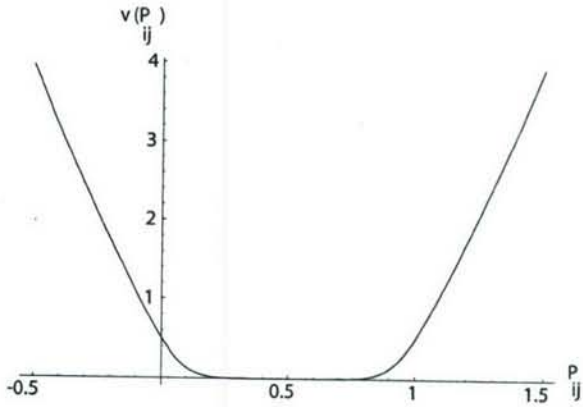

Fig. 3. Unit segment potential function. In the total cost function, numbers $P_{ij} \in [0;1]$ contribute much less than numbers P_{ij} outside this range. Minimization of w will attract all P_{ij}s toward the inside of the unit segment.

IV. Embedding Distributions in Temporal Sequences

As illustrated in the example shown in Fig. 2, the probabilistic representation of odors and intensities fits well the random nature of excitations received from the olfactory epithelium. The Markov model is also a natural candidate for a simple approximation of the dynamics behind spike interactions driven by the receptors. The olfactory bulb, however, should be considered a deterministic system which has no random variables other than the input received from the epithelium. Moreover, the olfactory bulb is capable of self-excitatory activity in response to the input. This may be the factor contributing to both high sensitivity and high selectivity of the sense of smell [15]. From this perspective, it seems reasonable to regard the olfactory bulb as an active medium rather than a passive relay of receptor signals. The olfactory bulb actively produces firing activity in response to the receptor signals [16].

A sequence of interspike intervals complying with a given interval distribution can be generated in a deterministic dynamical system. The simplest such system is a one-dimensional map constructed by solving the inverse Frobenius–Perron problem [17]. The overall goal of the search for a sequence generator is to be able to represent the odor information by a distribution of interspike intervals. A simple shift map can be constructed directly from the probabilistic operator used in approximation (6), as described in detail in [18].

First, a piecewise linear map $f : [0;N] \to [0;N]$, $[0;N] \subset R$ is derived from probabilities included in the operator P

$$f(x) = \frac{1}{P_{ij}}\left(x - j + \sum_{m=1}^{i} P_{mj}\right) + N - i,$$
$$\text{if } j - \sum_{m=1}^{i} P_{mj} \le x < j + P_{ij} - \sum_{m=1}^{i} P_{mj}. \tag{12}$$

As shown in Fig. 4, map f is composed of N^2 linear segments corresponding to N^2 numbers P_{ij}. The slopes of the segments are simply $1/P_{ij}$. To evaluate $f(x)$, the pair of indexes i and j

appropriate for a given x needs to be identified using the condition provided by (12).

By scaling the domain and range of map f, the dynamical system generating temporal sequence $\{\tau_k\}$ can be defined with the help of shift map h

$$h(\tau) = \frac{\tau_{\max}}{N-1} f\left(\frac{N-1}{\tau_{\max}}\tau\right). \tag{13}$$

Regardless of the initial condition chosen, subsequent mappings with h will determine sequence $\{\tau_k\}$ whose distribution of values converges to the invariant distribution of process (6). A deterministic dynamical system

$$\tau_{k+1} = h(\tau_k) \tag{14}$$

may be regarded as a generator of realizations of neural signals for a given distribution of interspike intervals.

A numeric example of shift-map synthesis is shown in Fig. 5. Three interspike-interval distributions $\boldsymbol{p}_A^*$, $\boldsymbol{p}_B^*$, and $\boldsymbol{p}_C^*$ are selected randomly to characterize three hypothetical odors A, B, and C. The bars represent probabilities p_n of respective time intervals as defined by (5). The horizontal axis is normalized such that interval $N\tau_{\max}/(N-1)$ corresponds to 1. Shift maps h_A, h_B, and h_C are evaluated for the example odors and shown in the middle row of figures also in time-normalized coordinates. The maps have N disconnected branches, however, vertical lines connecting the branches are added to enhance the graphs. Starting with a random initial interval, each map iterated 3000 times according to (14) produced a temporal sequence. The sequences are shown in the bottom row of figures. Each interval in a sequence is indicated as a point whose vertical coordinate is the normalized time. This way the density of points reflects the original distribution plots if rotated clockwise by 90°.

V. Frobenius Filter for Temporal Sequences

It is broadly accepted that the olfactory bulb provides support for a pattern recognition mechanism for odor detection and classification. Not all of the recognition is taking place there, but definitely the process is initiated in the olfactory bulb. Assuming that the temporal sequences of interspike intervals are carriers of odor information, an implementation of signal processing system (14) can be proposed. Ultimately, the goal is to demonstrate usefulness of the proposed mechanism in odor recognition.

The signal processing scheme shown in Fig. 6 will be referred to as the Frobenius filter. The input to the filter is a temporal sequence whose interspike intervals are determined by the random variable τ_{in} with values governed by the probability distribution $\boldsymbol{p}_{\text{in}}$ defined as in (5). Distribution $\boldsymbol{p}_{\text{in}}$ characterizes an odor.

The Frobenius filter is simply a shift map with the feedback loop controlled by a random switch. The switch operation is described by a two-valued stochastic process $\xi : \{0,1\} \times N \to R$. The filter is producing time intervals based on the switch position. At every interval k, the switch position depends on the value of ξ_k governed by probabilities

$$\Pr(\xi_k = 1) = c \tag{15}$$

$$\Pr(\xi_k = 0) = 1 - c \tag{16}$$

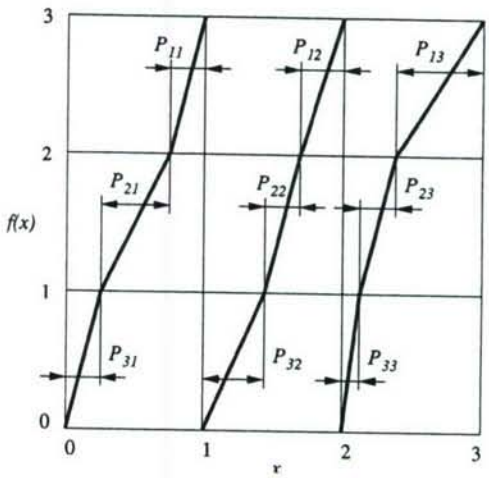

Fig. 4. Example of a piecewise linear shift map $f(x)$. Function f is composed of N continuous branches $f_j : [j-1; j) \to [0; N]$. If x is chosen randomly from the uniform distribution over the range $(0; N)$, the conditional probability P_{ij} that $f(x) \in (i-1; i)$ given the fact $x \in (j-1; j)$ can be evaluated by $P_{ij} = \|f_j^{-1}([i-1; i])\|$. Example with $N = 3$ shown.

where $c \in [0; 1]$ is a constant parameter. When $\xi_k = 1$, the filter is receiving the input τ_{in}. The opposite position of the switch ($\xi_k = 0$) lets the shift map determine the output time interval based on the previous interval as in (14). The overall filter equation reads

$$\tau_{k+1} = h\left[\xi_k \tau_{\text{in}} + (1 - \xi_k)\tau_k\right]. \tag{17}$$

The notion of the switch is an attempt to model a competition between the input and the feedback. Its random operation is inherited from the random nature of the input temporal sequence.

The three shift maps h_A, h_B, and h_C, introduced in Fig. 5, are used to illustrate the function of the Frobenius filter. Each of the shift maps was stimulated at the input by values generated by probability distributions $\boldsymbol{p}_A^*$, $\boldsymbol{p}_B^*$, and $\boldsymbol{p}_C^*$ representing three different odors. Fig. 7 shows all possible input-filter combinations arranged in the following nine pairs:

$$\begin{array}{lll} (\boldsymbol{p}_A^*, h_A) & (\boldsymbol{p}_B^*, h_A) & (\boldsymbol{p}_C^*, h_A) \\ (\boldsymbol{p}_A^*, h_B) & (\boldsymbol{p}_B^*, h_B) & (\boldsymbol{p}_C^*, h_B) \\ (\boldsymbol{p}_A^*, h_C) & (\boldsymbol{p}_B^*, h_C) & (\boldsymbol{p}_C^*, h_C). \end{array} \tag{18}$$

In each instance, $K = 20\,000$ values random values τ_{in} were drawn from the input distribution and applied with probability $c = 0.5$ to the filter. The values drawn were also sorted in the ascending order and stored. In the sorted input sequence $\{u_i\}$ the following property holds: $i < j \Rightarrow u_i \leq u_j$. When plotted, the graph of the sorted sequence would resemble the shape of the cumulative distribution function of the random variable τ_{in}.

The realization of the sequence $\{\tau_k\}$ generated by the Frobenius filter for K iterations were also sorted in the same manner. The sorted output sequence $\{t_i\}$ was then compared to the sorted input sequence in Fig. 7. More precisely, the graphs in the figure are the sequences of quadratic distances $\{(u_i - t_i)^2\}$ in each of the nine instances. The horizontal line is the mean-square value of the distance $\overline{(u_i - t_i)^2}$. As seen in the figure, the input-output sequences generated in pairs

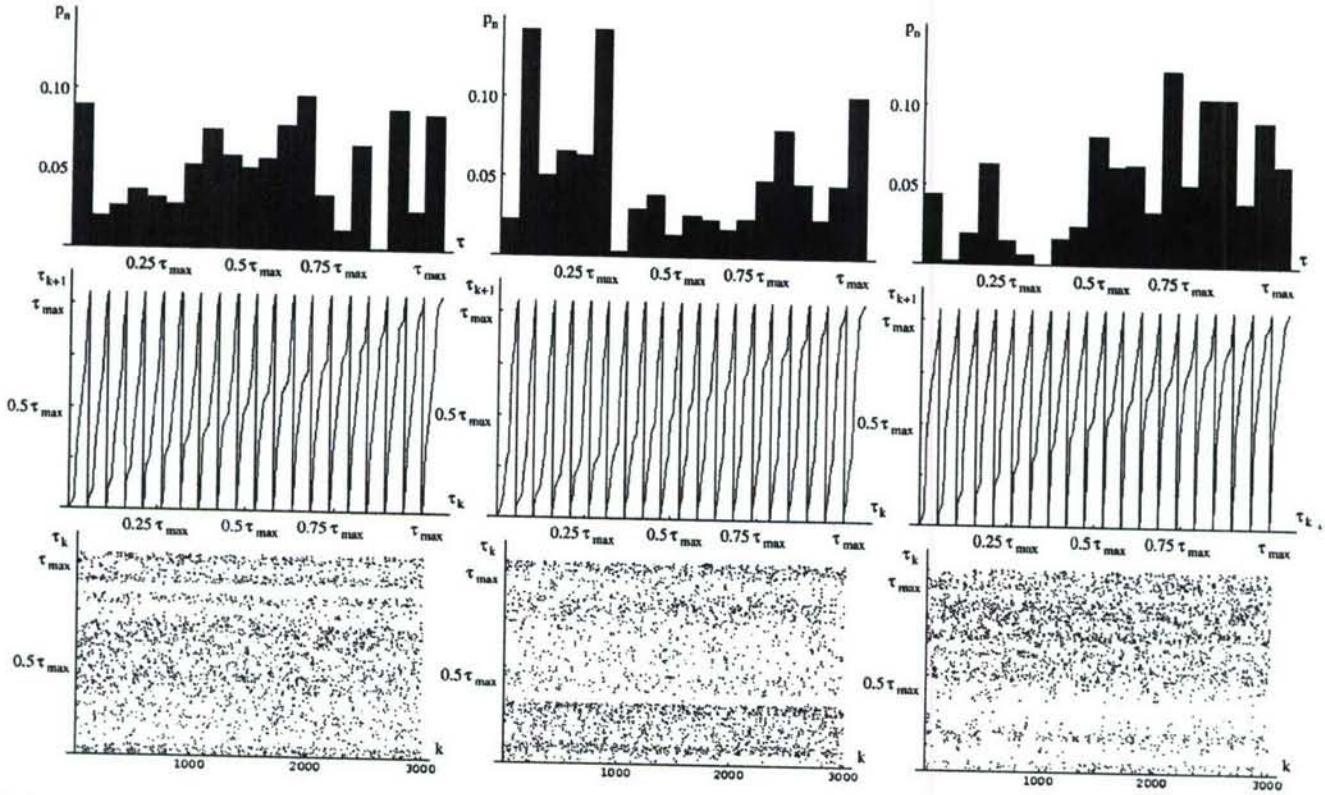

Fig. 5. Synthesis of temporal-sequence generators. Three example interspike-interval distributions with $N = 20$ representing three different odors are shown in the top row. The corresponding shift maps and distributions of values of generated temporal sequences are shown underneath. The time interval axes are normalized to the range of $(0; 1)$. Each graph in the bottom row contains 3000 points representing interspike intervals placed vertically according to the length of the interval.

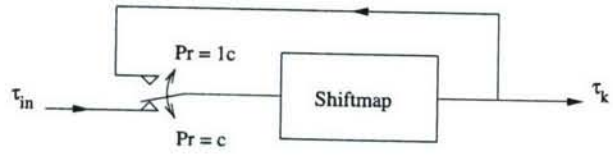

Fig. 6. Frobenius filter is a shift map with input. Either the input interval τ_{in} or the present output interval τ_k is transformed into the next output interval τ_{k+1}.

$(\boldsymbol{p}_A^*, h_A)$, $(\boldsymbol{p}_B^*, h_B)$, and $(\boldsymbol{p}_C^*, h_C)$ are synchronized in a sense that the quadratic distance between input and output interval distributions is small. The distances in all the other pairs are significantly larger. By detecting low distance between the input and the output of the filter, an odor recognition mechanism can be devised.

Two examples of realizations of the input and output temporal sequences are shown in Figs. 8 and 9. The proposed mechanism uses a pattern matching phenomenon which signals successful detection as a decreased distance between parameters of the input and the output neural signals. The pattern matching is not based on coherence of the two signals. As shown in the figures, no similarity in realizations of the input and the output can be observed in either the matched or unmatched odor-filter pairs. In case of the matched pair, the similarity is in the statistical properties of the input and the output signals.

Value $c = 0.5$ used in the experiment is the midpoint of the probability range. The value of c may be selected to optimize the performance with respect to different numbers of odors and filters. The extremes correspond to no-input ($c = 0$) and the open-loop ($c = 1$) conditions. In this regard, c represents the strength of the input coupling. With no input, the entire system becomes a simple pattern-matching mechanism. In the open-loop condition, the output is driven by the input through the filter mapping h. In both cases if the input is a stationary process, the filter output is also stationary and the distance $u_i - t_i$ can be evaluated. However, there will be no gain resulting from the synchronizing effect imposed by the switch.

VI. Conclusion

The details of how the cells of the olfactory bulb could encode the information in the way described in this paper are not discussed here. The goal set for this work was to describe the simplest method of encoding information in temporal sequences and show the input-output interactions which can lead to an odor detection and encoding mechanism. All the computations are very simple. No memory is necessary, only the last time interval is locally kept in the evaluation of the next time interval in the output sequence. Actual neurons are capable of performing such a storage with their inherent leaky integration.

The computational complexity of the model depends on the resolution N of the interspike interval distributions. It determines the dimensionality of the Markov transition matrix. Minimization (11) is the most time-demanding computation involved in the approach and takes a significant amount of time to evaluate. The minimization may be regarded as the learning process.

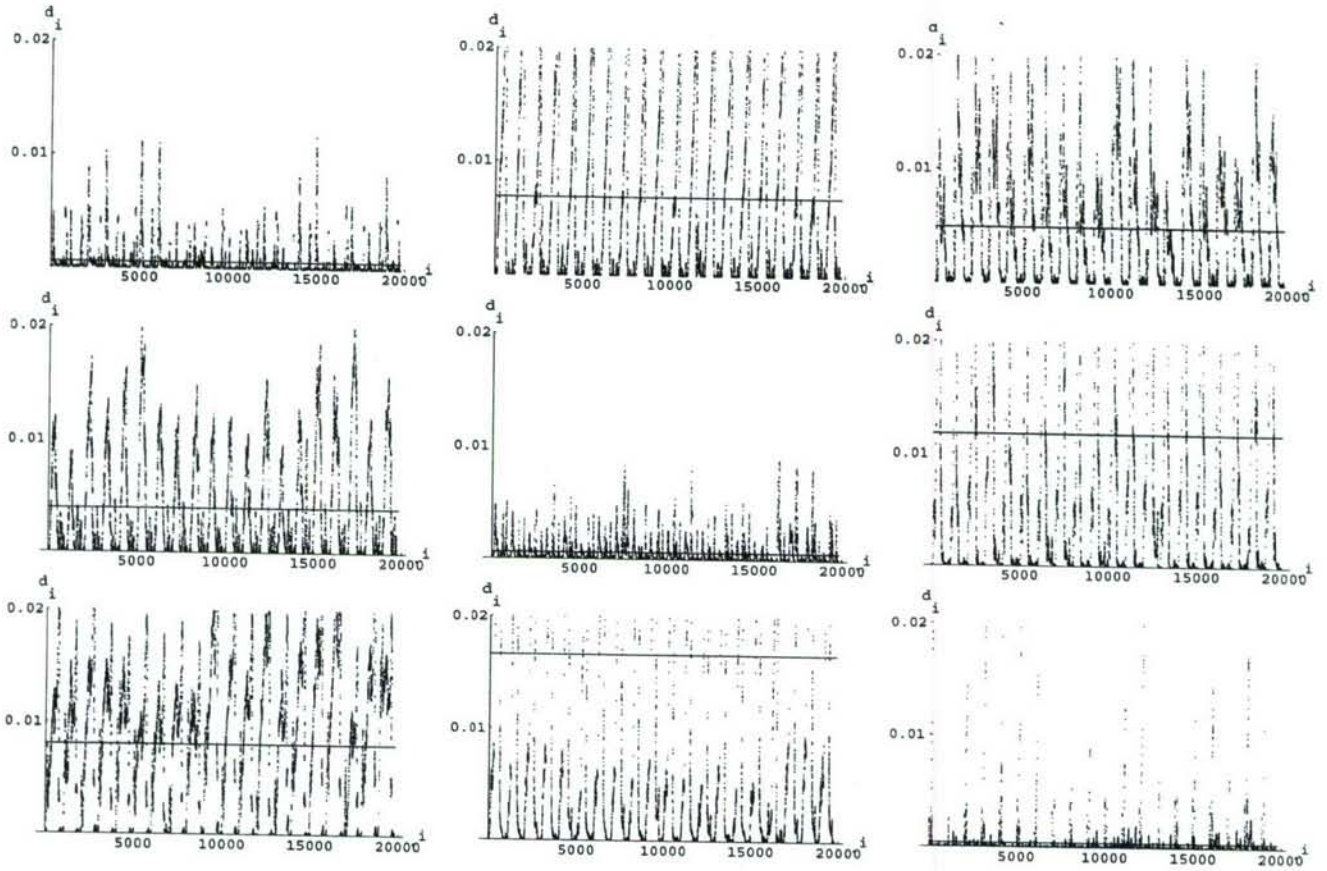

Fig. 7. Nine instances of a Frobenius filter stimulated by an input distribution for 20 000 iterations. Quadratic distance $d_i = (u_i - t_i)^2$ between cumulative distributions of interspike intervals at input u_i and output t_i of the filter shown. The graphs are arranged according to (18).

Fig. 8. Realizations of the input (top) and output (bottom) temporal sequences for a matched pair (p_A^*, h_A). A fragment containing 100 spikes shown.

Fig. 9. Realizations of the input (top) and output (bottom) temporal sequences for unmatched pair (p_B^*, h_A). A fragment containing 100 spikes shown.

The shapes of the shift maps shown in Fig. 5 are not crucial for in the operation of the Frobenius filters. The proposed shapes are just samples of infinite possibilities chosen for mathematical simplicity. In fact, any mapping that is mixing and expanding [19] can be used in the Frobenius filter. Such mappings develop continuous invariant distributions and guarantee ergodicity of the temporal sequence in a sense that the invariant distribution is reachable from any initial condition. Temporal sequences at the output of the filter have a very strong ability of encoding information in the time scale. It is sufficient to isolate just a few consecutive spikes to be able to identify the shift map which generated the spikes and effectively identify the encoded odor.

ACKNOWLEDGMENT

The authors would like to acknowledge inspiring discussion and help from Prof. J. S. Kauer, Tufts University School of Medicine, Medford, MA.

REFERENCES

[1] T. A. Dickinson, J. White, J. S. Kauer, and D. R. Walt, "Current trends in 'artificial-nose' technology," *Trends Biotechnol.*, vol. 16, no. 6, pp. 250–258, June 1998.

[2] N. Caticha, J. E. P. Tejada, D. Lancet, and E. Domany, "Computational capacity of an odorant discriminator: The linear separability of curves," *Neural Computat.*, vol. 14, pp. 2201–2220, 2002.

[3] A. Manwani and C. Koch, "Detecting and estimating signals in noisy cable structures, I: Neuronal noise sources," *Neural Computat.*, vol. 11, pp. 1797–1829, 1999.

[4] R. W. Friedrich and G. Laurent, "Dynamic optimization of odor representations by slow temporal patterning of mitral cell activity," *Science*, vol. 291, pp. 889–894, Feb. 2001.

[5] J. S. Kauer, "Real-time imaging of evoked activity in local circuits of the salamander olfactory bulb," *Nature*, vol. 331, pp. 166–168, July 1988.

[6] J. P. Rospars, P. Lansky, P. Duchamp-Viret, and A. Duchamp, "Spiking frequency versus odorant concentration in olfactory receptor neurons," *BioSystems*, vol. 58, pp. 133–141, 2000.

[7] ——, "Characterizing and modeling concentration-response curves of olfactory receptor cells," *Neurocomput.*, vol. 38–40, pp. 319–325, 2001.

[8] J. White, K. A. Hamilton, S. R. Neff, and J. S. Kauer, "Emergent properties of odor information coding in a representational model of the salamander olfactory bulb," *J. Neurosci.*, vol. 12, no. 5, pp. 1772–1780, May 1992.

[9] J. S. Kauer, "Contributions of topography and parallel processing to odor coding in the vertebrate olfactory pathway," *Trends Neurosci.*, vol. 14, no. 2, pp. 79–85, Feb. 1991.

[10] J. Hopfield, "Pattern recognition computation using action potential timing stimulus representation," *Nature*, vol. 376, pp. 33–36, July 1995.
[11] M. Lysetskiy, A. Lozowski, and J. M. Zurada, "Invariant recognition of spatio-temporal patterns in the olfactory system model," *Neural Process. Lett.*, vol. 15, pp. 225–234, June 2002.
[12] A. G. Lozowski and B. L. Noble, "Processing temporal sequences," in *Proc. 45th Midwest Symp. Circuits and Systems (MSCAS'02)*, vol. 1, Tulsa, Oklahoma, Aug. 4–7, 2002, pp. 180–183.
[13] B. Quenet and D. Horn, "The dynamic neural filter: A binary model of spatiotemporal coding," *Neural Computat.*, vol. 15, pp. 309–329, 2003.
[14] A. Budak, *Passive and Active Network Analysis and Synthesis*. Prospect Heights, IL: Waveland Press, 1991.
[15] T. A. Dickinson, J. White, J. S. Kauer, and D. R. Walt, "A chemical-detecting system based on a cross-reactive optical sensor array," *Nature*, vol. 382, pp. 697–700, Aug. 1996.
[16] J. White, T. A. Dickinson, D. R. Walt, and J. S. Kauer, "An olfactory neuronal network for vapor recognition in an artificial nose," *Biol. Cybern.*, vol. 78, no. 4, pp. 245–251, Apr. 1998.
[17] E. M. Bollt, "Controlling chaos and the inverse Frobenius-Perron problem: Global stabilization of arbitrary invariant measures," *Int. J. Bifurcation Chaos*, vol. 10, no. 5, pp. 1033–1050, 2000.
[18] D. Pingel, P. Schmelcher, and F. K. Diakonos, "Theory and examples of the inverse Frobenius-Perron problem for complete chaotic maps," *Chaos*, vol. 9, no. 2, pp. 357–366, 2000.
[19] G. Mazzini, R. Rovatti, and G. Setti, *Chaos-Based DS-CDMA:Introduction. Some Tools for Studying Chaos With Densities*. Berkeley, CA: Univ. of California Press, 2000.

Andrzej G. Lozowski (S'96–M'99) received the M.S. degree in electrical engineering with specialization in electronic circuits from the Warsaw University of Technology, Warsaw, Poland, in 1994, and the Ph.D. degree in computer science and engineering from the University of Louisville, Louisville, KY, in 1999.

He is currently an Assistant Professor and the Graduate Program Director in the Department of Electrical and Computer Engineering, Southern Illinois University, Edwardsville, IL. His research interests include nonlinear dynamics, analog circuit design and signal processing.

Mykola Lysetskiy (S'99) received the M.S. degree in physics from Kharkov State University, Kharkov, Ukraine, in 1997, and the Ph.D. degree in computer science and engineering from the University of Louisville, KY, in 2003.

He is presently a Postdoctoral Researcher in the Department of Anatomy and Neurobiology, University of California, Irvine.

Jacek M. Zurada (M'82–SM'83–F'96) is the S.T. Fife Alumni Professor of Electrical and Computer Engineering, University of Louisville, Louisville, KY. He is the coeditor of *Knowledge-Based Neurocomputing* (Cambridge, MA: MIT Press, 2000), *Computational Intelligence: Imitating Life* (Piscataway, NJ: IEEE Press, 1994), and the author of *Introduction to Artificial Neural Systems* (Boston, MA: PWS-Kent, 1992). He is the author or coauthor of more than 200 journal and conference papers in the area of neural networks and VLSI circuits.

Dr. Zurada has been the Editor-in-Chief of the IEEE TRANSACTIONS ON NEURAL NETWORKS since 1998. He was the recipient of the 2001 University of Louisville President's Distinguished Service Award for Service to the Profession. He is currently the President of the IEEE Neural Networks Society for 2004–2005. In March 2003, he was conferred the Title of the Professor by the President of Poland, A. Kwasniewski.

Available at
www.ElsevierComputerScience.com
POWERED BY SCIENCE DIRECT®

Neural Networks 17 (2004) 225–232

Neural Networks

www.elsevier.com/locate/neunet

Bifurcating neuron: computation and learning

Mykola Lysetskiy, Jacek M. Zurada*

Department of Electrical and Computer Engineering, University of Louisville, Louisville, KY 40292, USA

Received 18 June 2002; revised 24 September 2003; accepted 24 September 2003

Abstract

The ability of bifurcating processing units and their networks to rapidly switch between different dynamic modes has been used in recent research efforts to model new computational properties of neural systems. In this spirit, we devise a bifurcating neuron based on control of chaos collapsing to a period-3 orbit in the dynamics of a quadratic logistic map (QLM). Proposed QLM3 neuron is constructed with the third iterate of QLM and uses an external input, which governs its dynamics. The input shifts the neuron's dynamics from chaos to one of the stable fixed points. This way the inputs from certain ranges (clusters) are mapped to stable fixed points, while the rest of the inputs is mapped to chaotic or periodic output dynamics. It has been shown that QLM3 neuron is able to learn a specific mapping by adaptively adjusting its bifurcation parameter, the idea of which is based on the principles of parametric control of logistic maps [Proceedings of the International Symposium on Nonlinear Theory and its Applications (NOLTA'97), Honolulu, HI, 1997; Proceedings of SPIE, 2000]. Learning algorithm for the bifurcation parameter is proposed, which employs the error gradient descent method.

Keywords: Bifurcating neuron; Quadratic logistic map; Chaotic attractor; Saddle-node bifurcation; Period-3 orbit window

1. Introduction

Limitations of the static nature of artificial neural networks (ANN) stimulate investigation of biologically motivated neuron models with inherent dynamics, such as bifurcating and chaotic neurons (Farhat, 2000; Farhat & Eldefrawy, 1992; Farhat, Lin, & Eldefrawy, 1994; Holden, Hyde, Muhamad, & Zhang, 1992). In the networks composed of such neurons information is processed by convergence not only to a fixed point, but also to a limit cycle or chaotic attractor (Farhat, 2000; Farhat, Lee, & Ling, 1998; Hirsch & Baird, 1995; Lee & Farhat, 2001).

Artificial neurons commonly used to mimic dynamics of biological neurons are simplified versions of the Hodgkin-Huxley type model (HHM), such as, for instance, integrate-and-fire neurons. These models demonstrate very rich dynamics, with a variety of bifurcations and chaotic phenomena (Farhat & Eldefrawy, 1992; Farhat et al., 1994; Feudel et al., 2000; Holden et al., 1992; Izhikevich, 2000). For example, dynamics of interspike time interval of biological thermally sensitive neurons with increasing temperature (which is both its input and bifurcation parameter), undergoes transition to chaos via period-doubling cascade, intermittency and crises of chaotic attractors, emerging windows of periodic activity, etc. as shown in Fig. 1. (Feudel et al., 2000).

More typically, chaotic neural dynamics emerges at macro-level, in the network of dynamical units. Seminal results of Freeman and co-workers (Freeman, 1988) suggest that the state of the olfactory bulb in olfactory system, when unperturbed, is wandering within high-dimensional chaotic attractor. Applied input (odor) shifts the system to one of its low-dimensional attractors, 'wings', that correspond to the recognized odor.

Dynamics of the network of parametrically coupled logistic maps was explored in (Farhat, 1997, 2000; Farhat et al., 1998). It was shown that such networks may have enormous memory capacity due to the astronomical number of different coexisting dynamic attractors. The lattices of chaotic maps were studied in Dmitriev, Shirokov, and Starkov (1997), Kaneko and Tsuda (2000) and Sinha and Ditto (1998). Chaotic dynamics of a network was also explored in Adachi and Aihara (1997) and Hoshino, Usaba, Kashimori, and Kambara (1997), and applied to an engineering application: a search of an optimal solution of the traveling salesman problem (Tokuda, Nagashima, & Aihara, 1997). Encoding with the trajectory of the system's

* Corresponding author.
E-mail address: j.mzura02@louisville.edu, (J.M. Zurada).

0893-6080/$ - see front matter © 2003 Elsevier Ltd. All rights reserved.
doi:10.1016/j.neunet.2003.09.003

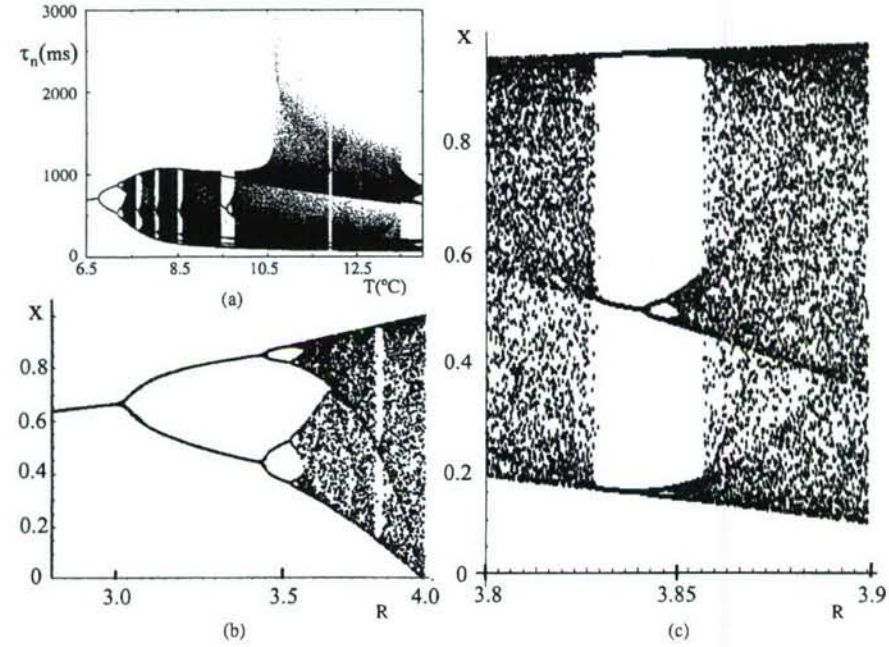

Fig. 1. (a) Bifurcation diagram of the modified Hodgkin-Huxley model of the thermally sensitive neuron. Interspike intervals τ_n versus bifurcation parameter, temperature T (From Feudel et al., (2000). *Chaos*, 10(1)). (b) Bifurcation diagram of quadratic logistic map $x_{t+1} = Rx_t(1 - x_t)$, x_t values versus bifurcation parameter R. (c) Zoomed in version of (b): Emerging of period-3 orbit.

state in the phase space realized in a network of FitzHugh–Nagumo spiking neurons was studied in Rabinovich et al. (2001).

In biological neural circuits, input may not be presented by initial conditions. It is, rather, one of the bifurcation parameters (Feudel et al., 2000; Fukai, Doi, Nomura, & Sato, 2000; Koch, 1999). Dynamics of thermally sensitive neurons (Braun, Eckhardt, Braun, & Huber, 2000; Feudel et al., 2000; Gilmore et al., 1999) is a good illustration of this idea. This input-as-a-bifurcation-parameter concept, explored in Farhat and Eldefrawy (1992), Farhat et al. (1994) and Holden et al. (1992) provides an insight of how microscopic fluctuations of an input may be able to change the system's global dynamics.

1.1. Why maps?

Biologically realistic modified Hodgkin-Huxley neuron models are barely analytically tractable due to a huge number of variables and bifurcation points. However, certain aspects of their activity, for example, the dynamics of the interspike time intervals, can often be described with dynamics of sine-circle and other maps, which are, generally, easier to work with Ermentrout and Kopell (1998) and Farhat and Eldefrawy (1992, 1994). In this article, as in Farhat (1997, 2000), Farhat and Lee (1998) and Lee and Farhat (2001) we use the dynamics of quadratic logistic maps (Figs. 1 and 2, Eq. (1)) (Holmgren, 1996; Ott, 1993) as an abstract model of a chaotic processing element

$$x_{t+1} = Rx_t(1 - x_t) \tag{1}$$

Bifurcation diagrams of QLM and modified HHM of thermal neurons are shown in Fig. 1(a) and (b). The reasons of their striking resemblance are saddle-node, period-doubling and other common basic bifurcations which underlie these dynamics. Period-doubling cascade route to chaos present in both of them is one of the fundamental bifurcation scenarios which is behind a huge number of processes—from a population dynamics in ecological systems, to chemical reactions, like the one of Belousov-Zhabotinsky (Kaneko & Tsuda, 2000). Computational abilities of the bifurcation processes in the logistic maps' dynamics have been studied extensively in a number of works (Farhat, 1997, 2000; Farhat & Eldefrawy, 1992; Farhat et al., 1994; Lysetskiy et al., 2002). In this article, we focus on one of the numerous bifurcation processes–collapse of chaos to a period-3 orbit in the QLM dynamics and its potential computational properties.

1.2. Dynamics

Here, we briefly review the QLM dynamics which is used in the following sections. With bifurcation parameter $R < 3$, the system $x_{t+1} = f[x_t]$ (Eq. (1)) has a single stable fixed point (Fig. 1(b)). First period-doubling bifurcation occurs when $R = 3$. With R increasing further, the system undergoes period-doubling cascade and at the critical point

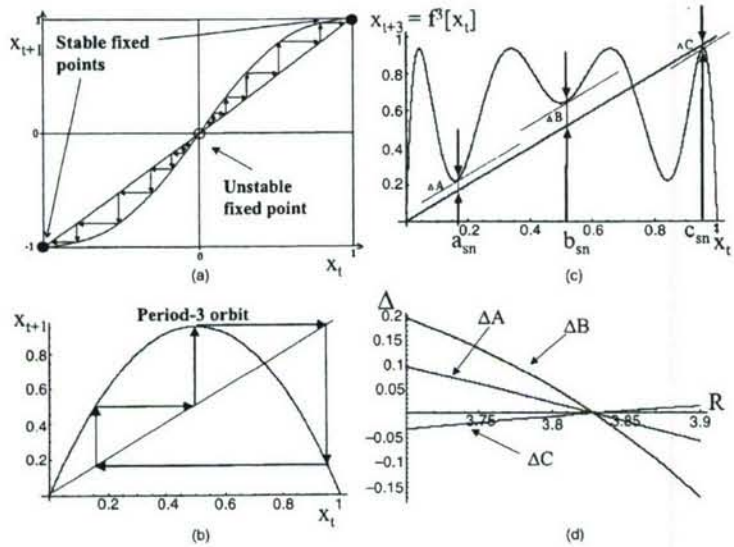

Fig. 2. (a) A neuron with a sigmoidal activation function as a logistic map and its dynamics. (b) Example of quadratic logistic map $x_{t+1} = Rx_t(1 - x_t)$ dynamics: period-3 orbit. (c) Third iterate of QLM $x_{t+3} = f^3[x_t] = f[f[f[x_t]]]$, $R = 3.75$: three stable fixed points are about to be born via bifurcations. (d) The distances ΔA, ΔB, and ΔC (Eq. (5)) to the corresponding bifurcation points a_{sn}, b_{cn} and c_{sn} (Eq. (3)) are identical only for a single critical value of R (in this working range of R).

$R_c \approx 3.57$ it becomes chaotic. Due to the fractal structure of the bifurcation diagram, there is an infinite number of values of R, at which chaotic attractors the system lives on collapse, producing stable periodic orbits.

In this article, we focus on the period-3 orbit which emerges when $R_3 \approx 3.828$ (Fig. 1(b) and (c)). Its appearance is due to three saddle-node bifurcations, giving birth to three stable and three unstable orbits out of chaos. How this phenomena happen can be easily seen graphically. Period-3 orbit of the map $f[x_t]$ (Fig. 2(b)) corresponds to a period-1 orbit (fixed point) of the map $f^3[x_t] = f[f[f[x_t]]]$ (Fig. 2(c)). Fixed point x^* of the system $x_{t+3} = f^3[x_t]$ can be defined as a point of intersection of curves $x_{t+3} = f^3[x_t]$ and $x_{t+3} = x_t$ (Figs. 2(c) and 3). Stability of x^* is defined by Eq. (2a–c)

$$\left|\frac{df^3[x]}{dx}\right| < 1; \tag{2a}$$

$$\left|\frac{df^3[x]}{dx}\right| = 1; \tag{2b}$$

$$\left|\frac{df^3[x]}{dx}\right| > 1; \tag{2c}$$

Fixed point x^* is stable, neutral or unstable if, respectively, condition (2a), (2b) or (2c) is satisfied.

When R is slightly less than R_3, map $f^3[x]$ has no stable fixed points and its state wanders within chaotic attractor (Figs. 1(c) and 2(c)). However, if $R = R_3$, the curve $x_{t+3} = f^3[x_t]$ touches the line $x_{t+3} = x_t$ simultaneously in three saddle-node bifurcation points a_{sn}, b_{cn} and c_{sn}, defined by Eq. (3)

$$\frac{df^3[x]}{dx} = 1 \tag{3}$$

This produces three neutral fixed points via three saddle-node bifurcations. The points, then, split into to three stable and three unstable solutions. We name them correspondingly A_s, B_s, C_s and A_u, B_u, C_u. The stable solutions exist while they satisfy Eq. (2a), but as R further increases they loose their stability via period-doubling bifurcations.

2. Input-induced bifurcations

2.1. Dynamics

In order to make the emergence of stable orbits compute, we shift function $f^3[x]$ vertically with input I (with weight w)

$$x_{t+3} = f^3[x_t] - wI \tag{4}$$

With this input, which is an additional bifurcation parameter, the system demonstrates quite different dynamics and bifurcation scenario. With $R < R_3$ it has no stable fixed points and lives on a chaotic attractor. Now, if we increase I starting from $I = 0$, the curve $x_{t+3} = f^3[x_t] - wI$ will touch the $x_{t+3} = x_t$ line at three distinct input values (Fig. 3). This happens because with

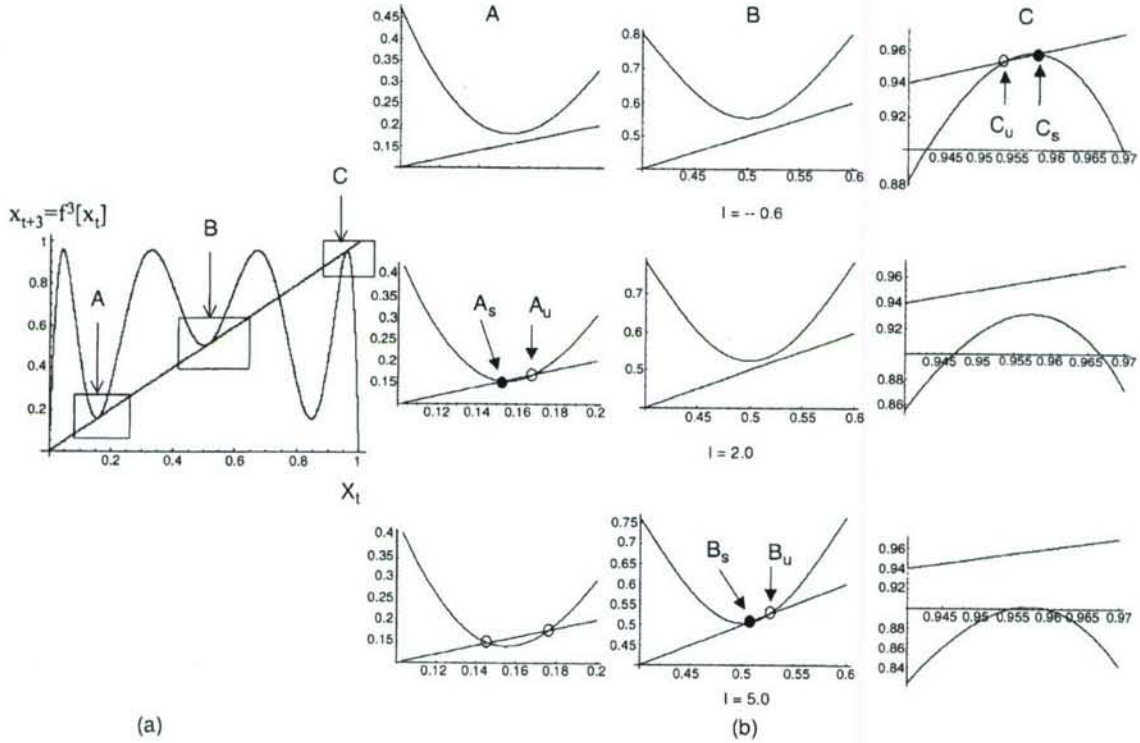

Fig. 3. (a) Function $x_{t+3} = f^3[x_t] = f[f[f[x_t]]] - wI$ of QLM3, $R = 3.805$. (b) Emergence and disappearance of fixed points via sequence of saddle-node bifurcations with different inputs. Black and empty circles correspond, respectively, to stable and unstable fixed points.

the same R the distances

$$\Delta A = f^3[a_{sn}] - a_{sn} \qquad \Delta B = f^3[b_{sn}] - b_{sn}$$
$$\Delta C = f^3[c_{sn}] - c_{sn} \tag{5}$$

at the bifurcation points a_{sn}, b_{sn} and c_{sn} (defined by Eq. (3)) are different (see Fig. 2(c) and (d)). The distances ΔA, ΔB, and ΔC are defined as the solutions of the equation

$$\Delta = f^3[x^*, R^*] - x^* \tag{6}$$

with a given R^* and x^*. Generally, Eq. (6) has multiple solutions. However, in the range of R we are interested in, the solution of Eq. (6) with x^* equal to a_{sn}, b_{sn} and c_{sn} and given R^* are unique, except for $R = R_3$, when $\Delta A = \Delta B = \Delta C = 0$ (Fig. 2(d)).

Thus, the shift $wI = \Delta A$ induces a single saddle-node bifurcation: the curve $x_{t+3} = f^3[x_t] - wI$ touches the line $x_{t+3} = x_t$ at a single point $x_t = a_{sn}$. It splits then into stable fixed point A_s and unstable A_u (Fig. 3b: column A, $I = 2.0$) when the shift is increased. The chaotic attractor collapses and the state of the system converges to A_s, as is shown in Fig. 4 ($I = 1.81$).

As I keeps increasing, A_s looses its stability via period-doubling bifurcation according to Eq. (2c). Dynamics of x undergoes cascade of these bifurcations and becomes chaotic (Fig. 4). Then, when the shift $wI = \Delta B$, another stable point B_s emerges via saddle-node bifurcation (Fig. 3b: Column B, $I = 5.0$). At this moment (chaotic) dynamics of x converges to the stable point B_s. (Figs. 3(b) and 4). The same bifurcation mechanism underlies the emergence of the stable fixed point C_s (and then, the loss of its stability) when I is negative, and the function $f^3[x]$ is shifted upward.

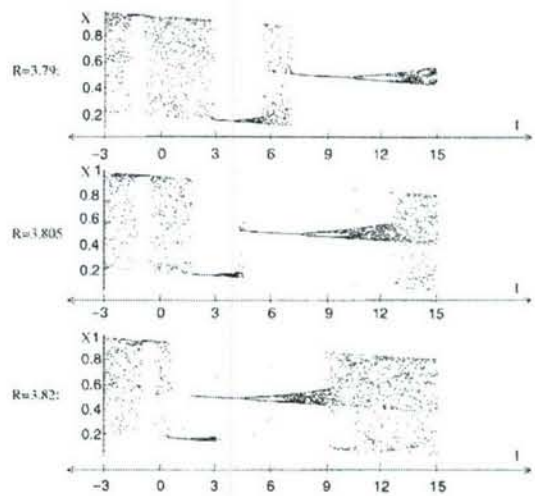

Fig. 4. Dynamics of the map $x_{t+3} = f^3[x_t] - wI$ with $R = 3.805$, versus I. Three input intervals are mapped onto three stable fixed points A, B and C.

Let I_{sn} and I_{pd} be the inputs that produce, correspondingly, a stable fixed point via saddle-node bifurcation (Eq. (2a)) and loss of its stability via period-doubling bifurcation (Eq. (2c)). The map's dynamics at the critical points A, B and C can be seen, then, as an analog of a perceptron, as it divides the input interval into two subintervals. One of them produces a stable fixed point and is defined as

$$I_{sn} < |I| < I_{pd} \tag{7}$$

where sign of I is the same as of the corresponding distance Δ (6). The inputs outside of this interval do not invoke a fixed point and the system remains chaotic or stays on a periodic orbit.

It should be noted that extension of the system for the case when **I** and **w** are vectors is rather straightforward. The QLM3 neuron $x_{t+3} = f^3[x_t] - \sum w_j I_j$ maps multidimensional space to the induced stable fixed point in the same way as it does with one-dimensional input (Fig. 4).

2.2. Simulation

In the following simulation example bifurcation parameter is set at $R = 3.808$. The reason behind this choice is that the widest period-3 orbit in the map's dynamics (Fig. 1(b) and (c)) emerges with $R_3 = 3.828$; $R_0 = 3.808$ is slightly less than R_3, so the system is chaotic, but its stable states can be produced by a small input.

The saddle-node bifurcation points, at which the curve $x_{t+3} = f^3[x_t] - wI$ touches $x_{t+3} = x_t$ line are defined by Eq. (2b): $a_{sn} = 0.1604$, $a_{pd} = 0.1501$, $b_{sn} = 0.5157$, $b_{pd} = 0.4851$, $c_{sn} = 0.9556$, $c_{pd} = 0.9588$. Input intervals Eq. (7) that produce emergence of fixed points A, B and C (with $w = 0.01$) are calculated with Eq. (2b and c) as follows

$$\begin{aligned} A &: I_{sn}^A = 1.81 < I < I_{pd}^A = 3.02 \\ B &: I_{sn}^B = 4.51 < I < I_{pd}^B = 7.48 \\ C &: I_{sn}^C = -0.53 > I > I_{pd}^C = -0.91 \end{aligned} \tag{8}$$

Simulation results (Fig. 4) demonstrate that QLM3 neuron maps the set of input intervals onto the set of invoked stable fixed points A, B and C.

It should be noted that if $I \neq 0$ the map $x_{t+3} = f^3[x_t] - wI$ no longer maps the interval [0,1] on itself. Two 'runaway' regions appear at the edges of the interval [0,1]. They are defined as: $0 < x < x_c$ and $1 - x_c < x < 1$, where x_c is the leftmost solution (for $x_c \in [0, 1]$) of equation $f^3[x^*] - wI = x^*$ if the shift is downward ($I > 0$), and x_c is its rightmost solution (for $x_c \notin [0, 1]$) if $I < 0$. In our simulations, where the input maximum, $I_{max} = 15$ is positive and $R = 3.805$, the critical value $x_c = 2.9 \times 10^{-3}$, which slightly restricts the set of initial conditions to $[x_c, 1 - x_c]$.

3. Learning

The sizes and centers of the intervals mapped by QLM3 neuron to its output states depend on R (Eqs. (6) and (8), Fig. 5) and w. To adjust w, one of the learning algorithms for the multilevel neurons would be appropriate, for example, the one described in Malinowski, Cholewo, and Zurada (1995).

We focus on the other option provided by QLM3 neuron—the learning of the bifurcating parameter R. It

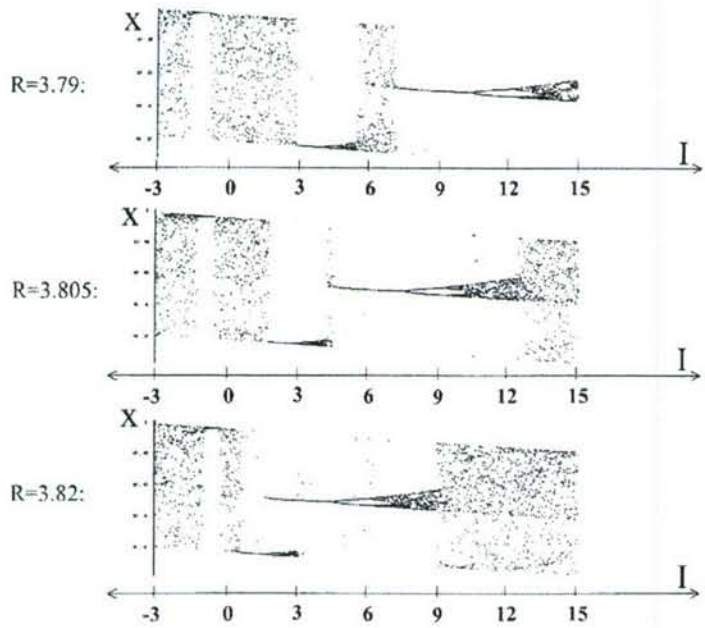

Fig. 5. Parameter-depending mapping: examples of the input intervals inducing stable fixed points with different values of bifurcation parameter R.

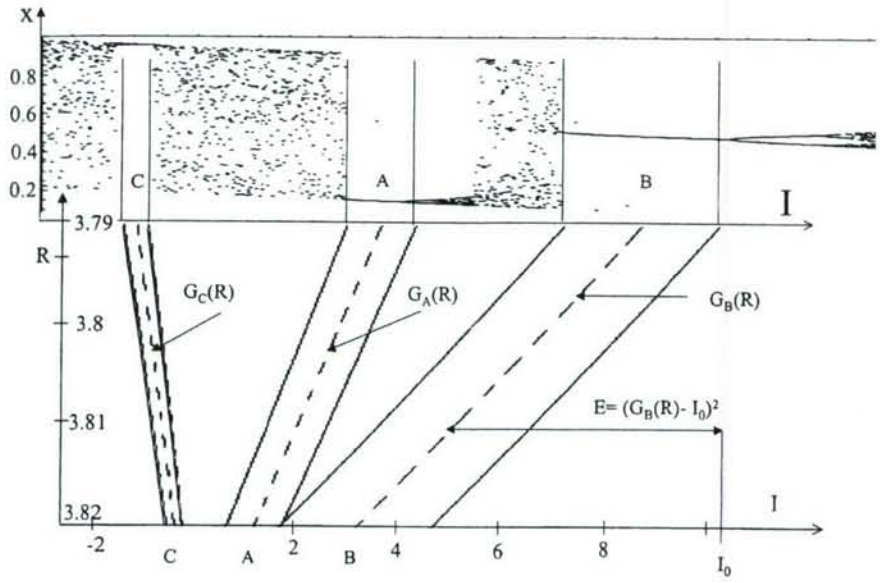

Fig. 6. The mapping of the input interval as a function of bifurcation parameter R.

is, in a sense, analogous to the optimizing the steepness of the activation function of a sigmoidal neuron to maximize the information of its output (Bell & Sejnowski, 1995).

The mapping of QLM3 neuron as a function of R is shown in Fig. 6, where the centers of mapped intervals (also functions of R) are described as curves $G_A(R)$, $G_B(R)$, $G_C(R)$. To make an input I_0 produce a desired output, for example a stable state A, R should be adjusted in a way to put I_0 into the interval mapped to A : $I^A_{sn}(R) < I_0 < I^A_{pd}(R)$ (Eq. (7)). Defining it more strictly, we want the input to be in the center of this interval, $I_0 = G_A(R)$, defined with Eqs. (5) and (9) as

$$G_A(R) = \frac{1}{2}(I^A_{sn}(R) + I^A_{pd}(R)) = \frac{1}{2}((f^3[a_{sn}, R] - a_{sn}) + (f^3[a_{pd}, R] - a_{pd})) \quad (9)$$

Thus, learning of mapping I_0 to A transforms to the task of minimizing the distance $|I_0 - G_A(R)|$ (Fig. 6). The error function can, then, be defined as a square of this distance

$$E(R) = (I_0 - G(R))^2 \quad (10)$$

This brings the error gradient learning rule to the following form

$$\Delta R = -c\frac{dE}{dR} = 2c(I_0 - G(R))G'(R) \quad (11)$$

where $G'(R)$ stands for the derivative of $G(R)$ and c is the learning coefficient.

To implement unsupervised learning the learning algorithm has to choose the centerline $G_J(R)$ which is closest to the applied input I_0: $E_J = \min_j [E_j], j\{ \in A, B, C\}$, and then the error E_J has to be minimized. In the case of supervised learning the corresponding centerline is defined by the teacher's signal.

Examples of simulations of the proposed learning algorithm (Eq. (11)) are shown in Fig. 7. The task was to learn mapping of input $I_0 = 6$ to the desired output B. With initial conditions $R_0 = 3.77$ and $R_0 = 3.82$ this input produces chaotic and period-2 orbits, respectively (Fig. 6). After 70 learning steps (Eq. (11)) R converged to $R = 3.805$ (Fig. 7(a)) and it produced desired output B (Figs. 4 and 5) with the errors $E = 6.7 \times 10^{-4}$ and $E = 4.4 \times 10^{-4}$ respectively. Dynamics of E is shown in Fig. 7(b). The learning coefficient used $c = 2 \times 10^{-6}$.

Thus, this learning method enables the QLM3 neuron to adjust adaptively its bifurcation parameter R to map certain input intervals to specific stable states (classes). The upgrade of R changes the mapping of all intervals/clusters (three, in our case) simultaneously (Figs. 5 and 6).

4. Discussion

This article explores computational abilities of controlling the collapse of a chaotic attractor to the stable orbits in the dynamics of a quadratic logistic map. Such control is implemented with an external input (additional bifurcation parameter) to the third iterate of QLM. The resulting processing unit, QLM3 neuron, demonstrates a richer repertoire of behavior than a classical artificial neuron with sigmoidal activation function. Besides saturated regions, where inputs from certain intervals/clusters invoke different stable states, QLM3 neuron also produces chaotic

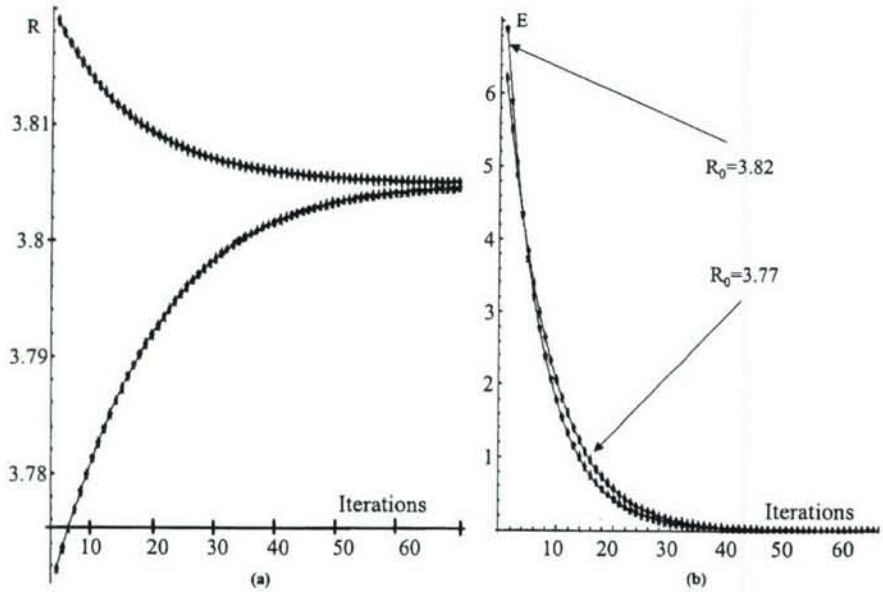

Fig. 7. (a) Dynamics of the bifurcation parameter R during learning. (b) Error E during learning.

or periodic dynamics in response to the rest of the inputs. Another potentially useful property of the QLM3 neuron is its ability to adjust adaptively its mapping by learning the bifurcation parameter value.

In this article, we used the emergence of period-3 orbit out of chaos which happens at $R \approx 3.828$. However, the appearances of a period-n orbit out of chaos, or, in other words, transitions of nth iterate from chaos to n fixed points are ubiquitous in the quadratic map's dynamics. For example, in the range of R from $R_c \approx 3.57$ (when the map's dynamics first becomes chaotic) to $R = 4$, there exist $(2^p - 2)/2p$ windows of period p orbits, where p is a prime number (Ott, 1993).

The map of nth iterate would look structurally similar to the map of the third iterate shown in Fig. 2(c), but it would have n saddle-node bifurcation points instead of 3. So, it would be possible to construct a QLM based neuron with a large number of stored stable states using other periodic orbits. It might be easier, though, to artificially generate a map with required number of saddle-node bifurcations.

Acknowledgements

This work was sponsored by the Department of the Navy, Office of Naval Research, Grant N000 14-01-1-0630. The content of this information does not necessarily reflect the position of the government.

We would like to thank Andrzej G. Lozowski for critical discussions and valuable comments on this manuscript. We also express thanks to the anonymous reviewers and the action editor, who have provided many insightful comments helpful for revision of this paper.

References

Adachi, M., & Aihara, K. (1997). Associative dynamics in a chaotic neural network. *Neural Networks, 10*(1), 83–98.

Bell, A. J., & Sejnowski, T. (1995). An information–maximization approach to blind separation and blind deconvolution. *Neural Computation, 7*, 1129–1159.

Braun, W., Eckhardt, B., Braun, H. A., & Huber, M. (2000). Phase–space structure of a thermoreceptor. *Physical Review E, 62*(5), 6352–6360.

Dmitriev, A., Shirokov, M., & Starkov, S. (1997). Chaotic synchronization in ensembles of coupled maps. *IEEE Transactions on Circuits and Systems I: Fundamental Theory and Applications, 44*(10), 918–926.

Ermentrout, G. B., & Kopell, N. (1998). Fine structure of neural spiking and synchronization in the presence of conduction delays. *Proceedings of the National Academy of Sciences, 95*(3), 1259–1264.

Farhat, N. (1997). Dynamical networks with bifurcation processing element (pp. 265–268). *Proceedings of the International Symposium on Nonlinear Theory and its Applications (NOLTA'97), Honolulu, HI.*

Farhat, N. (2000). Cortitronics: the way to designing machines with brain-like intelligence (*Vol. 4109*) (pp. 103–109). *Proceedings of SPIE*, Bellingham, WA: SPIE.

Farhat, N., & Eldefrawy, M. (1992). The bifurcating neuron: characterization and dynamics (*Vol. 1773*) (pp. 23–35). *In Photonics for computers, neural networks, and memories*, Bellingham, WA: SPIE.

Farhat, N., Lee, G. H., & Ling, X. (1998). Dynamical networks for ATR (pp. D1–D4). *Proceedings of RTO SCI Symposium on Non-Cooperative Air Target Identification Using Radar, published in RTO MP6, Mannheim, Germany.*

Farhat, N., Lin, S.-Y., & Eldefrawy, M. (1994). Complexity and chaotic dynamics in a spiking neuron embodiment (*Vol. CR55*) (pp. 77–88). *In Adaptive computing: Mathematics, electronics, and optics*, Bellingham, WA: SPIE.

Feudel, U., Neiman, A., Pei, X., Wojtenek, W., Braun, H., Huber, M., & Moss, F. (2000). Homoclinic bifurcation in a Hodgkin-Huxley model of thermally sensitive neurons. *Chaos*, *10*(1), 231–239.

Freeman, W. (1988). Strange attractors that govern mammalian brain dynamics shown by trajectories of electroencephalographic (EEG) potential. *IEEE Transaction on Circuits and Systems*, *35*, 781–783.

Fukai, H., Doi, S., Nomura, T., & Sato, S. (2000). Hopf bifurcations in multiple-parameter space of the Hodgkin-Huxley equations I. Global organization of bistable periodic solutions. *Biological Cybernetics*, *82*, 215–222.

Gilmore, R., Pei, X., & Moss, F. (1999). Topological analysis of chaos in neural spike train burst. *Chaos*, *9*(3), 812–817.

Hirsch, M., & Baird, B. (1995). Computing with dynamic attractors in neural networks. *Biosystems*, *34*, 173–195.

Holden, A. V., Hyde, J., Muhamad, M. A., & Zhang, H. G. (1992). In J. G. Taylor, & C. L. T. Mannion (Eds.), *Bifurcating neurons* (pp. 41–80). *Coupled oscillating neurons*, London: Springer.

Holmgren, R. A. (1996). *A first course in discrete dynamical systems*. New York: Springer.

Hoshino, O., Usuba, N., Kashimori, Y., & Kambara, T. (1997). Role of itinerancy among attractors as dynamical map in distributed coding scheme. *Neural Networks*, *10*(8), 1375–1390.

Izhikevich, E. M. (2000). Neural excitability, spiking and bursting. *International Journal of Bifurcation and Chaos*, *10*, 1171–1266.

Kaneko, K., & Tsuda, I. (2000). *Complex systems: Chaos and beyond*. New York: Springer.

Koch, C. (1999). *Biophysics of computation: Information processing in single neurons*. New York: Oxford University Press.

Lee, G., & Farhat, N. H. (2001). The bifurcating neuron network 1. *Neural Networks*, *14*, 115–131.

Lysetskiy, M., Lozowski, A. G., & Zurada, J. M. (2002). Bifurcation-based neural computation (pp. 2716–2720). *Proceedings of the IEEE International Joint Conference on Neural Networks, Honolulu, HI, May 12–17*.

Malinowski, A., Cholewo, T. J., & Zurada, J. M. (1995). Capabilities and limitations of feedforward neural networks with multilevel neurons (*Vol. 1*) (pp. 131–134). *Proceedings of the IEEE International Symposium on Circuits and Systems, Seattle, WA, April 30–May3*.

Ott, G. (1993). *Chaos in dynamical systems*. New York: Cambridge University Press.

Rabinovich, M., Volkovskii, A., Lecanda, P., Huerta, R., Abrabanel, H. D. I., & Laurent, G. (2001). Dynamical encoding by network of competing neuron groups: winnerless competition. *Physical Review Letters*, *87*, 068102.

Sinha, S., & Ditto, W. L. (1998). Dynamics based computation. *Physical Review Letters*, *81*(10), 2156–2159.

Tokuda, I., Nagashima, T., & Aihara, K. (1997). Global bifurcation structure of chaotic neural networks and its application to traveling salesman problems. *Neural Networks*, *10*(9), 1673–1690.

Lysetskiy M, Zurada, J.M., Temporal Binding, Segmentation and Attention Focusing in the Olfactory Model, Proc. International Joint Conference on Neural Networks, pp.1095-1100, Washington, D.C., July 16-19, 2001.

Temporal Binding, Segmentation and Attention Focusing in the Olfactory Model

Mykola Lysetskiy and Jacek M. Zurada

University of Louisville
Department of Electrical and Computer Engineering
Louisville, KY, 40208, USA
Email: m0lyse01@ubongo.spd.louisville.edu

Abstract

Biologically inspired model of the olfactory cortex is proposed which realizes mapping of the input pattern temporal structure to the spatial dynamic of the ensemble of output integrate-and-fire neurons. The temporal-to-spatial mapping and distributed representation of the model allows realization of both rough cluster classification and fine recognition of patterns within a cluster in parallel and as parts of the same dynamic process. The temporal structure of the system provides the base for the modeling of multi-pattern processing. The model is able to extract components of complex odor patterns (which are the spatio-temporal sequences of neural activity), segment and bind them temporally

1 Introduction

Flexible object recognition, feature binding and segmentation, attention focusing and other pattern processing tasks are hardly handled by pattern recognition techniques based on stationary principles. On the other hand, they are successfully resolved by biological neural systems, where different kinds of temporal dynamic and temporal correlations are believed to be underlying principles [2],[4],[11].

Olfaction is an example of such a system, in which spatio-temporal dynamics was a subject for numerous experimental studies [3],[9],[10],[12],[13], and theoretical modeling [1], [7], [16]. However, most odor recognition techniques do not make use of temporal encoding and processing. In such systems static patterns are recognized by the stationary pattern recognition methods, which do not appear to have much in common with biological temporal dynamics.

On the other hand, there are a number of olfactory cortex models which are based strictly on the known biological data and produce spatio-temporal dynamics similar to the one of experimental data [1], [16]. However, they do not explain the functional significance of this dynamic, which is believed to be related to cortical information processing.

Our model is an attempt to solve the problems of multi-pattern spatio-temporal processing the brain is dealing with using the tools which are believed to be present in the cortex. The temporal structure of our network provides the base for the solution of many higher-level tasks mentioned above. One of them is the problem of coarseness-sensitivity flexibility. A course enough system cannot distinguish fine variations of the patterns within a cluster, on the other hand, a sensitive enough system is not able to detect what cluster the slightly different patterns belong to. The architecture of a network of spiking neurons described in Section 3 is able to realize both fine and rough recognition of odors encoded as spatio-temporal sequences.

Another group of tasks handled by biological systems includes feature binding, segmentation, attention focusing and other multi-pattern recognition problems. There is experimental data that suggests that in the brain they are solved with the temporal processing [4],[8], and there are models that propose the possible mechanisms [2],[5],[11]. In section 4 we show that the temporal structure of our model allows us to realize the multi-pattern processing in the olfactory cortex.

2 Olfactory System

An odor identity is defined by a group of physical and chemical parameters of the odor's constituent molecules and their relative concentrations. However, these parameters are not clearly determined, nor is the

0-7803-7044-9/01/$10.00 ©2001 IEEE

correlation between their candidates and the odor properties [17]. For the sake of simplicity we assume that one constituent molecule possesses one of these crucial parameters and corresponds to one of the odor components. So, the odors are presented by the concentration vector $C = \{c_1, c_2, ..c_n\}$, where c_j is the concentration of j-th molecule.

In the olfactory systems odors are first perceived by hundreds (say n) of receptor neurons of the olfactory epithelium. These neurons are sensitive to different kinds of molecules and respond selectively to their presence with oscillatory firing. An odor is further encoded into a periodical temporal sequence of spatial patterns of synchronized oscillatory neural activity of the olfactory bulb/antennal lobe [7], [10], [13]. The spatial patterns are proved to be correlated with the odor components [9],[10],[12], but the functional significance of their temporal structure is unclear. Different experimental data supports two major hypothesis of its possible role. Such experiments as [10], [13] suggest that the temporal structure of firing of different ensembles contributes to encoding of odor identity in a certain combinatorial way. Other data shows that precise timing of a spike, or the phase of the periodic firing, depends on the stimulus intensity, that is the concentration of the corresponding component [3],[6]. These two hypothesis could coexist and compliment one another or be the parts of a more complicated neural code.

Our model realizes a mapping of the temporal relations of input patterns into spatio-temporal dynamic of the output activity. Although we follow the Hopfield's idea [6] and assume that the timing of a pattern's firing encodes the concentration of an odor, our system could still be employed if the temporal structure carried some other functional significance.

The spatio-temporal patterns in the olfactory bulb are believed to be formed in the following way: the greater the concentration of the odor component applied, the earlier the correspondent ensemble synchronizes its activity and fires [7]. According to the Hopfield's hypothesis [6], the corresponding concentrations c_j of n constituent molecules are encoded as absolute phases $\phi_1, \phi_2, .., \phi_n$ of ensemble's oscillation, related to reference phase of the cortical oscillation $\phi^{(r)}$. The respective phase shifts are then equal: $\varphi_j = \phi_j - \phi^{(r)}$. The functional relation between stimulus intensity and phase advance of the spikes has been proposed by Hopfield:

$$\varphi_j = \alpha \ln(c_j/\delta) \qquad (1)$$

where each phase shift is assumed to be proportional to the logarithm of the corresponding concentration, α is a coefficient and δ is a scale factor [6].

Such logarithmic scaling makes the relative phases of spatial patterns invariant to different concentrations of the same odor. The changing of the concentration of a multi-component odor results in a phase shift of the whole pattern, while the relative phase-shifts remain constant.

In our model we define an odor as a cluster of odor patterns, that have identical components with different relative concentrations. The system has to be rough enough to be able to recognize that different patterns may belong to the same cluster. On the other hand, it has to be sensitive enough to distinguish slightly different odors within a cluster.

In our network, recognition of an odor is represented by the firing of the neurons of a specific ensemble in a specific sequence. Cluster recognition and fine recognition are represented by activation of different neural sub-ensembles.

3 The Model

Our network consists of a layer of leaky integrate-and-fire neurons u_j, interconnected via arrays of intermediate delay-neurons d_k^{ji} (Figure 1). The neurons u_j are also connected with the layer of temporal inputs $s_j(t)$. These inputs simulate activity of the olfactory bulb and the neural layer functionally corresponds to the olfactory cortex that receives and processes those patterns.

The periodic inputs $s_j(t)$, $\{j = 1, ..n\}$ represent n spatial patterns which correspond to n components of odor concentration vector $C = \{c_1, c_2, ..c_n\}$. The inputs are presented as follows:

$$s_j(t) = s \sum_{k=1}^{\infty} \delta(t + \varphi_j - kT) \qquad (2)$$

where $\delta(t)$ is Dirac delta function, T is the signal's oscillation period, s is a spike's amplitude and the phase shifts φ_j encode concentrations of constituent molecules according to equation (1). An example of input pattern is shown in Figure 1.

There are three types of neurons in the layer. Each of them is characterized by its state, that is the neuron's membrane potential: $u_j(t)$ for the principal neurons,

$d_k^{ji}(t)$ for the delay neurons, and $x_k^{ji}(t)$ for the selective neurons. The neurons and inputs are connected with weights $w^{(neur)}$, $w^{(del)}$ and $w^{(sup)}$ (Figure 1)

As described below in equation (3), a neuron u_j receives corresponding input signal $s_j(t)$ from the j-th input and lateral signals $l_k^{ji}(t)$ (which are defined later in the section) from the activated neuron u_i, which are propagated and delayed by the delay-neurons d_k^{ji}.

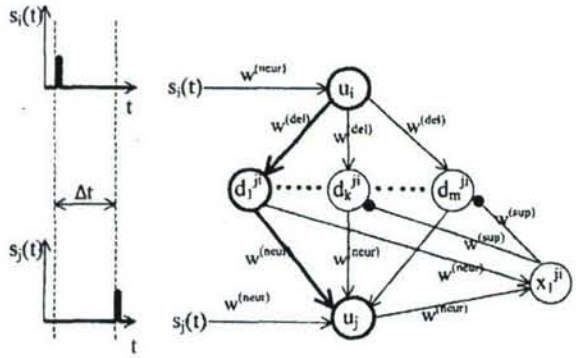

Figure 1: Network architecture. The neurons of activated sub-ensemble $\{u_i, d_1^{ji}, u_j\}$ are shown in bold. Arrows and black circles represent, correspondingly, excitatory and inhibitory connections.

When a neuron receives a spike, its potential $u_j(t)$ is increased by the weighted value $w^{(neur)}s_j(t)$, if it is a spike from input level, or $w^{(neur)}l_k^{ji}(t)=w^{(neur)}L[d_k^{ji}(t)]$ (operator L will be defined later in the section), if it is a spike propagated though a delay-neuron d_k^{ji}. If the potential of a neuron reaches its threshold value u_{thresh}, the neuron fires. Its output signal $l_j(t) = L[u_j(t)]$ produces a spike which is propagated to the array of delay-neurons that transfer the spike to all other neurons in the layer. At the same time its potential u_j is instantly reset to 0 as shown in (4). Additionally, the potential u_j is constantly decreasing with decay coefficient k. These mechanisms are employed by all the neurons in the model.

$$\frac{du_j(t)}{dt} = -ku_j(t) + w^{(neur)}s_j(t) + + \sum_{i:i\neq j}^{n}\sum_{k=1}^{m} w^{(neur)}L[d_k^{ji}(t)] \quad (3)$$

$$u_i(t^-) = u_{thresh} \Rightarrow u_i(t^+) = 0 \quad (4)$$

The operator L used above maps the functions of a neuron membrane potential to the function of the spikes $l(t)$ which this neuron produces. So, for example, $L[u_j(t)] = l_j(t)$ where $l_j(t)$ is equal to $s(t - t_{thresh})$ and t_{thresh} is the time when the value of membrane potential u_j reaches its threshold.

The parameters of the equation are set in such a way that in order for a neuron u_j to fire it needs to receive two spikes in the narrow time-window $\Delta t^{(u)}$. One spike $s_j(t)$, from the corresponding input neuron and another, $l(t) = L[d_k^{ji}(t)]$, from one of the delay-neurons (see details in section 5). An exception is made for the very first input spike in the first cycle, which alone is able to activate the corresponding neuron. This exception is made in order to add to the model the functional property of the networks like LEGION, where the global inhibition of the neurons depends on the number of the activated neurons [2]. Such inhibition ensures that the fewer neurons are activated, the greater is the probability for a neuron to fire. In our model the neurons are made more sensitive to the very first input spike, because there is no activation yet in the neuron layer. So, this first spike is enough for them to fire.

Delay-neurons in the arrays are integrate-and-fire neurons with added inherent propagation delays D_k, $\{k = 1..m\}$ defined as:

$$\frac{dd_k^{ji}(t)}{dt} = -kd_k^{ji}(t) + w^{(del)}L[u_i(t - D_k)] + + \sum_{q:q\neq k}^{m} w^{(sup)}L[x_k^{ji}(t)] \quad (5)$$

The parameters of the equation make the delay-neuron work as a delay-operator (details in section 5). When d_k^{ji} receives a spike at time t it fires at $t + D_k$. The values of delays D_k change gradually across the array as follows:

$$D_k = \frac{T(k - 1/2)}{m}, \{k = 1, ..m\} \quad (6)$$

where T is the oscillation period (2), and m is the number of the delay-neurons in the array.

As an example we consider a simple case, where an odor with two components $\{0, .., c_I, c_J, ..0\}$ is applied with $c_I > c_J$. For convenience we will be presenting

it further as $\{c_I, c_J\}$. When this odor is applied, the neuron u_I receives the input spike $s_I(t)$ first, at the moment t_1 and then u_J receives $s_J(t)$ at t_2.

The single spike s_I is enough for u_I to fire because of the exception mentioned above. The neuron u_I fires at the moment t_1 and sends spikes $L[u_I(t)]$ to all other neurons u_j , $\{j = 1..n, j \neq I\}$ via delay-arrays d_k^{ji}. The neurons u_j receive the delayed signals from d_k^{ji} at times $t + D_k$, $\{k = 1, .m\}$. However, it is not enough for them to fire because a spike from input level is also needed. Although all of them show subthreshold activation, only the neuron u_J which will receive the input spike s_J will actually reach the threshold and fire. Finally the neurons that fire are u_I, u_J and all intermediate neurons d_k^{JI} in the array which connects them.

The values of D_k set by (6) ensure that one and only one of the delay-neurons fires and sends a spike to the neuron u_J within the time window $\Delta t^{(x)}$. Although all of the delay-neurons in the array fired, only one of them actually contributes to the firing of the neuron u_J. To distinguish this contributing delay-neuron from others an additional layer of neurons x_k^{ji} is added (Figure 1). These neurons provide negative feedback $\sum_{q:q\neq k}^{m} w^{(sup)} L[x_k^{ji}(t)]$ to the intermediate neurons that did not contribute to the firing of u_J (5). This is done with integrate-and-fire neurons which work as coincident time neurons with the allowed time window Δt. Their parameters and functional properties are analogous to the neurons u_j.

$$\frac{dx_k^{ji}(t)}{dt} = -kx_i(t) + w^{(neur)} L[d_k^{(ji)}] + + w^{(neur)} L[u_j(t)] \qquad (7)$$

So, d_K^{JI} which contributed to the firing of u_J stays unchanged, while the rest of the intermediate neurons are suppressed and will not be sensitive to the spikes from u_i during time of suppression T_S, which is defined as follows:

$$T_S = \frac{1}{k} \ln \left(\frac{w^{(sup)}}{d_{thresh}/s - w^{(del)}} \right) \qquad (8)$$

Now at the output level there is a sequence of firing of neurons u_I, d_K^{JI} and u_I one after another. Firing of the neurons u_I and u_J indicates that an odor of the cluster $\{c_I, c_J\}$ is recognized. The firing of the specific intermediate delay-neuron d_K^{JI} indicates the relative concentration of two components, logarithm of which lays in the vicinity of the delay D_K of the corresponding delay-neuron:

$$D_K - \frac{T}{2m} < \alpha \ln \left[\frac{c_I}{c_J} \right] < D_K + \frac{T}{2m} \qquad (9)$$

The corresponding spatio-temporal dynamic is shown at the Figure 2b, left column. The parameters used in the simulation are described in Section 5.

4 Temporal Segmentation

According to the mechanism of formation of the input temporal sequence [7], if a mixture of several odors is applied, the corresponding spatio-temporal sequences are superimposed and the resulting input sequence contains patterns of all components of each odor. The stronger the component, the earlier its pattern fires, no matter which odor the component belongs to.

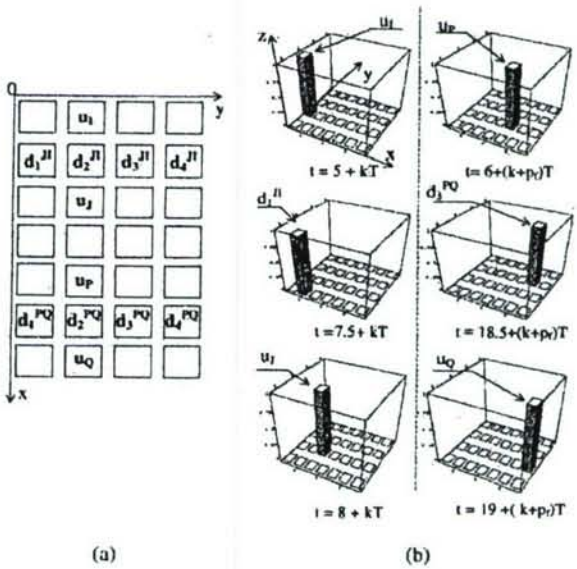

Figure 2: Temporal pattern segmentation. (a) Distribution of the neurons in the layer; (b) Spatio-temporal neural dynamics during first p_I (left column) and second p_I (right column) cycles. Axis z corresponds to the membrane potentials $u(t)$ or $d(t)$, $\{k = 1, ..p_I\}$, T is the period of oscillations

In order to segregate the odor patterns in time, one

of the ensembles should win and suppress the others for a period of several cycles. After that, due to the neural fatigue, the winning ensemble stops firing and the second strongest ensemble wins and fires during the next several cycles [2],[5],[7],[11]. To realize such pattern segmentation the modified network from the section 2 with additional neural interaction and neural fatigue function $F(p)$ is used:

$$\begin{aligned}\frac{du_j(t)}{dt} = & -ku_j(t) + \{w^{(neur)}s_j(t) + \\ + & \sum_{i:i\neq j}^{n}\sum_{k=1}^{m} w^{(neur)}L[d_k^{ji}(t)] + \\ + & \sum_{i:\forall z,u_i\cup u_j\notin E_z}^{n} w_{ji}^{(inter)}L[u_i(t)]\}F(p) \end{aligned} \quad (10)$$

where a neuron ensemble E_z, $\{z = 1,..Z\}$ is a group of neurons that correspond to the components of the same odor. All neurons which are not members of the same ensemble are interconnected with negative weights $w_{ji}^{(inter)}$. When a neuron u_i fires, it sends inhibitory signals $w_{ji}^{(inter)}L[u_i(t)]$ to the neurons that do not belong to any of the ensembles E_z in which the neuron u_i participates. The values of the membrane potential of those neurons are decreased by $w_{ji}^{(inter)}L[u_i(t)]$. They stay suppressed for the refractory period T_R during which they cannot fire regardless of the input signals received. T_R is determined as follows:

$$T_R = \frac{1}{k}\ln\left(\frac{w^{(inter)}{}_S}{u_{thresh} - 2w^{(neur)}{}_S}\right) \quad (11)$$

$F(p)$ is a step function with $F(p) = 1$, if $p < p_f$ and $F(p) = 0$, if $p > p_f$. The variable p is the number of times the neuron's potential reached its threshold, and p_f is the number of firings after which the neuron becomes insensitive to the inputs and stays silent for another p_f cycles.

The dynamics of the competition between ensembles is a quite complicated process [2], [7], because for a neuron in ensemble, probability to be suppressed depends on the statistical value of the difference of received inhibitory and excitatory spikes.

In our model, according to equation (10) and the exception for the first spike in the input sequence (Section 3), the first activated neuron suppresses the others, which are not in its ensemble and does not allow them to fire with 100% probability. So, the ensemble which contains the winning neuron, or, in other words, the odor with the strongest component always wins the competition first.

As an example we consider the case where two odors $\{c_I, c_J\}$ and $\{c_P, c_Q\}$ are applied to the network with the following order of the concentrations of their components: $c_I > c_P > c_J > c_Q$. The temporal sequence of input spikes is the same:$\{s_I(t), s_P(t), s_J(t), s_Q(t)\}$ The first of them $s_I(t)$ activates neuron u_I, which sends inhibitory signals to u_P and u_Q, and excitatory signal to u_J via array of the delay-neurons. When input spike $s_P(t)$ appears, the corresponding output neuron u_P is suppressed and will not respond to the impulse. Then input s_J activates neuron u_J, which already received excitatory signal from u_I. After that $s_Q(t)$ fails to activate neuron u_Q. Finally the neurons u_I and u_J fire, while u_P and u_Q remain silent. This way the odor $\{u_I, u_J\}$ is segmented from the background and attention is focused on it for the period of p_f cycles. Then, due to the neural fatigue $F[p]$, the neurons u_I and u_J stop firing and u_P and u_Q become activated, so the attention is now refocused at this odor. So, the odor patterns are temporally segregated and processed one at a time, as is shown at Figure 2.

5 Simulation

The neurons described by (3) and (7) work as coincident time detectors. They fire if two spikes arrive to a neuron within time window Δt, the size of which is defined by the parameters of the integrate-and-fire neurons as follows:

$$\begin{aligned}\Delta t^{(u)} &= -\frac{1}{k}\ln\left(\frac{u_{thresh}}{w^{(neur)}{}_S} - 1\right) \\ \Delta t^{(x)} &= -\frac{1}{k}\ln\left(\frac{x_{thresh}}{w^{(neur)}{}_S} - 1\right)\end{aligned} \quad (12)$$

where $\Delta t^{(u)}$ and $\Delta t^{(x)}$ are the time windows of neurons u_j and x_k^{ji} respectively. In our simulation $u_{thresh} = x_{thresh}$, so $\Delta t^{(u)} = \Delta t^{(x)}$, thus we will represent them both as Δt.

As well as this is essentially the property of the neurons used in the model, there was no need to implement them by the actual integrate-and-fire neurons. The neurons u_j were replaced by logic units u_j^*, characterized by its state $u_j^*(t)$ that has the following properties: Without inputs $u^*(t)$ is equal to 0. If u_j^* receives two spikes with weights $w^{(neur)}$ at the moments t_1 and t_2

with $t_2 > t_1$, Then:

IF $|t2 - t1| < \Delta t$

THEN $u^*(t_2^+) = u_{thresh}$

ELSE $u^*(t) = 0$

The rules for units x_k^{*ji} are analogous to the rules of u_j^*. State of d_k^{*ji} is defined as: $d_k^{*ji}(t) = d_k^{ji}(t) = L[u_i(t)]$.

The parameters used in the simulation are: $\alpha = 4$, $\delta = 1$, $s = 1$, $u_{thresh} = x_{thresh} = d_{thresh} = 1$, $w^{(neur)} = 0.75$, $w^{(del)} = 1.1$, $w^{(sup)} = -8.0963$, $w^{(int)} = -39.91$, $k = 0.2197$, $p_f = 3$, $\Delta t = 5$, $n = 4$, $m = 4$, $T = T_R = T_S = 20$.

Dynamic of an example simulation is shown in Figure 2, where the mixture of odors $\{u_I, u_J\} = \{100, 50\}$, and $\{u_P, u_Q\} = \{80, 3\}$ is applied. During first 3 cycles the neurons of the first odor fire in the following sequence: $\{u_I, d_1^{JI}, u_J\}$, (Figure 2b, left column). This indicates that the odor $\{u_I, u_J\}$ is recognized with the relative concentrations of its components defined by (9) as: $0 < \ln[\frac{c_I}{c_J}] < 1.25$. After 3 cycles $\{u_P, d_3^{JI}, u_Q\}$ becomes activated and suppresses in its turn the first ensemble (Figure 2b, right column). So, the ratio of the concentrations of the components of this odor is: $2.5 < \ln[\frac{c_P}{c_Q}] < 3.75$.

6 Discussion

Information in the brain is represented by spatio-temporal dynamics of neural ensembles in a distributed manner. Precise phase or timing of a single spike, or some more sophisticated fine structure of the spike trains are the candidates for the brain neural codes [4]. Different kinds of temporal correlation [2], [5],[11] and temporal-to-spatial mapping [15] also proved to be employed in the biological pattern processing.

So, the neural properties, principles and even the temporal-to-spatial mapping used in our model appear to have their biological prototypes. Although our system does not clarify the neural dynamics of a real biological cortex, we present an attempt to understand the principles of how the brain could use its "hardware" and temporal processing for the recognition tasks.

It is shown that the temporal structure of the proposed system allows realization of the recognition flexibility, and provides the base for the realization of higher-level tasks of multi-pattern processing such as pattern segmentation, feature binding, attention focusing and others.

Acknowledgment: This work was sponsored in part by the Department of the Navy, Office of Naval Research, Grant N000 14-01-1-0630. The content of this information does not necessarily reflect the position of the government.

References

[1] T.Ballain, P.Litaudon, J.L.Martiel and M.Cattarelli, "Role of the Net Architecture in Piriform Cortex Activity Analysis by a Mathematical Model", *Biological Cybernetics*, 79:323-336, 1998

[2] S.Campbell and D.Wang, "Synchrony and desynchrony in integrate-and- fire oscillators",*Proceedings of the IEEE International Joint Conference on Neural Networks*, Anchorage, Alaska, 2:1498-1503, 1998.

[3] P.Duchamp-Viret, B.Palouzier-Paulignan, A.Duchamp, "Odor Coding Properties of Frog Olfactory Cortical Neurons", *Neuroscience*, 74:885-895, 1996.

[4] H.Fujii, H.Ito, K.Aihara, N.Ichinose and M. Tsukada, "Dynamical Cell Assembly Hypothesis - The Theoretical Possibility of Spatio-temporal Coding in the Cortex", *Neural Networks*, 9(8):1303-1350, 1996.

[5] S.Grossberg, "How does the Cerebral Cortex Work? Learning, Attention and Grouping by the Laminar Circuits of Visual Cortex", *Spatial Vision*, 12:163-186, 1999.

[6] J.Hopfield, "Pattern Recognition Computation Using Action Potential Timing Stimulus Representation", *Nature*, 376:33-36, 1995.

[7] O.Hoshino, Y.Kashimori and T.Kambara, "An Olfactory Recognition Model Based on Spatio-temporal Encoding of Odor Quality in the Olfactory Bulb", *Biological Cybernetics*, 79:109-120, 1998.

[8] A.Jinks and D.Laing, "Temporal Processing Reveals a Mechanism for Limiting the Capacity of Humans to Analyze Odor Mixtures", *Cognitive Brain Research*, 8:311-325, 1999.

[9] J.Joerges, A.Kuttner, C.G.Galizia and R.Menzel, "Representations of Odour Mixtures Visualized in the Honeybee Brain", *Nature*, 387(6630):285-288, 1997

[10] G.Laurent, "Dynamical Representation of Odors by Oscillating and Evolving Neural Assemblies", *Trends in Neuroscience*,19:489-496, 1996.

[11] C.Malsburg, "The What and Why of Binding: The modeler's perspective",*Neuron*, 24:95-104, 1992.

[12] K.Ressler, S.Sullivan and L.Buck, "Information Coding in the Olfactory System: Evidence for a Stereotyped and Highly Organized Epitope map in the Olfactory Bulb", *Cell*, 79:1245-1255, 1994.

[13] M. Wehr, G. Laurent, "Odour Encoding by Temporal Sequences of Firing in Oscillating Assemblies", *Nature*, 384(6630):162-166, 1996.

[14] J.White, T.Dickinson, D.Walt and J.Kauer, "An Olfactory Neuronal Network for Vapor Recognition in an Artificial Nose", *Biological Cybernetics*, 78:245-251, 1998.

[15] J.Wiemer, F.Spengler, F.Joublin, P.Stagge, S.Wacquant, "Learning Cortical Topography from Spatiotemporal Stimuli", *Biological Cybernetics*, 82:173-187, 2000.

[16] M.Wilson and J.Bower, "Cortical Oscillations and Temporal Interactions in a Computer Simulation of Piriform Cortex", *Journal of Neurophysiology*, 67(4):981-995, 1992.

[17] P.Wise, J.Mats and S.William, "Quantification of Odor Quality", *Chemical Senses*, 25:429-443, 2000.

Lozowski A.G. and Noble B.L., ``Processing temporal sequences", Proc. of the 45th Midwest Symposium on Circuits and Systems, vol. 1, (Tulsa, Oklahoma), pp. 180-183, Aug. 4-7, 2002.

PROCESSING TEMPORAL SEQUENCES

Andrzej G. Lozowski and Bradley L. Noble

Southern Illinois University at Edwardsville, ECE Department
Edwardsville, IL 62026

ABSTRACT

The analysis of dynamical systems with nonintegrable continuous-time dynamics is oftentimes performed with the help of a Poincare map. This reduces the number of observed dimensions by one without a significant loss of generality in the results. Dynamics produced by the Poincare map, however, is still a sequence of real-valued quantities, difficult to represent in terms of electronic signals. Alternatively, a binary signal representing the time intervals between consecutive piercings through the Poincare section can be easily implemented in electronic circuitry.

1. INTRODUCTION

We introduce a temporal sequence to be a signal composed of Dirac deltas separated by a sequence of time intervals. The choice of the Dirac delta representation has no meaning other than marking certain instances in time. More formally speaking, a temporal sequence is a mapping $Z \rightarrow R$ (integer-to-real), which resembles the set-theoretical definition of a sequence.

Temporal sequences form a metric space. This allows for testing how close two temporal sequences are to each other. By defining a suitable metric, convergence of a dynamical system $Z \rightarrow (Z \rightarrow R)$ can be tested. The meaning of the introduced dynamical system description is a temporal sequence undergoing iterations. This formalism is sufficient to investigate Cauchy convergence as well as synchronization of two temporal sequences. Modifying the statistics of a temporal sequence as it is being generated can be considered a form of modulation. Information inscribed in the sequence in this manner would be detectable if the statistics of the unmodulated time sequence were known when received.

The main advantage of having the signal in the form of a temporal sequence is its suitability for binary representation. A simple electronic circuit (alternative designs have been introduced [1]) for hardware experiments with temporal sequences is presented in subsequent sections.

This work was sponsored by the Department of Navy, Office of Naval Research, Grant N00014-01-1-0630. The contents of this information does not necessarily reflect the position of the U.S. government.

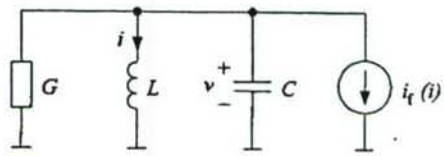

Figure 1: The LC tank circuit with negative conductance G and amplitude regulating current $i_f(i)$. The current-controlled current source is a Schmitt trigger circuit.

2. SIMPLE TEMPORAL SEQUENCE GENERATOR

The circuit includes a simple harmonic (linear) oscillator with a tank circuit and a negative conductance, as shown in Fig. 1. The negative conductance G supplies energy to cover for the dissipation from the actual LC components. In order to insure bounded oscillations, an amplitude stabilization technique is used by injecting current $i_f(i)$. Current i_f switches between one of two constant levels I_0 or $-I_0$. Every such switching decreases the magnitude of oscillations. The dynamic equations of the oscillator represent a second order system

$$C\frac{dv}{dt} = -Gv - i + i_f(i) \quad (1)$$

$$L\frac{di}{dt} = v \quad (2)$$

Whenever the injected current is constant $i_f = \pm I_0$, the solution $(v(t), i(t))$ is linear about the fixed point $(0, \pm I_0)$, as shown in Fig. 2. The frequency of oscillations and the envelope of magnitude expansion are determined by the eigenvalues of the Jacobian $\begin{bmatrix} -G/C & -1/C \\ 1/L & 0 \end{bmatrix}$. These eigenvalues are the complex conjugate pair $\lambda = -\frac{G}{2C} \pm i\frac{1}{\sqrt{LC}}$. Therefore the frequency of the oscillations is $f_0 = \frac{1}{2\pi\sqrt{LC}}$ and the magnitude follows the envelope $e^{-\frac{G}{2C}t}$.

The fixed point is a center of the oscillations spiraling outward. Current i_f selects the present location of the fixed point as either positive or negative constant I_0. The switching occurs when the trajectory gains enough magnitude to reach the vicinity of the opposite fixed point location. Since only a single variable i is used to determine the switching

0-7803-7524-6/02/$17.00 ©2002 IEEE

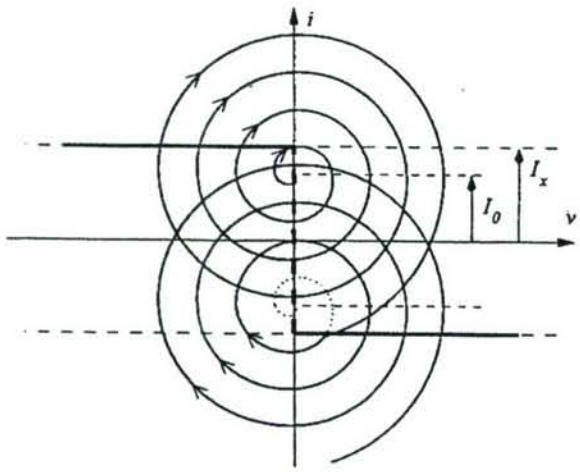

Figure 2: There is only a single fixed point in the phase space, however its location is switched between $\pm I_0$. The Poincare section $i = -I_x \text{sign}(v)$ is shown in bold.

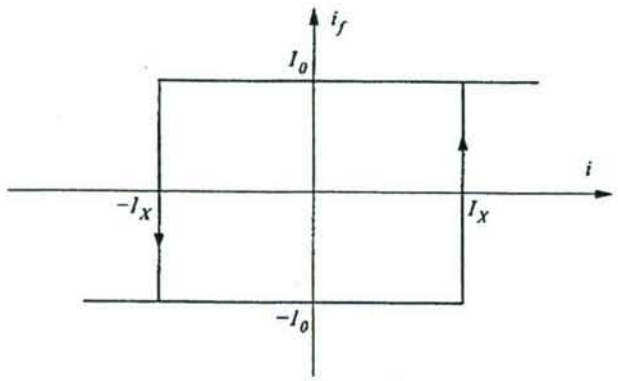

Figure 3: A Schmitt trigger injects current $i_f = \pm I_0$ to switch the fixed point location whenever inductor current i reaches value $\pm I_x$.

threshold, the circuit can be implemented using a simple Schmitt trigger. If the present fixed point is I_0 and the trajectory coordinate goes below the opposite fixed point $-I_0$, the fixed point is switched. Likewise, if the present fixed point is $-I_0$ and the current coordinate exceeds positive I_0, the fixed point is also switched. A constant I_x has been selected to adjust the threshold point for the fixed point switching. The described switching occurs at an instance t_0 as follows:

$$i_f(t_0^+) = \begin{cases} -I_0, & \text{if } i(t_0^-) = I_x \\ I_0, & \text{if } i(t_0^-) = -I_x \end{cases} \quad (3)$$

where $t_0^{\pm} = \lim_{h \to 0}(t \pm h)$. The hysteretic relationship between the currents i_f and i, shown in Fig. 3, is a source of nonlinearity of the circuit and provide its ability to oscillate chaotically.

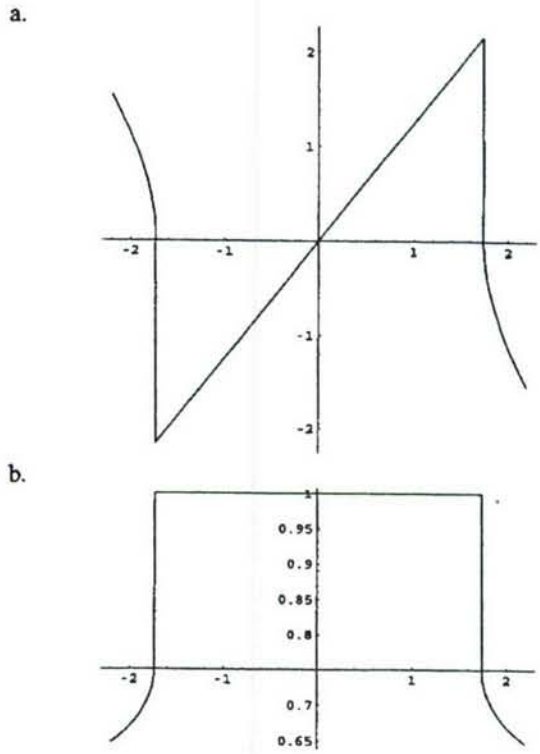

Figure 4: Graphs of functions f (top) and g (bottom). Note that axes of the graph in the bottom do not intersect in the origin.

The set of points in the phase space, corresponding to the change of state of the Schmitt trigger, is located on the bold discontinuous curve shown in Fig. 2. This curve, described by equation $i = -I_x \text{sign}(v)$, is selected to be the Poincare section of the oscillator dynamics. Note that only variable v is a meaningful coordinate of the events happening on the curve. The Poincare section determines a discrete-time dynamical system. It will be useful to express its equations using the following state description:

$$v_{n+1} = f(v_n) \quad (4)$$

$$T_n = g(v_n) \quad (5)$$

Sequence $\{v_n\}$ represents the coordinates of consecutive intersections of the oscillator trajectory with the Poincare section. Sequence $\{T_n\}$ represents time intervals between these intersections. Figure 4 shows graphs of functions f and g resulting from the oscillator dynamics example with $I_x/I_0 = 1.05$ and parameters GLC selected to obtain eigenvalues $\lambda = 2\pi(0.05 \pm 1.00i)$. With the help of these functions and equations (4) and (5), the dynamics on the Poincare section can be easily calculated without having to integrate the differential equations of the oscillator.

Sequences of v_n and T_n are not easy to obtain from the

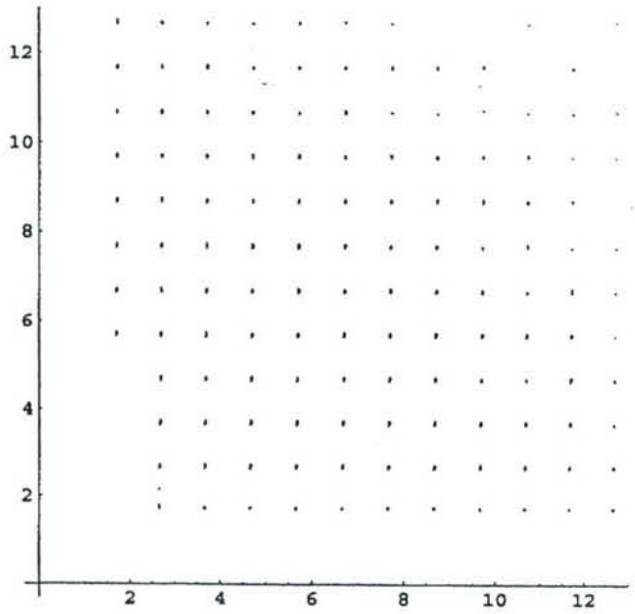

Figure 5: Graph of 50000 intervals between the Schmitt trigger transitions. Intervals τ_{k+1} are shown (vertically) in terms of preceding intervals τ_k (horizontally).

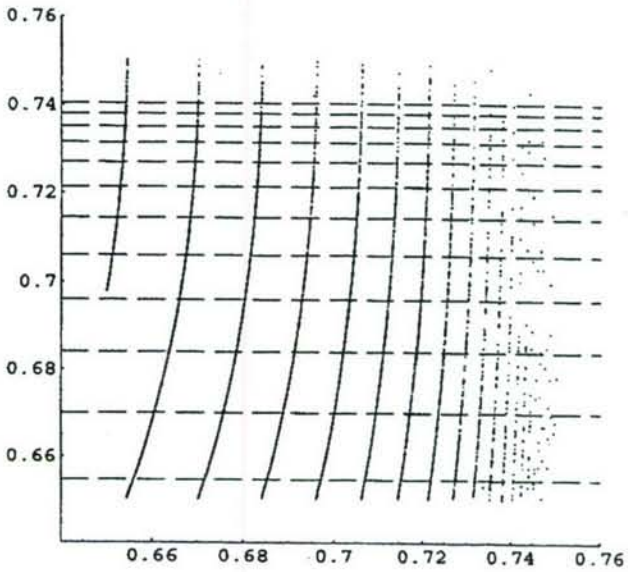

Figure 6: Mapping $T_{n_{k+1}} = h(T_{n_k})$. Final intervals $T_{n_{k+1}}$ are shown vertically versus preceding final intervals T_{n_k} (horizontally). Counting from the left, d_{k+1} is the number of the graph branch. Dashed lines separate variable ranges occupied by the branches.

electronic implementation of the oscillator. Another observable, readily available through measurement, is the state of the Schmitt trigger. Let $\{\tau_k\}$ be the sequence of time intervals between consecutive transitions of the Schmitt trigger. As illustrated in Fig. 2, every interval τ_k is composed of several full rotations of the trajectory about the fixed point and one final rotation taking less then 75% of period to hit the bold line on the opposite side. With the selection of example oscillator parameters, the period is $T_0 = 1$, which can be identified as the maximum value of function g in Fig. 4b. All intervals T_n less then period T_0 determine the final rotation before the Schmitt trigger transitions. The ordered set $\{n : T_n < T_0\}$ defines a sequence $\{n_k\}$ of indexes of such final intervals T_n. Prior to the n_k-th final interval T_{n_k}, there are $d_k = n_k - n_{k-1} - 1$ full rotations T_0. This provides a relationship between time interval sequences $\{\tau_k\}$ and $\{T_n\}$:

$$\tau_k = d_k T_0 + T_{n_k} \tag{6}$$

A question naturally arises as to whether sequence $\{\tau_k\}$ could be generated directly by a mapping. Even more specifically, is interval τ_{k+1} uniquely determined by the preceding interval τ_k? A number of interval pairs (τ_k, τ_{k+1}), generated using Equation (6), is displayed in Fig. 5. The grid pattern is an immediate consequence of the τ-interval being composed of a multiple of T_0 plus a final interval T_{n_k}. In fact, the final intervals carry all the information regarding the τ-sequence. As shown in Fig. 6, final interval T_{n_k} uniquely determines the successive final interval $T_{n_{k+1}}$.

Moreover, the graph of this relationship is composed of several branches. For a given T_{n_k}, the successive final interval is located on the d_{k+1}-st branch of the graph. This way, final interval T_{n_k} uniquely determines also the interval τ_{k+1}. The evolution of final intervals resembles iterations of the Bernoulli shifts. A mapping h and quantization scheme q can be developed by interpolating the graph in Fig. 6:

$$T_{n_{k+1}} = h(T_{n_k}) \tag{7}$$

$$d_{k+1} = q(T_{n_k}) \tag{8}$$

With the help of these two functions the mapping of τ-intervals can be explicitly devised as

$$\tau_{k+1} = q(\tau_k \bmod T_0)T_0 + h(\tau_k \bmod T_0). \tag{9}$$

Given an initial interval, Equation (9) allows for generating the τ-sequence same as the one produced by the original differential equation. However if certain limited precision level is assumed, mapping h will introduce uncertainty in the dynamics. There are infinitely many branches contained in the graph of mapping h. At higher argument values, corresponding to the right side of the graph in Fig. 6, even a slight fluctuation of argument, resulting from physical reality of implementation, will result in indeterminable value of the mapping. Such behavior is typical for nonintegrable dynamics. In order to avoid relying on individual trajectories of the dynamics being inspected, using its statistical

characterization may prove beneficial in practical applications. Let $D \subset (0, T_0)$ be both the domain and the range of mapping h. Let h_i be the i-th branch of mapping h, and unambiguously $h = \bigcup_{i=1}^{\infty} h_i$. Domain D is divided into infinitely many segments D_i. Each segment D_i is a preimage of the domain for a certain branch $D_i = h_i^{-1}(D)$. Segments D_1 through D_{12}, separated by the dashed lines in the range of mapping h, are shown in Fig. 6. A fraction of segment D_i which is mapped onto segment D_j is a subsegment $h_i^{-1}(D_j)$. Assume the initial interval T_{n_0} is selected randomly from domain D. If the dynamics determined by Equation (9) is ergodic, conditional probability P_{ij} that the successive interval T_{n_1} falls into segment D_j given that interval T_{n_0} is in segment D_i equals the ratio of the segment lengths:

$$P_{ij} = \frac{|h_i^{-1}(D_j)|}{|D_i|} \tag{10}$$

Numbers P_{ij} arranged in a matrix $P = [P_{ij}]$ describe probabilities of transitions from segment D_i to D_j at every iterative step. The first six rows and columns of matrix P evaluated numerically read

$$P = \begin{bmatrix} 0 & 0 & 0 & 0 & 0.528 & 0.471 & \dots \\ 0.121 & 0.346 & 0.237 & 0.137 & 0.091 & 0.065 & \dots \\ 0.114 & 0.360 & 0.226 & 0.146 & 0.096 & 0.056 & \dots \\ 0.133 & 0.357 & 0.232 & 0.136 & 0.084 & 0.056 & \dots \\ 0.093 & 0.338 & 0.259 & 0.148 & 0.094 & 0.065 & \dots \\ 0.121 & 0.365 & 0.218 & 0.135 & 0.095 & 0.063 & \dots \\ \dots & \dots & \dots & \dots & \dots & \dots & \dots \end{bmatrix} \tag{11}$$

Note that P is the transition matrix of a Markov process with states d_k associated with segments D_i. Matrix P is probabilistic, which means that the row-sums are always equal to 1. If ϕ is any initial probability distribution $\phi(u) = \Pr(d_0 = u)$, after k iterative steps the distribution evolves to be ϕP^k. The iterations eventually approach the invariant probability distribution $\phi^* = \lim_{k\to\infty} \phi P^k$. If mapping h is mixing [2] and expanding ($|h'(T_{n_k})| > 1$), the invariant distribution ϕ^* is uniquely determined by the parameters of the dynamical system [3], independent of the initial distribution ϕ. The dynamical system (9) generates observable time intervals τ_k with symbols d_k occurring according to the distribution ϕ^* shown in Fig. 7. This distribution is also the left eigenvector of matrix P associated with eigenvalue equal 1.

In conclusion, the first-order statistics of the time intervals generated by a dynamical system with oscillatory dynamics can be derived from its binary observable. The sequence of time intervals which displays a grid pattern in delayed coordinates contains a sequence of discrete symbols. Such a symbol sequence may be considered Markovian and the frequency of inter-symbol transitions can be estimated in order to determine transition probabilities.

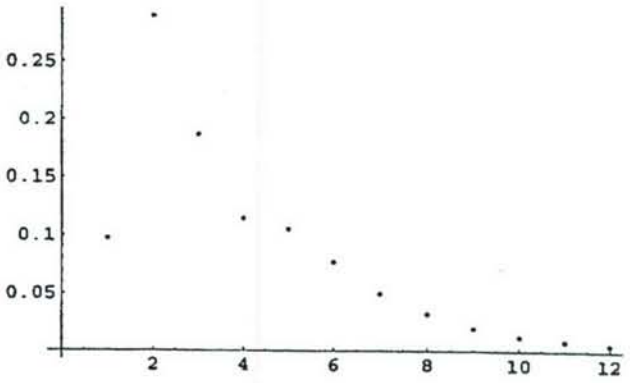

Figure 7: Invariant probability distribution ϕ^* for the dynamical system derived from time intervals τ_k. Probabilities of the first 12 states ($\Pr(d_k = 1)$ through $\Pr(d_k = 12)$) shown.

3. REFERENCES

[1] H. Nakano and T. Saito, "Synchronization in a pulse-coupled network of chaotic spiking oscillators," in *Proc. of the 45th Midwest Symposium on Circuits and Systems (MWSCAS'02)*, vol. 1, (Tulsa, Oklahoma), Aug. 4–7, 2002.

[2] M. Tabor, *Chaos and integrability in nonlinear dynamics. An introduction.* John Wiley & Sons, 1989.

[3] G. Mazzini, R. Rovatti, and G. Setti, "Chaos-based DS-CDMA:Introduction. Some tools for studying chaos with densities." Winter School in Chaotic Communications, University of California in San Diego, Jan. 23–26, 2000.

Bifurcation-Based Neural Computation

Mykola Lysetskiy, Jacek M. Zurada and Andrzej Lozowski*
University of Louisville
Department of Electrical and Computer Engineering
Louisville, KY, 40208, USA
Email: m0lyse01@ubongo.spd.louisville.edu
*Southern Illinois University at Edwardsville, IL
Department of Electrical and Computer Engineering

Abstract - Quadratic logistic map (QLM) is proposed as a generalized form of an artificial neuron (AN). Dynamics of the QLM not only exhibits computational abilities, but also has certain common features with the one of the modified Hodgkin-Huxley models of a neuron. The rest state of the QLM neuron is wandering within a chaotic attractor. Applied input is an additional bifurcation parameter of the system. Input of a certain range induces emergence of corresponding stable orbit. An arbitrary large number of attractors can be stored in a single QLM neuron. We explore the computational abilities of the QLM dynamics and argue that it may reflect certain aspects of dynamics of biological neurons.

I. INTRODUCTION

Limitations of the static nature of artificial neural networks (ANN) have inspired investigation in neuron models with inherent dynamics, such as spiking and chaotic neurons. In networks made of such neurons recognition is presented by convergence not only to a fixed point, but also to a limit cycle or even chaotic attractor [5]. Although this is a step toward modeling of the real brain processes, when these dynamic attractors are used in the framework of static NN, they simply replace static fixed points with the dynamic ones. As a result, they do not bring principally new computational properties.

Most artificial neurons commonly used for simulations are oversimplified versions of the Hodgkin-Huxley model (HHM), which, in turn, is a simplified model of the real neural processes.

However, HHM, as well as its modified versions (MHHM), demonstrate quite fascinating dynamics, with a variety of chaotic phenomena. For example, dynamics of interspike time interval of biological thermally sensitive neurons with increasing input (temperature) which is a bifurcation parameter of a system, undergoes transition to chaos via period-doubling cascade, intermittency and crises of chaotic attractors, emerging windows of periodic activity, etc., as shown in Fig. I. [3]. Chaotic dynamics emerges in neural systems at macro level as well. Seminal results of W.Freeman and co-workers [11] show that the state of the olfactory bulb, in olfactory system, when unperturbed, is wandering within high-dimensional chaotic attractor. This chaotic wandering is seen as a solution search. Applied input (odor) shifts the state of the system to the one of its low-dimensional wings, which corresponds to the recognized odor.

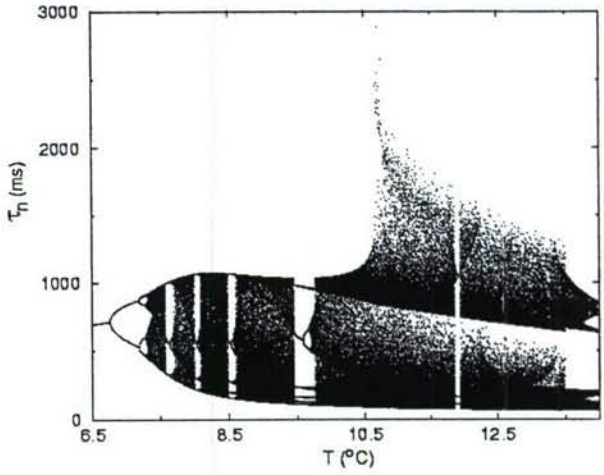

Fig. I. Bifurcation diagram of the modified Hodgkin-Huxley model of thermally sensitive neurons. Interspike intervals τ_n versus bifurcation parameter T (temperature). (From U.Feudel et al., *Chaos*,Vol. 10:1, 2000.)

This concept of chaotic search was further explored by [1],[8], and even applied to an engineering application: a search of an optimal solution of the salesman problem [12].

Another idea is that if chaotic wandering were controlled, the patterns could be stored as trajectories of the system's state in the phase space. That would give an enormous memory capacity and preserve some relations

0-7803-7278-6/02/$10.00 ©2002 IEEE

Lysetskiy M, Zurada, JM., Lozowski, A., Bifurcation-based Neural Computation, Proc. of the International Joint Conference on Neural Networks, pp. 2716-2720, Honolulu, Hawaii, May 12-17, 2002

(like similarity, for example) of stored patterns. However tempting, the concept has not been yet realized.

Sensitivity to small fluctuations and initial conditions is is another application of chaos possibly employed by the brain circuits to separate, for example, a tiny input from a strong background.

How exactly chaos is employed by the brain and how the computation principles of biological neural circuits are different from the ones of ANN is not well understood. However, one of the hints about this difference is the fact that in biological systems an input may not be presented by initial conditions. Instead, an input can be its bifurcation parameter. It is exactly the case in the HHM and MHHM, where external current is a bifurcation parameter of the dynamics of the neuron's potential. Dynamics of thermally sensitive neurons, where the temperature is a bifurcation parameter for a interspike interval dynamics [2],[3],[4] is a good illustration of this idea. This input-as-a-parameter hypothesis could explain how microscopic fluctuation of an input is able to change global dynamics of a system, which is often the case for biological sensory circuits. Subthreshold oscillations may be the biological mechanism to push the neuron close to the bifurcation state, and make it sensitive to the changes of bifurcation parameter (input) [7].

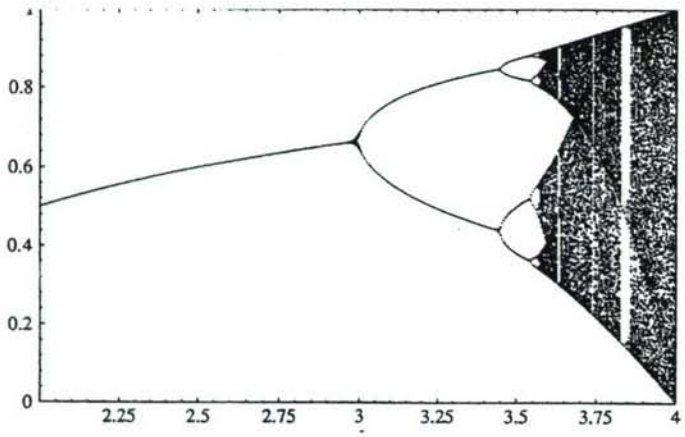

Fig. 2. Bifurcation diagram of quadratic logistic map $x^{t+1} = Rx^t(\mathrm{I} - x^t)$. x^t values (vertical axis) versus bifurcation parameter R (horizontal axis). (From R.A.Holmgren, Springer-Verlag, New York, 1996.)

Another hint about brain's possible computational principles comes from the necessity of a flexible dynamical structure of attractors which represent features and objects. ANN philosophy basically is: one pattern – one attractor. However, the brain have to deal online with multiple objects which are composite, constantly changing in time and with vaguely defined features. In order to handle this task the structure of attractors must not only be hierarchical but dynamical and flexible as well. Chaotic attractors undergoing structural transformations (as, for example, merging and segregation), caused by changing of bifurcation parameter, could be the mechanism used by the brain for this purpose.

In this paper we use the dynamics of quadratic logistic maps (See Fig. 2 and Eqn. (I)) [6],[10] as an abstract model of a chaotic neuron with great computational power. At a first glance the QLM is very far from both ANN and their biological prototypes, but, surprisingly, it turns out that QLM may actually be one of the the missing links between them.

A single classical neuron with a feedback and sigmoidal activation function $x^{t+1} = f[x^t]$ can be seen as a logistic map with three fixed points and their corresponding basins of attraction (Fig. 3). Sigmoidal form of the activation function used in ANN not only produces trivial dynamics with limited computational abilities, it also does not reflect subtle and sophisticated computational processes of a real biological neuron.

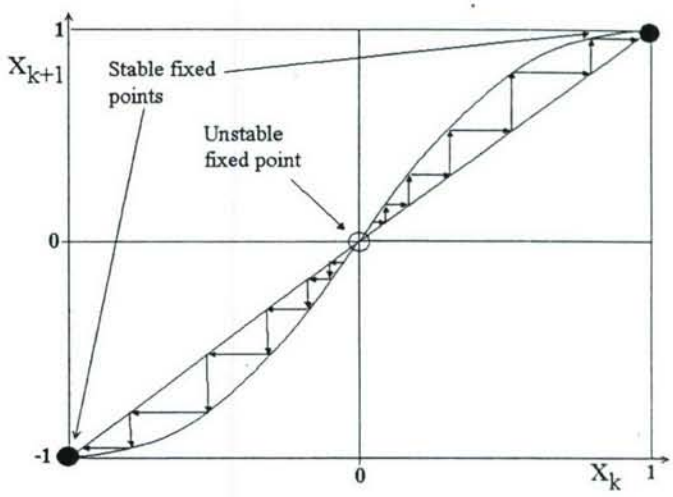

Fig. 3. A neuron with a sigmoidal activation function as a logistic map.

Although transformation function of QLM,

$$x^{t+1} = Rx^t(\mathrm{I} - x^t) \qquad (\mathrm{I})$$

is even simpler, its dynamics is tremendously rich, and thus, very promising from a computational point of view. With bifurcation parameter R increasing starting from a low value (see Fig. 2), the number of stable fixed points is constantly doubling till the system falls to chaotic attractors. In their turn, chaotic attractors undergo further transformations, such as merging and segregation with

0-7803-7278-6/02/$10.00 ©2002 IEEE

other chaotic attractors, collapses which produce stable periodic solutions, etc.

Bifurcation diagrams of QLM and MHHM of thermal neurons are shown in Figs. I. and 2. The reason of their amazing resemblance are saddle-node, period-doubling and other common basic bifurcations which underlie these dynamics. Period-doubling cascade route to chaos present in both of them is one of the fundamental bifurcation scenarios which is behind a huge number of dynamic processes – from a population dynamics in ecological systems, to chemical reactions, like the one of Belousov-Zhabotinsky [7],[9]. So, it is not an accident that dynamics of logistic maps may qualitatively reflect certain dynamical processes of biological neurons.

The question now is: what all this variety of bifurcation processes could give us in terms of computation? This is what we focus on in this paper.

II. DYNAMICS

When bifurcation parameter R is small ($R < 3$), the system $x^{t+1} = f[x^t]$ has a single stable fixed point (Fig. 2). Period-doubling bifurcation occurs when $R = 3$. With R increasing further, system undergoes period-doubling cascade and at the critical point $R_c \approx 3.57$ it becomes chaotic. The dynamics of the system is quite complicated and is still a subject of research. We focus on one of the numerous bifurcation phenomena: At certain values of R, for example at $R_3 \approx 3.828$, chaotic attractor the system lives on collapses, producing stable period-3 orbit (Figs. 2 and 4). This happens due to three saddle-node bifurcations, giving birth to 3 stable and 3 unstable orbits out of chaos. This period-3 orbit also undergoes a cascade of period-double bifurcations and the system falls to chaotic attractors again. Due to the fractal structure of the bifurcation diagram such windows of periodic orbits are ubiquitous and can be found at any interval of the bifurcation parameter. Period-3 orbit of the map $f[x^t]$ corresponds to a period-I orbit (fixed point) of the map $f^3[x] = f[f[f[x^t]]]$. Fixed point x^* of the system $x^{t+1} = f^3[x^t]$ is defined graphically as a point of intersection of curves $x^{t+1} = f^3[x^t]$ and $x^{t+1} = x^t$ (Fig. 3). x^* is stable if:

$$\left|\frac{df^3[x]}{dx}\right| < 1 \tag{2}$$

it is neutral if:

$$\left|\frac{df^3[x]}{dx}\right| = 1 \tag{3}$$

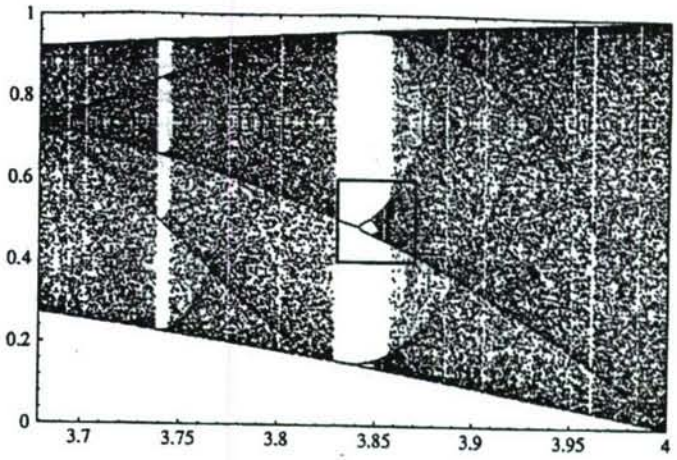

Fig. 4. Bifurcation diagram of QLM. Emerging of period-3 orbit. (From R.A.Holmgren, Springer-Verlag, New York, 1996.)

and unstable if:

$$\left|\frac{df^3[x]}{dx}\right| > 1 \tag{4}$$

With $R < R_3$ map $f^3[x]$ has no stable solution and thus wanders within chaotic attractor (Figs 2 and 4). When $R = R_3$ the curve $x^{t+1} = f^3[x^t]$ touches the line $x^{t+1} = x^t$ simultaneously in three points A, B and C, defined by (5):

$$\frac{df^3[x]}{dx} = 1 \tag{5}$$

which produce 6 intersections. This gives birth to 3 unstable and 3 stable solutions. We name them correspondingly A_1, B_1, C_1 and A_2, B_2, C_2 (see Fig. 5). Solutions A_2, B_2, C_2 are stable while they satisfy Eqn. (2). As R further increases they loose their stability via period-doubling bifurcation. In order to make this phenomena compute, we will explore another bifurcation scenario. Let $R = R_b$ be slightly less than bifurcation value R_3, when there is no stable fixed points and the system lives on the chaotic attractor. Now we add input $wInp$ (w stands for the connection weight) to the system, which shifts the function vertically in the following way:

$$x^{t+1} = f^3[x^t] - wInp \tag{6}$$

Now, if we increase gradually Inp starting from $Inp = 0$, the curve $x^{t+1} = f^3[x^t] - wInp$ will not touch the $x^{t+1} = x^t$ line at 3 points simultaneously as in the previous case, but at 3 distinct input values (Figs 5 and 6).

0-7803-7278-6/02/$10.00 ©2002 IEEE

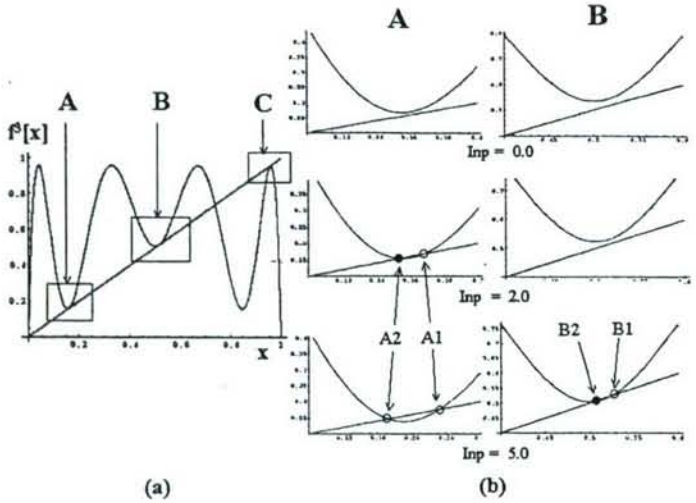

Fig. 5. (a) Function $f^3[x] = f[f[f[x^t]]]$ of QLM, $R = 3.808$. (b) Emergence and disappearance of stable orbits via the sequence of saddle-node bifurcations. Black and empty circles correspond, respectively, to stable and unstable fixed points.

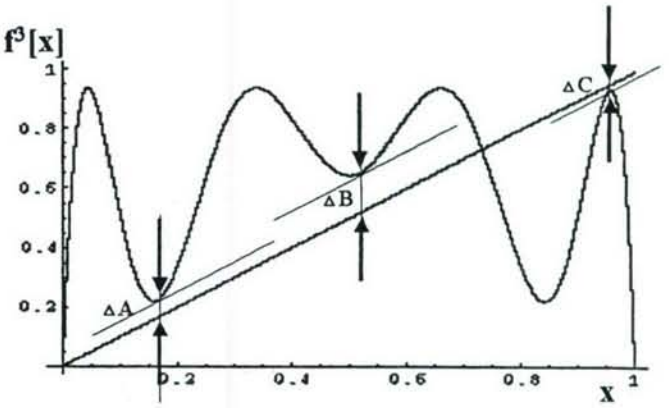

Fig. 6. Function $f^3[x] = f[f[f[x^t]]]$ of QLM, $R = 3.75$.

This happens so because the distances

$$\begin{aligned} \Delta\bar{A} &= f[\bar{A}] - \bar{A} \\ \Delta B &= f[B] - B \\ \Delta C &= f[C] - C \end{aligned} \tag{7}$$

are different and unique for different points ($\bar{A}$,B and C) for all $R < R_3$, as shown in Fig. 6. These differences are due to the different speed of the vertical changes $\frac{d\Delta\bar{A}}{dR}$ which depends on how far the point is from the origin.

When the shift $wInp = \Delta\bar{A}$ the curve $x^{t+1} = f^3[x^t] - wInp$ touches the line $x^{t+1} = x^t$, so a neutral fixed point $\bar{A}$ appears via saddle-node bifurcation which splits then into unstable fixed point $\bar{A}_1$ and stable $\bar{A}_2$ (Fig. 5b). The chaotic attractor collapses and the state of the system converges to the stable point $\bar{A}_2$, as is shown in Fig. 7 ($Inp = 1.5$).

As Inp keeps increasing two processes occur. Fixed point $\bar{A}_2$ looses its stability due to (4). Also, when the shift $wInp = \Delta B$, another stable point B_2 emerges via saddle-node bifurcation by the same mechanism (Fig. 5b). At some moment the state of the system jumps from $\bar{A}_2$ that is looses its stability to B_2 that becomes stable (Fig. 5b). The same bifurcation mechanism underlies appearance of a stable fixed point C_2 when Inp is negative and the system is shifted upward.

3 different input intervals have been mapped onto 3 different attractors. By exploring windows with different periods, any desirable number of intervals can be stored to a single neuron.

It is worthwhile to note that the shape of the function $f^3[x]$ has not been specially designed for this kind of computation, so only 3 saddle-node bifurcation points can be explored with specific $R = R_b$. It is easy to construct a function of specific shape with numerous saddle-node bifurcation points which would make the number of input intervals stored practically unlimited with their sizes arbitrary chosen.

III. SIMULATION

Simulation of the QLM dynamics was performed with parameter $R_b = 3.808$. The reason behind this choice is that the widest period-3 orbit (Fig. 4) emerges with bifurcation parameter $R_3 = 3.828$. $R_b = 3.808$ is slightly less than R_3, so the system is chaotic, but its stable states can be produced by a small input. The saddle-node bifurcation points, where the curve $x^{t+1} = f^3[x^t] - wInp$ touches the $x^{t+1} = x^t$ line are defined by (3) as follows: $\bar{A} = 0.161$, $B = 0.515$, $C = 0.955$.

Stable fixed points $\bar{A}2$, $B2$ and $C2$ loose their stability via double-period bifurcations when they reach the following values: $\bar{A}_2^b = 0.150$, $B_2^b = 0.484$, $C_2^b = 0.959$, defined by (4).

Input intervals that produce emergence of attractors $\bar{A}$, B and C with $w = 1$ are defined, respectively as follows:

$$\begin{aligned} \bar{A}: &\quad \Delta\bar{A} = 0.015 < wInp < \Delta\bar{A}_2^b = 0.026 \\ B: &\quad \Delta B = 0.039 < wInp < \Delta B_2^b = 0.070 \\ C: &\quad \Delta C = -0.004 > wInp > \Delta C_2^b = -0.007 \end{aligned} \tag{8}$$

Simulation results are shown at Fig. 7.

0-7803-7278-6/02/$10.00 ©2002 IEEE

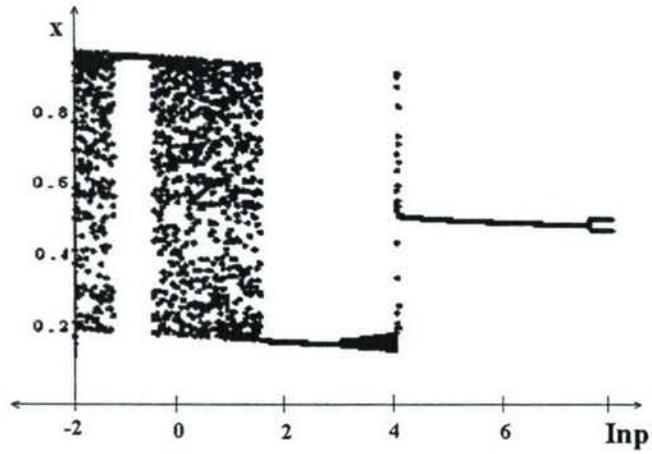

Fig. 7. Dynamics of the map $x^{t+1} = f^3[x^t] - wInp$ (with $R = 3.808$) versus applied input. Three input intervals are mapped onto three attractors

IV. DISCUSSION

We have shown that quadratic logistic map can be considered as a more general neural model with great computational abilities. QLM demonstrate dynamics which, at certain level, has certain common features with the one of biological neurons.

Bifurcation transition that we used (emerging of period-3 window out of chaotic attractor), is only one of numerous phenomena of QLM dynamics. Other chaotic processes of QLM could provide us with more computational abilities and possibly with some cues to understand certain aspects of dynamics of biological neurons. Such process as, for example, transformations of chaotic attractors of QLM may reflect dynamic transformations of the global state of the biological neural system during the recognition process. Appearance and then merger of several chaotic attractors to a single big chaotic attractor may correspond to a recognition of parts of a composite object, their binding, and then recognition of the object as a whole. Thus we argue that dynamics of quadratic logistic maps could be a useful tool for exploring computational abilities of artificial and biological neurons.

Acknowledgment: This work was sponsored by the Department of the Navy, Office of Naval Research, Grant N000 14-01-1-0630. The content of this information does not necessarily reflect the position of the government.

References

[1] *M.Adachi and K.Aihara, "Associative Dynamics in a Chaotic Neural Network", Neural Networks, Vol. 10:1, pp 83-98, 1997.*

[2] *W.Braun, B.Eckhardt, H.A.Braun, M.Huber, "Phase-space structure of a thermoreceptor", Physical Review E, Vol. 62:5, pp 6352-6360, 2000.*

[3] *U.Feudel, A.Neiman, X.Pei, W.Wojtenek, H.Braun, M.Huber, and F.Moss, "Homoclinic bifurcation in a Hodgkin-Huxley model of thermally sensitive neurons", Chaos, Vol. 10:1, pp 231-239, 2000.*

[4] *R.Gilmore, X.Pei and F.Moss, "Topological Analysis of chaos in neural spike train burst" ,Chaos, Vol. 9:3, pp 812-817, 1999.*

[5] *M.Hirsch and B.Baird, "Computing with Dynamic Attractors in Neural Networks", Biosystems, Vol. 34, pp 173-195, 1995.*

[6] *R.A.Holmgren, A First Course in Discrete Dynamical Systems, Springer-Verlag, New York, 1996.*

[7] *F.C.Hoppensteadt, E.M.Izhikevich, Weekly Connected Neural Networks, Springer-Verlag, New York, 1997.*

[8] *O.Hoshino, N.Usuba, Y.Kashimori and T.Kambara, "Role of Itinerancy Among Attractors as Dynamical Map in Distributed Coding Scheme", Neural Networks, Vol. 10:8, pp 1375-1390, 1997.*

[9] *K.Kaneko and I.Tsuda, Complex Systems: Chaos and Beyond, Springer-Verlag, Berlin Heidelberg New York, 2000.*

[10] *G.Ott, Chaos in Dynamical Systems, Cambridge University Press, New York, 1993.*

[11] *C.Skarda, and M.Freeman, "How brains make chaos in order to make sense of the world", Behavioral and Brain Sciences, Vol. 10:161-195, 1987.*

[12] *I.Tokuda, T.Nagashima and K.Aihara, "Global Bifurcation Structure of Chaotic Neural Networks and its Application to Traveling Salesman problems", Neural Networks, Vol. 10:9, pp 1673-1690, 1997.*

Hemachand Narem, Zurada, JM., Lozowski, A., Simulation of Pulse Distibution Observed in Olfactory Bulb, Proc. of the Artificial Neural Networks in Engineering (ANNIE 2004) Conference, St. Louis, Missouri, November 7-10, 2004, pp.791-799

SIMULATION OF PULSE DISTRIBUTION OBSERVED IN OLFACTORY BULB

HEMACHAND NAREM
University of Louisville
Kentucky
Department of Electrical
and Computer Engineering

JACEK M. ZURADA
University of Louisville
Kentucky
Department of Electrical
and Computer Engineering

ANDRZEJ G. LOZOWSKI
Southern Illinois University, Edwardsville,Illinois
Department of Electrical and Computer Engineering

Abstract

According to experimental studies, interspike intervals (ISI) are responsible for odor information encoding occurring in the olfactory bulb. In this paper a method is described for generating ISI that hypothetically mimics the temporal encoding of odor information. The ISI is generated by the dynamical system derived from a Markov process synthesized to incorporate the ISI as its invariant distribution. The ISI distribution is the principal eigenvector of the transition matrix of Markov process. An algorithm using Nelder - Mead to synthesize the transition matrix through a cost function minimization is presented.

1 INTRODUCTION

A sense on smell (or Olfaction) allows vertebrates and other organisms with olfactory receptors to identify the odorant molecules. A particular group of receptors is excited by a specific group of odorants (Dickson et al. 1998). The sensory olfactory receptors response to the odorants is then passed to the olfactory bulb for detection. The function of the olfactory bulb is to relay the input obtained from the olfactory receptors into a set of easily interpretable signals to the brain. The characteristics of the signals is assumed to be the following (Lozowski et al. 2004):

1. The spikes mark instances of time when the neurons fire and their shape is not a significant factor.
2. The average value of the signal is affected by spikes since signal is a time sequence of spikes and also they fluctuate between occurring more or less frequently.
3. The code division of information conveyed by a single signal is possible because the interspike intervals may follow a distinct and a repetitive behavior, in simple words spikes may occur in a certain temporal pattern.
4. Synchronization between the signal sources may cause two or more signals to exhibit cross-correlation.If the synchronized signals assume a certain spatial distribution, a set of such signals will manifest a spatio-temporal pattern.

According to a recently proposed principle of pattern processing with ISI distribution which hypothetically mimics the olfactory system encoding (Lozowski et al. 2004), the feature of odor molecules could be encoded

with ISI distribution produced by a dynamical system. The dynamic system is derived from a Markov process synthesized to incorporate the ISI distribution which is the principal eigenvector of Markov process.

This paper discusses the means of encoding odor information in the olfactory bulb and suggests an implementation for encoding by using a biological neural circuit of spiking integrate-and-fire neurons. This paper also discusses an algorithm using Nelder - Mead to synthesize the transition matrix through a cost function minimization.

2 SIGNAL ENCODING IN OLFACTORY BULB

Olfactory receptors located in the olfactory epithelium region are hard-wired to detect a specific odor component. On one end of the receptor there is a dendrite which receives signals from odorants, on the other end is an axon, which projects to the olfactory bulb. Thus olfactory epithelium the input stage to the olfactory system.

The olfactory receptors also called sensory neurons produce spikes, whose frequency (f) of spiking depends on the concentration of the odorants at olfactory epithelium. The larger the intensity of the odorants at olfactory epithelium the more frequent the sensory neurons spike (White et al. 1991). The concentration information is temporally modulated at the glomerular inputs of the olfactory bulb, therefore the perception of odor intensity must be related to the interspike intervals ($\tau = 1/f$) (Lozowski et al. 2004). If the odor intensity increases, the intervals of spiking decreases at a different rate for each basic odorant due to the differences in their conversion gains.

A much more compressed way to describe odors is through distributions of interspike interval probabilities, which is more relevant to the signals presented to the mitral inputs. Let the interspike intervals be quantized into N ranges with cutoff τ_{max}. Maximum time difference between evoked and spontaneous activity of the receptors is τ_{max}. A single neural signal can represent an odor with the interspike interval τ probability distribution $\mathbf{a}$=$(a_1, a_2, ...a_N)$,which is formally a vector of probabilities by Lozowski et al.(2004):

$$a_n = \begin{cases} Pr(\frac{n-1}{N} < \tau \leq \frac{n}{N}\tau_{max}) & \text{if } n < N \\ Pr(\tau_{max} < \tau) & \text{if } n = N \end{cases} \tag{1}$$

The transformation of the odor into spikes is a dynamical process. The odor information is embedded in the time realizations of signals and can be retrieved only through observation of these signals for a period of time. Statistical analysis of the neural signals retrieves the probability distribution of the interspike intervals. A simple stochastic process can be modeled to have the statistical properties representing a given odor through the probability distribution.

Let a^* according to Lozowski et al.(2004) represent the probability distribution of odor at a steady state, i.e. after all transient response has vanished. A first order approximation of a dynamical system for the odor leads to Markov process with an invariant probability distribution of a^*. Let A $(N \times N)$ be the transition matrix of the Markov process (Lozowski et al. 2002)

$$a(k+1) = Aa(k) \tag{2}$$

The invariant distribution is the eigenvector of transition matrix A associated with the unit eigenvalue: $a^* = Aa^*$, thus we call the invariant distribution as the principal eigenvector of the Markov process.

The realization of the introduced Markov process is a sequence of interspike intervals τ_k. The interval range is defined to be $T_n = [\frac{n-1}{N}\tau_{max}; \tau_{max})$ if $n < N$, and $T_n = [\tau_{max}, \infty)$ otherwise, where the interval range index n is defined in the same manner as in Rospars et al. (2001). Operator A may be developed by using optimization to have a^* as its invariant distribution of interspike intervals over a period of time. The

elements of the operator are denoted by A_{ij}, so that $A = [A_{ij}]$, where i and j are the row column indices. Number A_{ij} is the probability that in the Markov process (Lozowski and Noble 2002) an interval from the range τ_i will follow the interval from the range τ_j (Lozowski et al. 2004):

$$A_{ij} = \frac{Pr(\tau_{k+1} \in T_i \text{ and } \tau_k \in T_j)}{Pr(\tau_k \in T_j)} \tag{3}$$

For a given a^* starting with some random A_{ij}'s, Nelder-Mead Simplex method of optimization can be used to find the A_{ij}'s corresponding to a minimum cost function value. As all A_{ij}'s are probabilities, they must be real numbers in the range (0,1). Based on this we define a components of cost function Eq. (4) namely quadratic error Eq. (5) and penalty function Eq. (6).

$$F(A) = F_q(A) + F_c(A) \tag{4}$$

Operator A is a probabilistic matrix whose column vectors are normalized probability distributions. Therefore, the columns of A sum up to 1. The cost function component $F_q(A)$ calculates the error of deviation for this condition (Lozowski et al. 2004):

$$F_q(A) = \sum_{j=1}^{N} \left(1 - \sum_{i=1}^{N} A_{ij}\right)^2 \tag{5}$$

The penalty function component of the cost function $F_p(A)$ calculates the sum of individual element penalties, which defines the error due to a particular element swaying out of range 0 to 1. This can be represented by the Eq. (6).

$$F_p(A) = \sum_{i=1}^{N}\sum_{j=1}^{N} \begin{cases} -A_{ij} & \text{if } A_{ij} < 0 \\ (A_{ij} - 1) & \text{if } A_{ij} > 1 \\ 0 & \text{otherwise} \end{cases} \tag{6}$$

Operator A is a well defined transition matrix of Markov process Eq. (2) if $F(A)$=0. The goal of optimization procedure is to develop operator A with the constraint that a^* is its principal eigenvector associated with eigenvalue 1. To simplify the operator synthesis, matrix A will be assumed to be diagonalizable : $A = B\Lambda B^{-1}$. The diagonal matrix $\Lambda = \text{diag}(\lambda)$ is composed of N eigenvalues λ=($\lambda_1, \lambda_2, ..., \lambda_N$) of A. Let $\lambda_1 = 1$. The convergence of the dynamical system Eq. (2) depends on the radius of the remaining λ_i's, for $i > 1$, assuming that $|\lambda_i| < r < 1$ and the radius is kept low to improve the convergence rate. In this paper the value of r was fixed to be equal to 0.2. Operator A is diagonal in the basis constructed with the column vectors of B. Since λ_1=1, the first column vector of B is a^*. All other entries B_{ij}, $j > 1$, are the variables in the optimization process. Their initial values are selected randomly from the uniform distribution in the range (-1;1). The optimization process is explained in the next section.

3 SIMPLEX METHOD FOR FUNCTION MINIMIZATION

The Nelder-Mead Simplex method for function minimization (Nelder and Mead 1965) of multiple variables is a classical, very powerful local descent algorithm, which depends on the comparison of function values at the vertices of a general simplex and not on the objective function derivatives. The comparison of function values at vertices is followed by the replacement of the vertex with the highest value by a new point generated in the process of optimization. The simplex adapts itself to the local landscape, and contracts on to the final minimum.

0.2753 0.0753 0.0751 0.0752

0.2766 0.4765 0.2765 0.2765

0.0995 0.0994 0.2994 0.0993

0.3486 0.3487 0.3488 0.5487

Costfunction minimized to 5.33096E-21

Figure 1: **An example for transition matrix of a four stage Markov process generated by simulator using simplex minimization method**

As described in the previous section the first column of the matrix B is the principal eigenvector a^*, the remaining $N(N-1)$ variables in matrix B have to be adjusted to obtain optimum operator A. So, initially considering minimization of a function of $N(N-1)$ variables, thus a simplex of $N(N-1)$ dimensions needs $N(N-1)+1$ points which are formed by randomly selecting values (in the range (-1;1)) for the variables in matrix B and corresponding transition matrices, cost functions ($Y_{(1\times N(N-1)+1)}$) are formed. The $N(N-1)$ variables in each matrix are treated as vertices of the simplex, thus the vertices of simplex are $P_0, P_1, ..., P_{N(N-1)}$. The cost function at point P_i is denoted as Y_i, the highest value among the cost functions is denoted as Y_h (Y_h=$max_{i=0}^{N(N-1)}Y_i$), and the lowest value among the cost functions is denoted as Y_l(Y_l=$min_{i=0}^{N(N-1)}Y_i$). $\overline{P}$ is defined as the centroid of the points with $Y_i \neq Y_h$ and the distance from point P_i to P_j is represented by $[P_iP_j]$.

The simplex goes through a sequence of geometric transformations (expansion-step 1, reflection-step 2, contraction-step 6 and multi-contraction-step 7) at each stage of comparison by replacing the highest by a new point. The optimization process is as follows (R. Chelouah et al. 2003):

1. Determine the $Y_l, Y_h, \overline{P}$ and calculate $P^* = (1+\alpha)\overline{P} - \alpha P_h$ calculate the cost function at P^* as Y^*.
2. If $Y_l < Y_l$ then form p** and go to step(3) else go to step(4) $P^{**} = (1+\gamma)P^* - \gamma\overline{P}$, calculate the cost function at P^{**} as Y^{**}.
3. If $Y^{**} < Y^*$ then replace P_h by P^{**} and go to step(5).
4. If $Y^* > Y_i$ for all Y_i except Y_h go to step(6).
5. Replace P_h by P^* and go to step(8).
6. If $Y^* < Y_h$ replace P_h by P^*. Form $P^{***} = \beta P_h + (1-\beta)\overline{P}$ and calculate the cost function at P^{**} as Y^{**}.
7. If $Y** > Y_h$ then replace P_i by $\frac{(P_i+P_l)}{2}$, i =0:N, else replace P_h by P^{**}
8. Check if Y_l has reached satisfactory value or zero, if so the optimum value for the matrix B is P_l.

The transition matrix A shown in Fig. 1 is formed with the matrix B obtained from simplex method of minimization. A simple shift-map can be constructed from the probabilistic operator by used in approximation Eq. (7), as described in detail Pingel et al. (2000).

$$f(x) = \frac{1}{A_{ij}}\left(x - j + \sum_{m=1}^{i} A_{mj}\right) + N - i, if j - \sum_{m=1}^{i} A_{ij} \leq x < j + A_{ij} - \sum_{m=1}^{i} A_{mj} \tag{7}$$

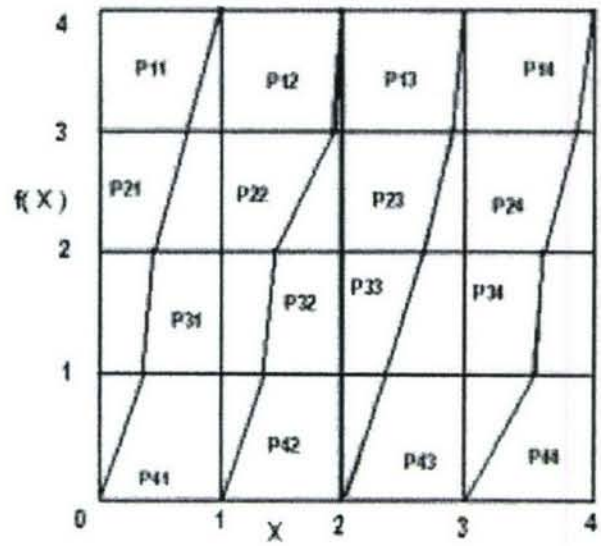

Figure 2: **Example of a piece-wise linear shift map $f(x)$ for the transition matrix shown in Fig. 1**

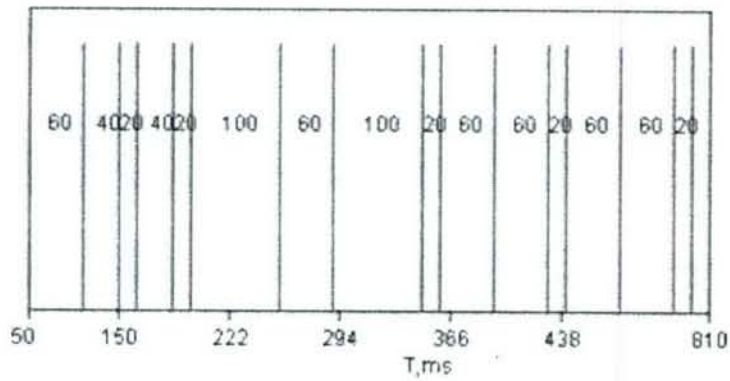

Figure 3: **An example of spike train with specific ISI distribution produced in response to the input pattern *I*={*0.41,0.28,0.41,0.31,0.34*}**

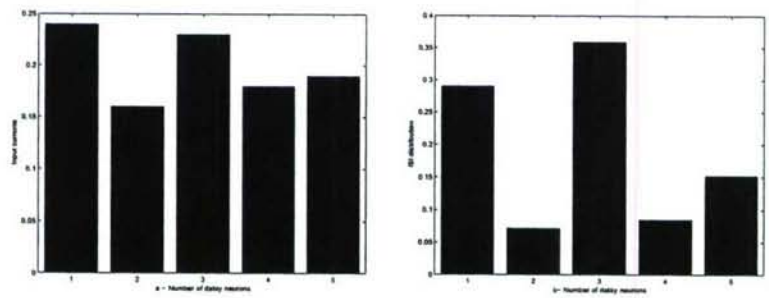

Figure 4: **The pattern of normalized input currents (a) and the resulting ISI distribution (b) of the spike train.**

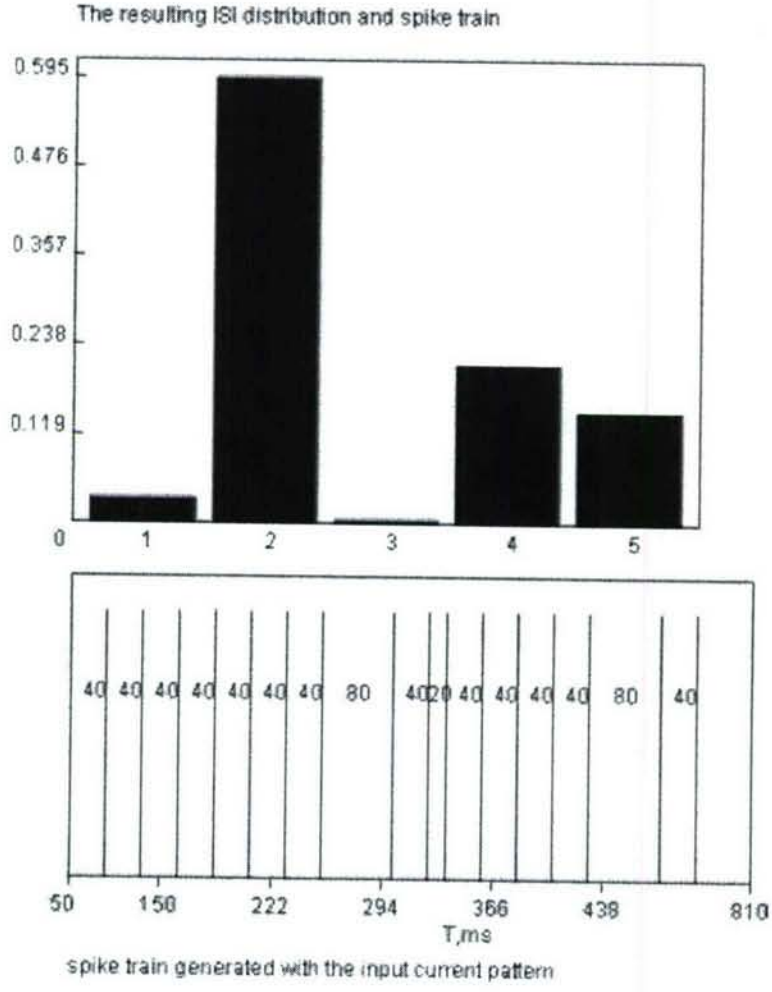

Figure 5: **ISI distribution and spike train produced by the ISI simulator**

```
0.2936 0.0936 0.09367  0.0936
0.3004 0.5004 0.3005   0.3005
0.3238 0.3239 0.5238   0.3239
0.082  0.082  0.0821   0.282
Costfunction minimized  to 1.2418E-20
```

Figure 6: **Transition matrix with principal eigenvector a^*={ 0.117,0.3755,0.4047,0.1025} generator generated by the simulator**

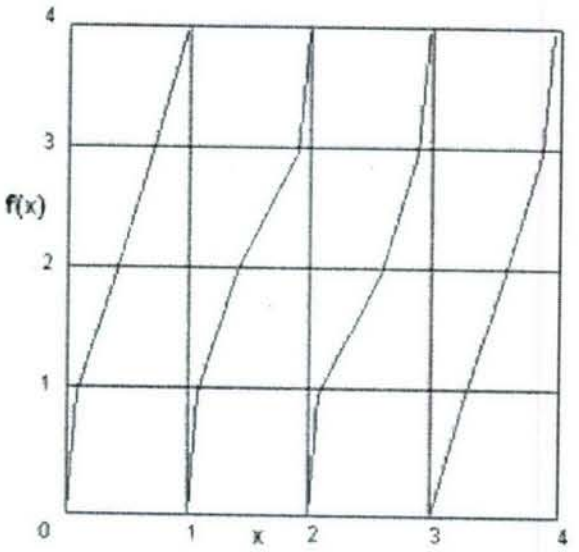

Figure 7: **Shiftmap of the transitoin matrix shown in the Fig. 6**

A piece-wise linear map as shown in the Fig. 2 $f : [0; N] \rightarrow [0; N], [0, N] \subset R$ is derived from probabilities included in the operator P.

4 INTERSPIKE INTERVAL GENERATOR

An example of a spike train produced in response to the input pattern $I = \{0.41, 0.28, 0.41, 0.31, 0.34\}$ is shown in Fig. 3. The diagram of the normalized input pattern $I_{norm} = \{0.24; 0.16; 0.23; 0.18; 0.19\}$ and the resulting ISI distribution of 10 seconds spike train are shown in Fig. 4. Here $\rho(ISI_n)$ is the probability of occurrence of the interspike intervals.

Simulator for the interspike interval generator and can be visited at
'$http://ci.uofl.edu/currentwork/narem/SIMULATOR/spikegen$'. Fig. 5 shows the example of a spike train produced in response to the input pattern $I = \{0.34, 0.55, 0.27, 0.44, 0.40\}$ and the resulting ISI distribution of 10 second spike train.

Simulator for transition matrix generator can be visited at
'$http://ci.uofl.edu/currentwork/narem/SIMULATOR/tranmatrix$'. Transition matrix generated by the simulator and the cost function for the transition matrix with principal eigenvector
a^*={0.117,0.3755,0.4047,0.1025} is shown in the Fig. 6. The resulting shift map of the transition matrix is shown in the Fig. 7.

5 CONCLUSIONS

This paper describes a simplest method of encoding information in temporal sequences and show input-output interactions which lead to an odor detection and encoding mechanism. This paper also describes a simulator which generates spike trains with the input controlled distributions of interspike intervals. This paper also describes Simplex method for function minimization, a multi-variable function minimization technique.

ACKNOWLEDGMENTS

This work was sponsored by the Department of Navy, Office Of Naval Research, Grant N00014-01-1-0630. The contents of this information does not necessarily reflect the position of the U.S. government.

REFERENCES

Chelouah, R., and Siarry, P., 2003, "Genetic and Nelder-Mead Hybridzed for a more accurate global optimization of continuous multimina functions" *European Journal of Operational Research*, vol. 148, Iss 2, pp.335-348.

Dickson, A.T., White, J., Kauer, J.S., and Walt, R.D., 1998, "Current trends in 'artificial-nose' technology," *Trends in Biotechnology*, Vol. 16,pp.250-258.

Lozowski, G.A., and Noble, L.B., 2002, "Processing Temporal Sequences," in *proc. of the 45th Midwest Symposium on circuits and systems (MSCAS'02)*, vol. 1, (Tulsa, Oklahoma), pp.180-183.

Lozowski, G.A.,Lysetskiy, M., and Zurada, M.J., 2004, "Signal Processing with Temporal Sequences in Olfactory systems," *IEEE Transactions on Neural Networks* (to be published).

Lysetskiy, M., 2003, "Input-Controlled Neural Dynamics And Its Statistics In The Olfactory System Pattern Processing," Ph.D. Dissertation, *University Of Louisville,Louisville,Kentucky.*

Nelder, A.J., and Mead, R., 1965, "A Simplex method for function minimization," *Computer Journal*,vol.7, pp.308-313.

Pingel, D., Schmelcher, P., and Diakonos, F.K., 2000, "Theory and examples of the inverse Frobenius-Perron problem for complete chaotic maps," *Chaos*, vol. 9, no.2,pp.357-366.

Rospars, P.J., Lansky, P., Duchamp-Viret, P., and Duchamp, A., 2001, "Characterizing and modeling concentration-response curves of olfactory receptor cells," *Neurocomputing*, vol. 38-40,pp.319-325

White, J., Hamilton, A.K., Neff, R.S., and Kauer, S.R., 1991, "Emergent properties of odor information coding in a representational model of the salamander olfactory bulb," *Journal of Neuroscience*, Vol. 12. pp.

Index

5.3 List of Published Papers

Journal Papers

Lysetskiy M, Lozowski A, and Zurada JM, "Temporal-to-spatial dynamic mapping, flexible recognition and temporal correlations in olfactory cortex", Biological Cybernetics, 87(1):58-67, 2002.

Lysetskiy M, Lozowski A, Zurada, JM, "Invariant Recognition of Spatio-temporal Patterns in the Olfactory System Model", Neural Processing Letters, 15(3):225-234, 2002.

Lozowski A.G., Lysetskiy M., and Zurada J.M., "Signal Processing with Temporal Sequences in Olfactory System", IEEE Transactions on Neural Networks, vol.15, No.5, September 2004, pp.1268-1275

Lysetskiy M and Zurada JM, "Bifurcating neuron: Computation and Learning", Neural Networks, 17(2): 225-232, 2004.

Conference Papers Published in Proceedings

Lysetskiy M, Zurada, J.M., Temporal Binding, Segmentation and Attention Focusing in the Olfactory Model, Proc. International Joint Conference on Neural Networks, pp.1095-1100, Washington, D.C., July 16-19, 2001.

Lozowski A.G. and Noble B.L., Processing temporal sequences, Proc. of the 45th Midwest Symposium on Circuits and Systems, vol. 1, (Tulsa, Oklahoma), pp. 180-183, Aug. 4-7, 2002.

Lysetskiy M, Zurada, JM., Lozowski, A., Bifurcation-based Neural Computation, Proc. of the International Joint Conference on Neural Networks, pp. 2716-2720, Honolulu, Hawaii, May 12-17, 2002

Hemachand Narem, Zurada, JM., Lozowski, A., Simulation of Pulse Distibution Observed in Olfactory Bulb, Proc. of the Artificial Neural Networks in Engineering (ANNIE 2004) Conference, St. Louis, Missouri, November 7-10, 2004, pp.791-799

Other Conference Presentations

Lysetskiy M, Lozowski A, Zurada, JM., "Invariant Recognition of Spatio-temporal Patterns in the Olfactory System Model", Fifth International Conference on Cognitive and Neural Systems, Boston, Mass., 2001

Lysetskiy M, Zurada, JM, Synaptic balancing guided by spike-timing-dependent plasticity in olfactory cortex model, Neural Information and Coding Workshop (NICW), Snowbird, Utah, 2003

Lysetskiy M., Lozowski A.G., and Zurada J.M., "Neural Dynamics: Encoding with Chaos and Statistics", Ninth Annual Kentucky EPSCoR Conference, Lexington, Kentucky, Abstract no. 54, May 12, 2003

Lysetskiy M., Zurada, J.M., "Possibility of synaptic balancing and spike-timing-dependent synaptic plasticity in the olfactory cortex", Seventh International Conference on Cognitive and Neural Systems, Abstract no. 13, p. 95, Boston, Mass., May 29-31, 2003

Modeling of Spatial and Temporal Dynamics in Biological Olfactory Systems

April 8, 2004

Jacek M. Zurada
Department of Electrical and Computer Engineering
University of Louisville, Louisville, KY

Andy G. Lozowski
Department of Electrical and Computer Engineering
Southern Illinois University, Edwardsville, IL

[1]This presentation is available at http://www.ee.siue.edu/~alozows/library/presentations/onr.04 with ID = onr and password = onr

Contents

1 Introduction

- Goal: Capture how information is processed in olfactory system
- Foundations: Consultations with neurophysiologists and published research
- Methods: Computer modeling of global behavior
- Conclusions: Neural information representation and processing
- Implications: Technological applicability (communications)

2 Anatomy of vertebrate olfactory system

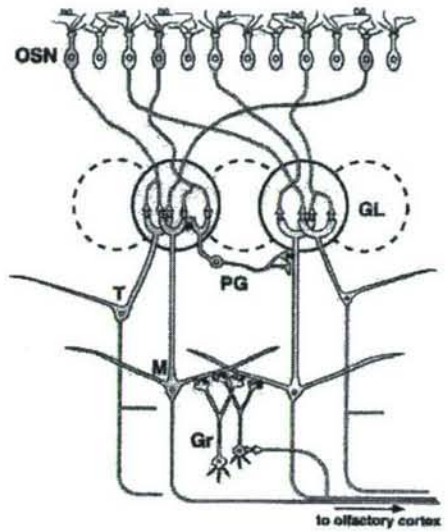

Figure 1: Olfactory bulb functional anatomy. Abbreviations: M - Mitral cells; T - tufted cells; Gr - Granulle cells; PG - Periglomerular cells; OSN - Olfactory sensory neurons; (from Mori K, Nagao H, and Yoshihara, Y, *Science*, 286(5540):711-715, 1999).

3 Formal description of neural signals

Shape of individual spike is insignificant. The Dirac delta function is a model of spike fired at t=0:

Neural spikes mark instances of time. The signal is a time sequence of spikes:

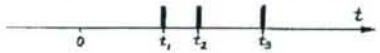

$$\text{For sequence } S = \{t_1, t_2, \ldots\}, \text{ neural signal is } s(t) = \sum_{t_i \in S} \delta(t - t_i) \tag{1}$$

Spikes may occur in a certain temporal pattern. More precisely, the inter-spike intervals may follow a distinct and repetitive behavior.

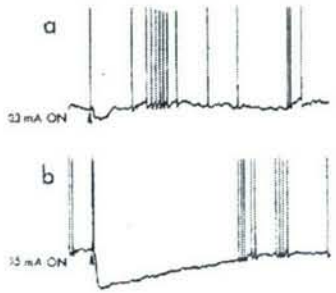

Figure 2: Intracellular responses of a mitral/tufted cell (from K. A. Hamilton and J. S. Kauer, *Brain Research*, 338 (1985) 181-185

4 Temporal modulation[1]

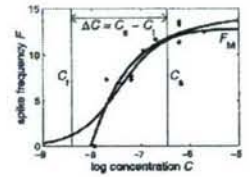

Figure 3: Concentration-response curve with logistic and arctan fittings. Response properties: maximum firing frequency F_M, threshold C_t, saturation C_S, and dynamic range $C_S - C_t$. From: Rospars, Lansky, Duchamp, *BioSystems* 58 (2000) 1333–141.

$$s(m) = \frac{1}{m - m_t} \tag{2}$$

$$\tau(m) = \left(\frac{2}{\pi} f_m \arctan \beta \log \frac{m}{m_t}\right)^{-1} \tag{3}$$

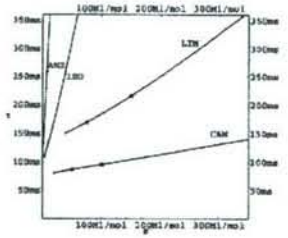

Figure 4: Interspike intervals of receptor firing versus incremental sparsity s of odorant. Investigated odorants: anisole (ANI), camphor (CAM), isoamyle acetate (ISO), and limonene (LIM).

First-order approximation with two parameters: minimum interval and gain

$$\tau = \tau_0 + Gs \tag{4}$$

[1]Term *temporal modulation* is adopted from G. Laurent.

5 Interspike interval densities

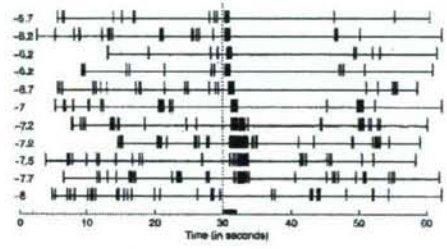

Figure 5: Recordings from a neuron at increasing concentrations of the odorant (limonene), with 30 s prestimulus (spontaneous), 2 s stimulation (vertical dotted line indicates onset of stimulation) and 30 s poststimulus activities. Concentrations C (in log mol/l) are given on the left.

Remark on Central Limit Theorem[1]

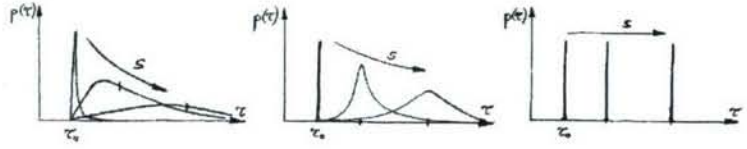

Figure 6: Probability density of average interspike intervals. Convergence of 1 (left), 100 (middle), and 40000 (right) receptors shown at three odor concentration levels.

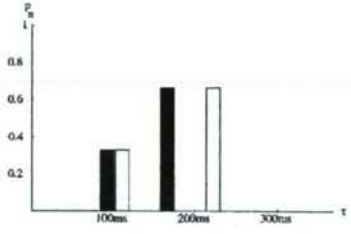

Figure 7: CAM (0.5 mol) and LIM (0.75 mol) mixed with 100 Ml of air (filled bars) and then diluted in additional 100 Ml of air (empty bars). Example with $N = 20$ and $\tau_{max} = 350$ ms shown.

[1] http://www.statisticalengineering.com/central_limit_theorem.htm

6 Stochastic representation of densities

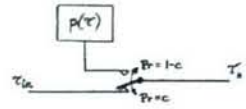

Figure 8: Markov filter

A Markov process with the invariant distribution equal p^* could serve as a first order approximation of a dynamical system for that odor. Let NxN matrix P be the transition matrix of the Markov process

$$p(k+1) = Pp(k) \tag{5}$$

7 Shift maps can generate interspike densities

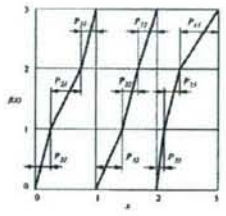

Figure 9: Example of a piece-wise linear shift map $f(x)$. Function f is composed of N continuous branches $f_j : [j-1; j) -> [0; N]$. If x is chosen randomly from the uniform distribution over the range $(0; N)$, the conditional probability P_{ij} depends on the segment slope. Example with $N = 3$ shown.

8 Odors as shift maps

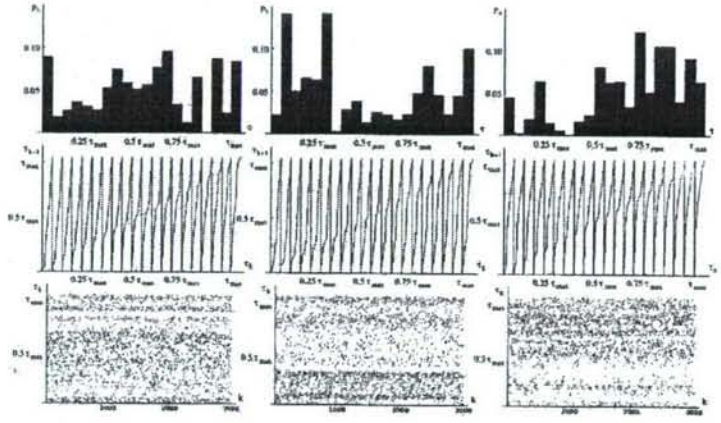

Figure 10: Synthesis of temporal sequence generators. Three example interspike interval distributions with $N = 20$ representing three different odors are shown in the top row. The corresponding shift-maps and distributions of values of generated temporal sequences are shown underneath. The time interval axes are normalized to the range of $(0; 1)$. Each graph in the bottom row contains 3000 points representing interspike intervals placed vertically according to the length of the interval.

9 Shift map with input (Frobenius filter)

$$\Pr(z_k = 1) \quad = c \tag{6}$$
$$\Pr(z_k = 0) \quad = 1 - c \tag{7}$$

c is a constant parameter, $0 < c < 1$. The overall filter equation reads:

$$\tau_{k+1} = h[z_k \tau_{\text{in}} + (1 - z_k)\tau_k] \tag{8}$$

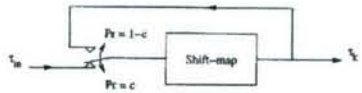

Figure 11: Frobenius filter is a shift-map with input. Either the input interval τ_{in} or the present output interval τ_k is transformed into the next output interval τ_{k+1}.

10 Olfactory system as pattern recognition

$$\begin{matrix} (p_A^*, h_A) & (p_B^*, h_A) & (p_C^*, h_A) \\ (p_A^*, h_B) & (p_B^*, h_B) & (p_C^*, h_B) \\ (p_A^*, h_C) & (p_B^*, h_C) & (p_C^*, h_C) \end{matrix} \tag{9}$$

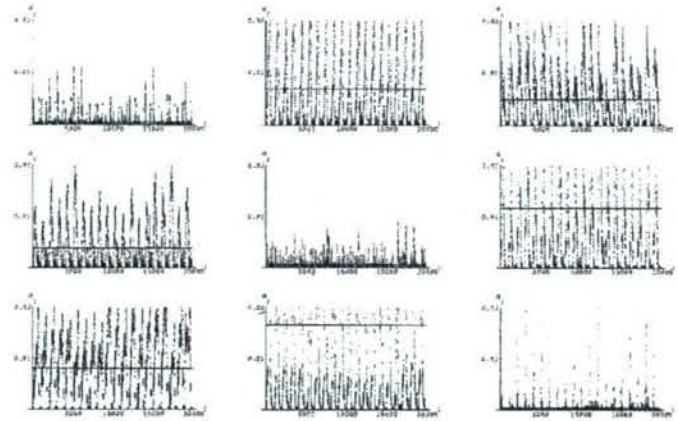

Figure 12: Nine instances of a Frobenius filter stimulated by an input distribution for 20000 iterations. Quadratic distance $d_i = (u_i - t_i)^2$ between cumulative distributions of interspike intervals at the input u_i and output t_i of the filter shown.

11 Time sequences

Figure 13: Realizations of the input (top) and output (bottom) temporal sequences for a matched pair (p_A^*, h_A). A fragment containing 100 spikes shown.

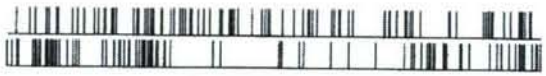

Figure 14: Realizations of the input (top) and output (bottom) temporal sequences for unmatched matched pair (p_B^*, h_A). A fragment containing 100 spikes shown.

12 Deliverables

- Formal specification of system in Mathematica
- MATRIX - numerically efficient Markov approximator in Matlab
- GENERATOR - numerically efficient sequence generator in Matlab
- MATRIX - portable in Java
- GENERATOR - portable in Java

13 Implications

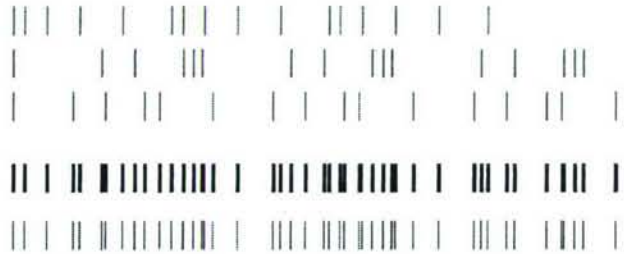

Figure 15: Superimposed temporal sequences

14 Communication types

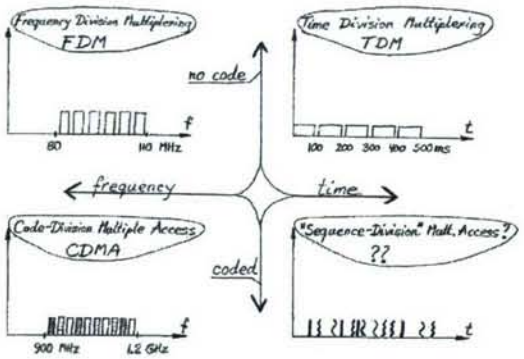

Figure 16: Communication schemes

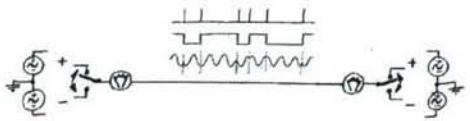

Figure 17: Implementation

15 Analog implementation of the sequence generation

There are many possible electronic circuits capable of generating temporal sequences from a shift map. Discrete example is shown in the figure. More elaborate communication systems would require VLSI implementation.

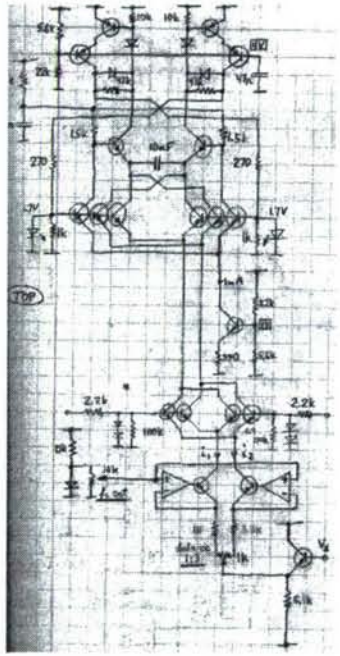

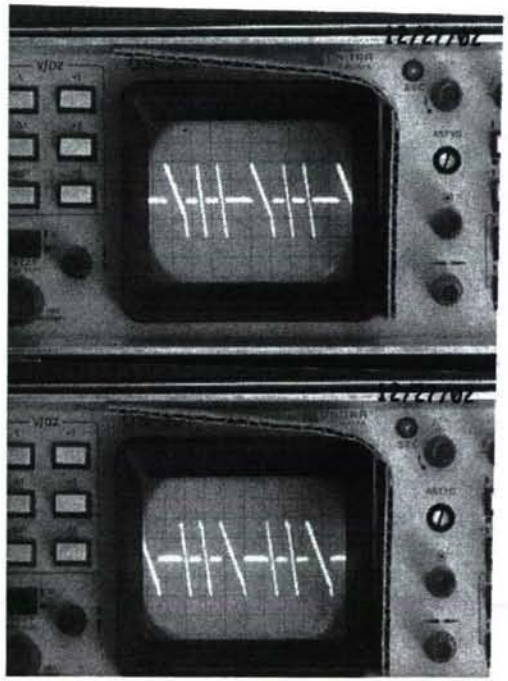

16 Digital Sequence Locking Loop (SLL)

Digital implementation of "Sequence Locking Loop" is fisible and robust. System similar in structure to the Phase Locking Loop - the electronic building block of all present communication systems.

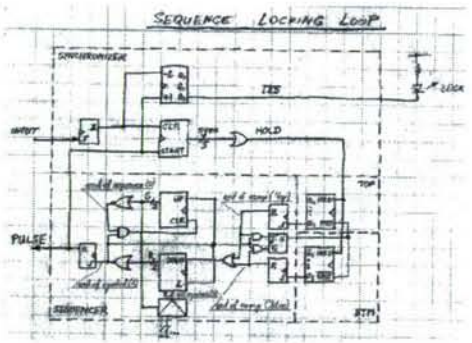

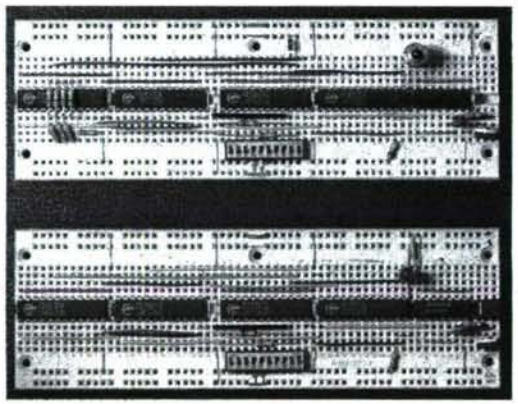

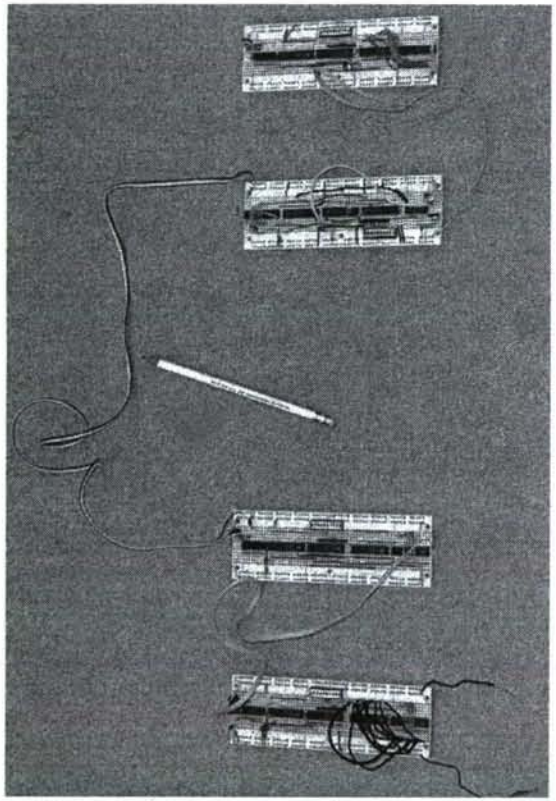

17 Possible application

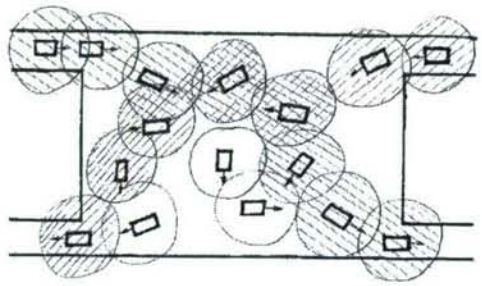

Figure 18: Access negotiation